300

THE THERMODYNAMIC AND IONIC TRANSPORT PROPERTIES OF TERNARY MOLYBDENUM SULPHIDES

KUNG YIP CHEUNG, B.Sc., M.Sc.

A thesis submitted for the degree of Doctor of Philosophy
of the University of London

Department of Metallurgy and Materials Science,
Imperial College of Science and Technology,
University of London.

November, 1978

THE THERMODYNAMIC AND IONIC TRANSPORT PROPERTIES OF TERNARY MOLYBDENUM SULPHIDES

K. Y. CHEUNG

Abstract

A lithiation reaction involving n-butyllithium reagent was developed. It was used to perform the screening test on solid solution electrode materials. A spectroscopic analysis of the reagent by UV spectrophotometry was also attempted. The difficulties of using this reagent are discussed.

Copper molybdenum sulphides ($Cu_xMo_6S_{8-y}$) were prepared from the elements. The phases with x=2 and $0<y<1$ were studied by x-ray diffraction. Samples of density about 98% theoretical value were prepared by the hot-pressing technique. The change of lattice parameters as a function of x value was studied and little variation was found when the copper content was altered by coulometric titration. By means of solid state electrochemical techniques, the thermodynamic and ionic transport properties of the compound were measured as a function of temperature. These data are discussed in terms of the population of two copper sites. A copper ionic conductivity of 0.113 $(ohm.cm)^{-1}$ was measured at $400^{\circ}K$, a value which is comparable to the best copper ionic conductors.

The techniques of ionic exchanging $Cu_2Mo_6S_{8-y}$ and lithiating Mo_6S_{8-y} were used to prepare lithium molybdenum sulphide. Satisfactory results were achieved with the latter technique. The hot-pressed samples were studied by solid state electrochemical methods. The lithium activity in $Li_{2.2}Mo_6S_{7.7}$ was calibrated with respect to a fresh lithium deposit on a nickel substrate. However, no other thermodynamic data could be obtained from the sample. A poor chemical diffusion coefficient of lithium ions in the sample was determined. An explanation of the slow diffusion rate is suggested.

ACKNOWLEDGEMENTS

I would like to thank Dr. B.C.H. Steele for his guidance, encouragement and understanding throughout the course of this study, and Dr. G.J. Dudley for his discussion and assistance on the theoretical and experimental side of the project. My sincere gratitude goes to Mrs. S.C. Lloyd-Williams for her expertise and willingness to offer help in languages, without it, the literature would not be comprehensive nor would this thesis be readable.

I am also indebted to the technical staff at Imperial College who, in one way or the other, have helped to make the present investigation possible. I would thank all my colleagues and friends for their assistance and companionship, without them, the last three years would not have been so stimulating, fascinating and memorable. Among the long list of names, I would like to express my special thank to Peter Fung and Susie Yim who typed the manuscript and Jim Boff and Mike Storey who proofread the thesis and made many valuable suggestions and comments.

This work is financially supported by UKAEA, Harwell, to which, I am most grateful.

Table of Contents

	Page
Abstract	i
Acknowledgements	ii
Table of Contents	iii
List of Figures	vi
List of Tables	viii
List of Symbols	ix

Chapter 1: INTRODUCTION

I. General Remarks	1
II. Fast Ionic Conduction	1
1. Simple Hopping Model	1
2. Factors Responsible for Fast Cu(I) and Ag(I) Ionic Conductors	3
3. Lattice Engineering, An Approach to Synthesis of New Solid Electrolytes for Alkali Ions	5
III. Solid Solution Electrodes (SSE)	7
IV. Three-dimensional SSE Materials	9

Chapter 2: THE SCREENING TECHNIQUES EMPLOYING n-BUTYLLITHIUM (n-BuLi) AGENT

I. Introduction	11
II. Lithiation by n-Butyllithium	12
III. Kinetics Studies on Lithiation by n-Butyllithium	13
IV. Experimental	17
V. Results & Discussion	
1. Vanadium Pentoxide	19
2. Vanadium Dioxide	23
3. UV Spectrophotometry Analysis	27
VI. Conclusion & Suggestions for Further Work	32

Page

Chapter 3: COPPER MOLYBDENUM SULPHIDES

I. Introduction 35

II. Aspects of Ternary Molybdenum Sulphides, Literature Survey and Deduction

1. The Crystal Structure of the Chevrel Phases 35
2. The Electronic Structure of the Chevrel Phases 40
3. The Delocalisation of M Ions 43
4. Ionic Conductivity in the Chevrel Compounds 47
5. The Non-stoichiometry of Chevrel Phases 53

III. Preparation, Specimen Fabrication and Characterisation of Copper Molybdenum Sulphide

1. Experimental Procedures 57
2. Results & Discussions
   2-1 Phase study of $Cu_2Mo_6S_{8-y}$ 58
   2-2 Hot-pressing of $Cu_2Mo_6S_{8-y}$ Phases 65

IV. The Phase Study of $Cu_xMo_6S_{7.59}$ 67

1. Experimental Procedures 69
2. Results & Discussions 71

V. Solid State Electrochemical Study of Copper Molybdenum Sulphide

1. Experimental 74
2. Results & Discussions
   2-1 Thermodynamic Studies 76
   2-2 Ionic Transport 81

VI. Summary and Conclusions 84

Chapter 4: LITHIUM MOLYBDENUM SULPHIDES

I. Introduction 86

II. Preparation, Characterisation and Fabrication of Lithium Molybdenum Sulphides 86

1. Ionic Exchange
   1-1 Introduction 87
   1-2 Experimental 88
   1-3 Results & Discussions 89

	Page
2. Lithiation of the Binary Chevrel Phase	93
2-1 Experimental	93
2-2 Results and Discussions	94
(a) The binary phase	94
(b) Lithium molybdenum sulphide	98
3. Hot-pressing Lithium Molybdenum Sulphide	
3-1 Experimental	100
3-2 Results & Discussions	100
III. Electrochemical Studies on Lithium Molybdenum Sulphide	
1. Lithium Solid Electrolytes	101
(a) LISICON	101
(b) LISPO	104
2. Calibration of Lithium Activity in the Lithium Molybdenum Sulphide	107
2-1 Experimental	107
2-2 Results & Discussions	109
3. Thermodynamic Properties of Lithium Molybdenum Sulphide	111
4. Transport Properties of Lithium Molybdenum Sulphide	112
4-1 Experimental	112
4-2 Results and Discussions	112
IV. Summary & Conclusions	116
CONCLUDING REMARKS AND FURTHER WORKS	117
APPENDIX MATHEMATICAL BACKGROUND OF THE DIFFUSION MEASUREMENT	119
REFERENCES	127

Figures

		Page
1.	Rection Kinetics of Lithiation of TiS_2 & TiS_3 by n-BuLi	14
2.	Effect of the Addition of Excess n-BuLi to Equivalent Slurries of V_2O_5, TiS_2 & MoO_3	16
3.	Resistance Change of a V_2O_5 Single Crystal upon Lithiation	20
4.	X-ray Diffraction Results for Lithiated V_2O_5	22
5.	Reaction Kinetics of Lithiating VO_2 by n-BuLi	24
6.	X-ray Diffraction Results for Lithiated VO_2	25
7.	Cell EMF of $Li(s)/Li^+(PC)/Li_xVO_2$	26
8.	Optical Absorbances of n-BuLi Solutions	28
9.	Optical Absorbances of n-BuLi Solutions	29
10.	Optical Absorbance Change as a Function of Time	31
11.	Optical Absorbance Change as a Function of Reaction Time	33
12.	The Idealised Structure of $PbMo_6S_8$	37
13.	Energy Levels for the Mo_6S_8 Cluster	42
14.	The Positions of M_1 & M_2 Sites	45
15.	Site Occupancy of M_1 & M_2 Sites as a Function of Copper Content	46
16.	Relationship between α_R Value & Delocalisation	49
17.	The Intercluster Mo-Mo Distance & a_R Value as a Function of Copper Content	51
18.	Relationship between a_R & Intercluster Molybdenum-molybdenum distance	52
19.	Phase Diagram of $Pb_xMo_6S_{8-y}$	54
20.	Formation of MoS_2 as a Function of Sulphur Content	61
21.	Lattice Parameters of $Cu_2Mo_6S_{8-y}$ as a Function of (8-y)	62
22.	Lattice Parameters of $Pb_{1.05}Mo_6S_{8-y}$ as a Function of (8-y)	64
23.	The Electrochemical Set-up for $Cu_xMo_6S_{7.59}$ sample Preparation	70
24.	Lattice Parameters of $Cu_xMo_6S_{7.59}$ as a Function of x	73
25.	Experimental Set-up for 6-point Conductivity Measurement on $Cu_xMo_6S_{7.59}$	75
26.	Cell EMF of $Cu(s)/T/Cu_xMo_6S_{7.59}$	77
27.	Partial Molar Enthalpy of Copper in $Cu_xMo_6S_{7.59}$	79

		Page
28.	Partial Molar Entropy of Copper in $Cu_xMo_6S_{7.59}$	80
29.	Ionic Conductivity & Activation Energy for Diffusion of Copper in $Cu_xMo_6S_{7.59}$	82
30.	Chemical Diffusion Coefficient of $Cu_xMo_6S_{7.59}$	83
31.	Molten Salt Exchange Apparatus	90
32.	X-ray Diffraction Results of the Studies of Thermal Stability of $Mo_6S_{7.7}$	97
33.	Experimental Set-up of 4-point DC Conductivity Measurement on LISICON	103
34.	Ionic Conductivity of LISICON	105
35.	Assembly of the $Li_{2.2}Mo_6S_{7.7}$ Electrochemical Cell	108
36.	Voltage Decay between the Lithium Reference Electrode & $Li_{2.2}Mo_6S_{7.7}$	110
37.	Voltage Response across the Ionic Probes in Transient Measurements	113
38.	The Plot of log $\lvert V_{2\infty} - V_2 \rvert$ against Time	114

Tables

		Page
1.	The Parameters of Beer's Law Obtained in UV Spectrophotometry Studies	30
2.	Members of the Series $M_xMo_6S_8$	36
3.	Comparison of Crystallographic Data of Three Selected Chevrel Phases	39
4.	Structural Parameters of Delocalised Ions in Chevrel Phases	48
5.	Analytical Results of $Cu_2Mo_6S_{8-y}$	59
6.	Results of the Phase Studies of $Cu_2Mo_6S_{8-y}$	60
7.	Hot-press Results of $Cu_2Mo_6S_{8-y}$	66
8.	Comparison of Lattice Parameter Changes on Hot-pressing at 1325°C	68
9.	Comparison of Fast Copper Ionic Conductors	84
10.	Results of Ionic Exchange on Copper Chevrel Compounds	91
11.	X-ray Diffraction Results of Lithium Molybdenum Sulphides and the Binary Phase	99
12.	Results of Hot-pressing $Li_xMo_6S_{8-y}$	100
13.	X-ray Diffraction Results for LISICON	102
14.	Ionic Conductivities & the Activation Energy for Conduction of LISICON	106
15.	Experimental Results on the Calibration of Lithium Molybdenum Sulphide	108

Abbreviations and Symbols

a_i	chemical activity of i species
C	concentration
$\tilde{D}$	chemical diffusion coefficient
d	density or jump distance
E_a	activation energy for diffusion
E_f	Fermi energy
EMF	electromotive force
E_n or En (n: number)	electrode n
F	Faraday constant
G	Gibbs free energy
H	enthalpy
i	current density
J_i	flux of i species
L	length of the specimen
O.C.V.	open-circuit voltage
R	universal gas constant
r.t.	room temperature
S	entropy
T	absolute temperature or Takahashi compound
t	time
TP	ternary phase
w.r.t.	with respect to
X	distance
x, y, z	variations of composition
z_i	charge of i species
1,2	Subscripts for electron and ion respectively
α	geometric factor
β	fraction of the species free to move
$\bar{\mu}_i$	electrochemical potential of i species
μ_i	chemical potential of i species
ν	average jump frequency
ν_o	attempt frequency
σ_i	ionic conductivity
σ_o	total electrical conductivity
τ	characteristic time
φ	average electrical potential

CHAPTER 1

INTRODUCTION

I. General Remarks:

Recently, there is an increasing interest in the study of solid state fast ionic conductors. The emergence of the new 'Solid State Ionics' field, a name used to describe the ionic behaviour in solids, is mainly due to the growing emphasis on energy conservation and alternative energy sources. As a result of a considerable amount of effort, solid materials exhibiting high ionic conductivity at ambient temperature are discovered. These materials can be used as solid electrolytes and are nowadays more often considered for use in place of the traditional liquid electrolytes in battery design. It is understandable that the conductivity of solid electrolytes will be unlikely to be better than liquid electrolytes. Furthermore, a good solid/solid interface fabrication is still an unsolved problem. In return, the all solid-state cell construction minimises the problems of corrosion, self discharge and leakage and hence improves the cell life. This is an important specification for industrial,medical, military and domestic applications.

When the high energy density battery is considered a lithium system is always a prime candidate because of its high voltage and light weight. Its high sensitivity to water and damp air, however, allows it to be used only with molten salts, solid state and aprotic solvent electrolytes. This is the reason why the fast ionic conductors for lithium, as electrolyte and electrode materials, become the central interest in this fast developing field.

II. Fast Ionic Conduction:

1. Simple Hopping Model:

The theoretical expression for diffusion coefficient D of ramdomly diffusing species is

$$D = \alpha\ d^2\ \nu \qquad [1]$$

where α is the geometric factor, d is the jump distance and ν is the average jump frequency. The last term can be expressed as

$$\nu = \beta\ \nu_o\ \exp\ (-\Delta G_m/RT) \qquad [2]$$

where β is the fraction of the species that is free to move, ν_o the attempt frequency and ΔG_m is the free energy of migration. When the average jump frequency in equation [1] is substituted by equation [2] and the free energy term is expressed in its enthalpy (ΔH_m) and entropy (ΔS_m) constituents, one can have

$$D = \alpha\ d^2\ \beta\ \nu_o \exp\ (\Delta S_m/R) \exp\ (-\Delta H_m/RT) \qquad [3]$$

When the transport occurs via defects , the value of β is obviously the defect concentration in the vicinity of the diffusing species. In high purity ionic compounds, the defect concentration is low and determined by the free energy change forthe formation of the intrinsic defect pair (Schottky or Frenkel pair),

$$\beta = \exp\ (-\Delta G_f/RT) \qquad [4]$$

The slope of a plot of ln D vs T^{-1} gives $-(\Delta H_m + \Delta H_f)/R$. In solids with a large concentration of defects,the β value will be temperature independent. When this is the case, the slope of the ln D vs T^{-1} plot becomes $-\Delta H_m/R$.

By the Nernst-Einstein relationship, the diffusion coefficient can be related to the conductivity (σ)

$$\sigma = DC\ z^2F^2/RT \qquad [5]$$

where C is the concentration of mobile species, F is the Faraday constant and R is the universal gas constant. Equation [5] can then be substituted by equation [3],

$$\sigma = C\ \beta\ d^2\ \nu_o\ \alpha\ (z^2F^2/RT) \exp\ (\Delta S_m/R) \exp\ (-\Delta H_m/RT) \qquad [6]$$

Comparing equation [6] with the Arrhenius type equation:

$$\sigma = (\sigma_o/T) \exp(-E_a/RT), \qquad [7]$$

the prefactor σ_o can be expressed as

$$\sigma_o = c \beta d^2 \nu_o \alpha (z^2F^2/R) \exp(\Delta S_m/R) \qquad [8]$$

For fast ionic conduction, a low activation energy E_a is a necessary condition. As discussed above, the value of E_a will be small if a large concentration of available sites is present in the lattice. In addition to this, low activation energy for migration is also important. This can be achieved when the 'bottleneck' of the diffusion passage is wide enough to minimise the constraint on the lattice while the ions are squeezing through. This decrease of the energy barrier, which the ions have to surmount before diffusion, also happens when the ions are stable at the transition state. On the other hand, a large concentration of mobile ions are required to provide high conductivity. This condition is never met if the ions are residing in a deep potential well. This perhaps explains why the prefactor of fast ionic conductors is orders of magnitude lower than normal ionic conductors.

2. Factors Responsible for Fast Cu(I) and Ag(I) Ionic Conductors

Among the long list of fast ionic conductors, the Cu(I) and Ag(I) conductors form the most popular group. Indeed, the best solid ionic conductor known to date is $RbAg_4I_5$ with an Ag ionic conductivity 0.12 $(ohm.cm)^{-1}$ at 20°C and an activation energy of 0.07 eV (1). Armstrong et al. (2) postulated the conditions for fast ionic conduction in simple compounds as:

(a) a large number of vacant crystallographic sites available for the mobile ions,

(b) these vacant sites should be energetically nearly equivalent to the sites being occupied by the mobile ions, and

(c) a low activation energy of motion.

Considering the cation-cation and cation-anion interactions in simple cubic systems, these authors found these conditions are most readily realised when the cations are monovalent and stable in tetrahedral and trigonal coordination.

Ag(I) and Cu(I) are monovalent cations with d^{10} election configuration. A remarkable characteristic of these two ions is their ability to form compounds with low coordination number. This property greatly stabilises the structural configuration at the transition state which is often trigonal in the simple cubic systems. This ability also appears to be linked to their tendency to polarise other ions. The ineffectively shielded nuclear charge attracts electrons and the covalent bonds thus formed, too, stabilise the intermediate position. This enhancement of the stability of the intermediate position is clearly more favourable if the anion is more polarisable. With all these unique properties, it is understandable to find such an abundance of Cu(I) and Ag(I) conductors.

Another class of Cu(I) and Ag(I) conductors is the addition compounds of their halide salts with bulky alkali halides (MX) or nitrogenous organic base halides (QX). The conductivity is usually improved by orders of magnitude. The actual effect of the addition on the conductivity properties is not fully understood because very little structural information is available. In a recent paper (3), Raleigh proposed that the addition of a small amount of the large cation forces the structure into a greater degree of face-sharing of the halide coordination polyhedra than in the single salt. In AgI, all iodine atoms are tetrahedrally bonded with silver atoms occupying every other tetrahedral site. The transport occurs when a silver atom moves through the common face of two iodine tetrahedra. When MI or QI is added, the octahedrally coordinated minority cation requires more anion than the single salt can supply. The structure is therefore altered to increase the face-sharing of the iodide tetrahedra. The transport of silver ions is hence improved as more 3-dimensional interconnection of the passage is available. The introduction of MI or QI octahedra is also believed to stabilise the lattice which should be distorted if only tetrahedra are present.

Among the long list of this class of compounds, the addition

compound consisting of cuprous bromide and 1,4-dimethyl-1,4-diaza-bicyclo (2,2,2) octane dibromide is selected as part of the present investigation. This compound, first reported by Takahashi et al (4), has an ionic conductivity of 3×10^{-2} $(ohm.cm)^{-1}$ at 20°C, the highest copper conductivity ever known. It is difficult at this stage to point out whether this high conductivity is also due to the increase of face-sharing of the anion polyhedra. This compound, nevertheless, is suitable to be used as solid electrolyte in the electrochemical study of fast copper ionic conductors.

3. Lattice Engineering, An Approach to Synthesis of New Solid Electrolytes for Alkali Ions

Apart from seaching the literature to look for compounds with possible fast ionic conduction, it is more fruitful to design a lattice which is optimum for ionic transport. This is the approach adopted by Goodenough et al. (5) and Hong (6) to synthesise new compounds exhibiting high alkali ion conductivity. Typical examples are $Na_3Zr_2Si_2PO_{12}$ with sodium ionic conductivity equal to $0.2\ (ohm.cm)^{-1}$ at 300°C which is comparable with the best β"-alumina, and $K_{1.9}Mg_{0.95}Si_{1.05}O_4$ with a resistivity at 300°C equal to 28 ohm.cm, the lowest reported for potassium ion conductors.

The crystallographic principles laid down by Hong (6) include primarily a rigid, 3-dimensional skeleton having an interstitial space interconnected in at least one dimension and partially occupied by alkali ions. The network is formed by the linkage of either MO_4 tetrahedra, MO_6 octahedra, or both. The availability of nearly equivalent crystallographic sites is provided by the partial occupancy of the interstices which, in turn, enhances the β term in equation [7]. To increase conductivity, the jump distance (d) should not be too long and more important, the activation energy (ΔH_m) has to be low. This can be achieved by increasing the diameter of the bottleneck of the passage. The accepted criterion is twice the sum of the radius of the diffusing ion and the anion on the framework. This value is 4.0 Å for lithium ions to diffuse through an oxide lattice.

Unlike Cu(I) and Ag(I) ions, alkali ions do not have a polarisable electron shell. The chance of a favourable intermediate

position for the ions can be improved by increasing the ionicity of the bonding so that the ions are less site specific. For this, the electron cloud around the anion on the framework has to be pulled towards the skeleton. This polarisation can occur in two ways: (a) the anions can bond with more than 2 cations of the framework, and (b) the anions can form strongly covalent bonds within the framework. One point which has to be stressed is that when the anion bonds to four or more network cations, the coordination requirement brings the anions together and a close-packed sub-lattice is formed. This greatly reduces the size of the passage and retards the diffusion. If each anion is linked to three network cations, the transport is most likely to be one- or two-dimensional. β-alumina is a very good example, in which, the oxygen atoms at the boundary of the diffusion layer are bonded to 3 aluminium atoms in the spinel block. The ensure the weakest interaction between the framework and the diffusing alkali ions as well as the rigidity of the skeleton, strong σ and π bonds within the framework are needed. It is therefore advisable to select the strongly covalent complexes such as SiO_4^{4-}, PO_4^{3-} or SO_4^{2-} and transition metal cations having an empty d orbital as building blocks.

All the effort, so far, has concentrated on oxides. However the oxygen ion is known to form strong covalent bonds with lithium. This is the reason why Hong (7), when constructing the lattice for lithium transport, had to increase the bonds to the oxygen ions to four to avoid the possible interaction between the framework and the mobile ions. In order to achieve this, the average valency of cations within the skeleton should be less than two if only tetrahedra are present. Such a condition can be satisfied by incorporating alkali ions into the network. As mentioned, the increased anion coordination reduces the size of the bottleneck. Indeed, the size of the parallelogram-like bottleneck of $Li_{14}Zn(GeO_4)_4$ is 3.54 x 5.22 Å and the conduction is 2-dimensional. The conductivity at 300°C of this so-called LISICON was measured recently (8) to be 2.8×10^{-3} $(ohm.cm)^{-1}$ which indicates the reported value is an order of magnitude too high.

The scientific merit of lattice engineering is demonstrated by the achievements on sodium and potassium, and perhaps to a lesser extent, on lithium ionic conductors. The crystallographic factors

used in this approach would also serve as useful guideline in interpreting the conductivity results. Since its emergence, a lot of interest along this line has been stimulated and it should become a more important branch of the field when the present known compounds are explored.

III. Solid Solution Electrodes (SSE):

In solid electrolyte materials, the electronic conductivity is suppressed. If a material possesses a reasonable electronic conductivity, it can be used as an electrode material. The possibility of introducing ionic conductivity in electrode materials also draws a lot of attention to this development.

Traditionally, electrochemical discharge is interpreted in terms of a disproportionation reaction between the reactants. Taking MoO_3 as example, the reaction:

$$2\ Li + MoO_3 \rightarrow Li_2O + MoO_2 \qquad \Delta G$$

is believed to take place. However, as pointed out by Whittingham (9), the free energy change (ΔG) of the reaction does not correspond to the recorded voltage value. It is, in fact, the formation of the ternary phase Li_xMoO_3 which gives rise to the observed behaviour. These so-called intercalated compounds have been found extremely promising as cathode materials in secondary batteries involving alkali metals. The best-known compound is titanium disulphide which has been extensively studied and is already in commercial production.

Titanium disulphide TiS_2 is a layer compound with (S-Ti-S) 'sandwiches' held together through the van der Waal's interaction between the layers. Lithium can be readily and reversibly inserted into and removed from the vacant gap. During these processes, there is no cleavage nor formation of any strong bonds. The lithium ion is residing in a shallow potential well, that enables the processes to occur reversibly and rapidly. Indeed, a fast lithium diffusion is recorded with $\tilde{D}$ reaching 2×10^{-8} cm^2/s at r.t. (10), which makes possible a satisfactory current density during the operation.

From the structural point of view, for compounds to behave in this manner, they have to be homogeneous over a large range of non-stoichiometry. For a material MY, this means that the x value in

Li_xMY has to be as large as possible without the separation of a new phase. The ternary phase should then be treated as a solid solution consisting of the dissolved lithium and the host MY lattice. To accommodate the dissolved alkali ions, space in the lattice is obviously needed. Materials with built-in vacancies will be ideal for this purpose. The open structure also satisfies the requirement for fast ionic conduction. Suitable alteration to introduce electronic conductivity to the solid electrolyte materials would be a possible way to search for new electrode materials of this sort.

Experimental evidences (11) have been acquired to support the view that when lithium dissolves into TiS_2, electrons are donated to the electron band of the host lattice and lithium is in the ionic form at its crystallographic sites. The energy of the dissolved species therefore comprises the ionic and electronic terms. Splitting the chemical activity of species A in the solid state into its two constituents

$$a_A = a_{A^+}^{cry} + a_e$$

where a_A, $a_{A^+}^{cry}$ and a_e are chemical activities of A particles in the solid state, A^+ ions in their crystallographic sites and electrons respectively. The working specification of a constant voltage of a battery requires the chemical activity of A in the solid state to be constant. The constancy of the term $a_{A^+}^{cry}$ can be ensured by the availability of equivalent crystallographic sites. The same argument also applies to the electronic term, for which a vacant high density electron state is required. The Fermi energy (the term determines the electrochemical activity of electrons) in this situation will only drift slightly as the concentration of A increases. Although the band structure of TiS_2 is not available in the literature, it has been proposed that there is an energy gap separating a conduction band for 6 electrons from a valence band (12). The availability of electron states therefore maintains a relatively unchanged Fermi energy for a wide range of A dissolution. It must be emphasised that the band structure of most compounds is sensitive to the change of the crystal structure. Incorporation of A species, however minute the disturbance on the crystal structure it may cause, is bound to alter the band structure to a certain extent. It is also because of this that a rigid framework compound is needed before the

electronic contribution to the a_A value can be studied.

Steele (13,14) has introduced the term 'Solid Solution Electrode' (SSE) to describe materials with this kind of behaviour. The desired properties for a SSE material can be summarised as:

(a) Good electronic conductor and the availability of a vacant high density electronic state
(b) Homogeneity over large range of nonstoichiometry
(c) Rapid chemical diffusion of electroactive species in the host lattice
(d) A high solubility of the electroactive species in the host
(e) Rapid transfer of electroactive species across the SSE/electrolyte interface
(f) Stable in relevant electrolyte phases
(g) Cheap and easily fabricated

IV. Three-dimensional SSE Materials:

The solid ionic conductors can be classified in terms of crystal structures:

(a) One-dimensional conductors with uni-directional tunnels in the lattice. The best known example is Na_xWO_3 in which the chemical diffusion coefficient $\tilde{D}$ of sodium was determined to be 10^{-15} cm^2/s at 300°C when $x = 0.6$ (15)
(b) Two-dimensional conductors which are represented by transition metal dichalcogenides. The characteristic of this type of layer compound is the vacant plane which is readily available for diffusing species. A typical $\tilde{D}$ value of lithium in TiS_2 is 2×10^{-8} cm^2/s at r.t. (10).
(c) Three-dimensional conductors, in which passages for diffusing species are interconnected throughout the three-dimensional framework of the host lattice. Electrolytes belonging to this classification have been synthesised by making use of the lattice engineering principles (5,6).

The chemical diffusion coefficients of alkali metals in materials in category (a) are generally too poor to be worth considering as cathode material in batteries. On the other hand, two-dimensional conductors, though they have a better ionic

transport, suffer from lattice expansion when guest ions intercalate between the layers. In TiS_2, the c axis dilates by 10% when it is fully intercalated. This property restricts the use of layer compounds in solid-state batteries, in which the solid-state interfaces will be disintegrated by the lattice expansion. The three-dimensional conductors are at the present time most attractive of all. They satisfy the major laid-down criteria and will be a very important element to justify the application of solid-state battery systems.

The object of the present investigation is to find new SSE materials, preferably three-dimensional, suitable for use in a secondary lithium battery. Although the desired properties of these materials are listed, it is still difficult to decide which type of lattice is likely to allow rapid ionic transport. In view of the abundance of fast copper ionic conductors, the search for suitable candidates is also extended to this group of compounds. Because of the low potential and relatively low stability, the practical interest of copper conductors is low too. Nevertheless, for its earier handling, the system is still very interesting from the academic point of view. A basic understanding of one system will be helpful to the studies of another. Moreover, if a three-dimensional conductor could be found, there should be a reasonable chance to substitute the mobile ion with other alkali ions. This strategy is adopted in this project and the investigations will be reported and summarised.

CHAPTER 2

THE SCREENING TECHNIQUES EMPLOYING n-BUTYL-LITHIUM (n-BuLi) AGENT

I. Introduction:

In the search for promising SSE materials, it would be very useful to have a reagent which reacts with materials analogous to the half-cell reaction under consideration, viz. the incorporation of lithium into the electrode materials. The rate of this reaction will be related to the associated chemical diffusion in the solid matrix. Employing this reagent in conjunction with a suitable analytical technique, the amount of lithium and the rate of its dissolution into the material can be estimated. The applicability of the material as a SSE in the lithium cell can be assessed by its performance in this screening test.

n-Butyllithium has been found to be an effective reagent for this screening purpose. It was first mentioned by Armand (16) in oonnection with work on chromium oxide/graphite. It was later used extensively and successfully on the studies of transition metal chalcogenides (17-22). The use of n-BuLi as a screening agent is preferable to other agents because it is a convenient reagent and the reaction is free from complicating side reactions. Other agents, like lithium metal solutions in liquid ammonia or naphthalene in tetrahydrofuran (23) can also introduce lithium into the materials under study. However, the extreme reactivites of lithium metal makes the reaction difficult to perform and quite often co-insertion of polar solvents into the host lattice takes place.

Using n-BuLi solution in hydrocarbon, the activity of lithium is reduced to a value corresponding to 1.0-1.4 V against lithium metal (24). The lower lithium activity allows somewhat less restricted experimental environments and probably limits the possibilities of other side reactions, for instance, the transition-metal-catalyzed formation of $LiNH_2$ from lithium in ammonia. The problem of co-intercalation of large solvent molecules leading to

the degradation of the crystalline form of the hosts can also be avoided. Since the solvent and reaction products are both hydrocarbons which do not intercalate into the materials being tested, the change of the crystalline form of the hosts upon the introduction of lithium can be studied. This is important in understanding the behaviour of SSE materials, and particularly for their use in solid state cells in which change of lattice parameters is a severe restriction.

II. Lithiation by n-Butyllithium:

The intercalation of lithium into the materials (MY) by n-BuLi is usually represented as:

$$x(n - C_4H_9Li) + MY \rightarrow Li_xMY + \frac{x}{2}\ (n - C_8H_{18})$$

The values of x depend on the material.

n-BuLi exists in hexane solution as a hexamer, its chemistry is conveniently thought of as arising from $Li^+(n\text{-}Bu)^-$. It is reasonable to envisage the reaction as an electron transfer from Bu^- and lithium ion intercalation to balance the charge. A further study has led Dines (17) to propose a more detailed mechanism: (a) generation of active species in the solution, which may be a tetramer, dimer or monomer; (b) surface absorption on the materials and activation of the adsorbant; (c) electron transfer from the lithium-carbon bond to the solids; (d) diffusion of the alkali into the lattice and the dimerisation and diffusion of the alkane into the solution. The reaction rate was found to be dependent on the concentrations of both reactants indicating that (a) and (b) are the rate determining steps.

A problem of using n-BuLi as a lithiation agent is the uncertainty of the effect of lithium n-butoxide (n-BuOLi). The presence of lithium n-butoxide is inevitable because it is impossible to exclude all the oxygen gas which reacts with n-BuLi forming n-BuOLi. There is no available information about the

reaction between n-BuOLi and materials like TiS_2. The much decreased lithium activity in butoxide is likely to prevent any reaction occurring between n-BuOLi and the material being investigated.

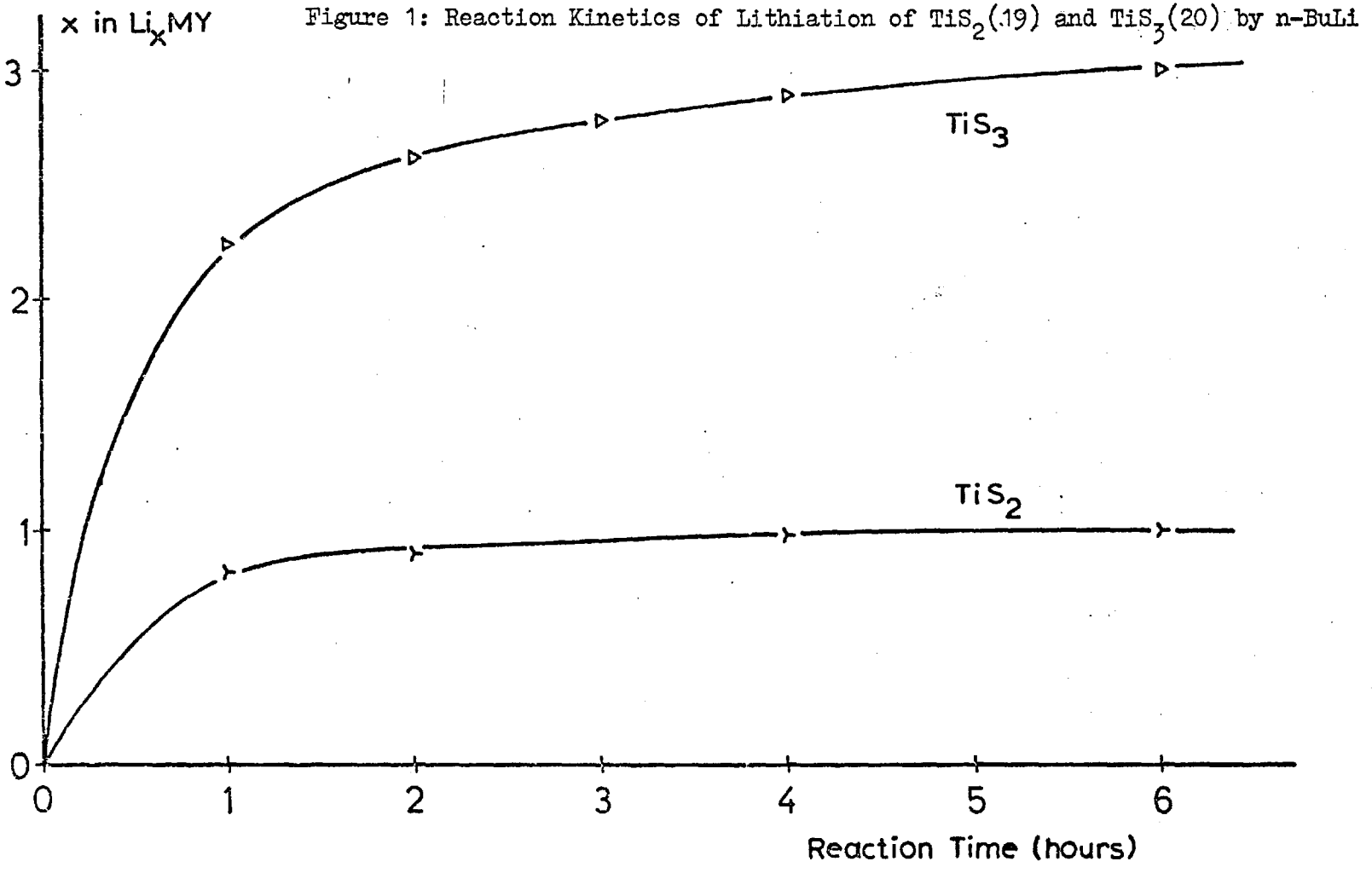
It should be pointed out that the dimerisation of the two alkyl radicals in step (d) is not the only way to terminate the reaction. A disproportionation reaction can also occur to give butane and butene as products. This also explains why it is unreliable to analyse the octane quantity formed as an indicator of the chemical stoichiometry of lithiation.

III. Kinetic Studies on Lithiation by n-Butyllithium

As outlined in the criteria of a SSE material, it is not only the solubility of lithium in the materials but also the fast solid state diffusion of lithium that is of concern. Therefore, it would be desirable if the lithiation rate can be monitored by suitable methods and the associated diffusion rate of lithium can be estimated. The screening ability of the agent will then be considerably extended.

The most common method of following the lithiation rate is tracing the consumption of n-BuLi by acid-base titration. This type of experiment has been performed on TiS_2 (19) and TiS_3 (20). As shown in fig. 1, rapid incorporation is evident in both cases. The maximum solubility in TiS_2 is one lithium atom per mole of TiS_2, while in TiS_3, the value reaches 3 lithium atoms per mole of TiS_3. One difficulty of this analysis is the frequent sampling of the n-BuLi aliquots which is tedious and inaccurate without a good dry box. Apart from this, lithium butoxide and lithium hydroxide are always found in n-BuLi solution. Because of these basic species, the acid-base titration gives high experimental error. They can be eliminated by double titration (25) in which 1,2-dibromoethane is used to react with n-BuLi while other basic substances remain unreacted and are subsequently analysed by acid-base titration. It is interesting to note that V_2O_5 was used as an analytical reagent to determine the concentration of n-BuLi (26).

Figure 1: Reaction Kinetics of Lithiation of TiS_2(19) and TiS_3(20) by n-BuLi



n-BuLi is oxidised by V_2O_5 and the amount of the reduced vanadium is back-titrated with standard Ce(IV) solution. This quantity is taken to be equivalent to the reacted n-BuLi and hence the concentration of n-BuLi is determined.

It is attempted to develop an in-situ spectroscopic technique to monitor the reaction of n-BuLi with SSE material. Such a technique would avoid the necessity of repeated sampling of the reagents and hence limit the errors introduced during these processes. Examination of the literature indicates that nuclear magnetic resonance (NMR) and ultraviolet (UV) absorption methods are both suitable for this purpose (27). Using NMR, concentration of n-BuLi can be determined within 5% down to 0.1 M. A more important advantage of using this technique is the separation of the possible impurities. On NMR spectra, n-BuOLi and LiOH when present should appear at different chemical shift values. UV methods are equally accurate at concentrations down to 10^{-3}M. The authors found that at 285 nm Beer's law was obeyed and an absorptivity of 91 l/mole.cm was calculated. However, these measurements require reliable calibration of concentration, and NMR was used as a concurrent technique in the development. In the present investigation, development concentrates on the UV method because spectrophotometers are readily and widely available.

In addition to the analysis of the remaining n-BuLi reagent, direct measurements on the materials have also been devised to trace the reaction rate. The microscopic method (22) utilises the property of a clear n-BuLi solution, so that direct observation of the physical change on the sample appearance is possible. Chianelli observed under a microscope a front created at the edge of the TiS_2 crystal and it moved towards the centre as the lithiation proceeded. The front was formed due to the 10% lattice expansion of the intercalated phase. The time for this movement was 4-5 hours for an average crystal of about 50 μm. As figure 2 shows, temperature change of the solid specimen can be monitored as a measure of the rate of the process (24). As lithium intercalates into the host lattice, its activity also decreases. The enthalpy term of the corresponding free energy change is released as heat which causes the temperature to rise. The

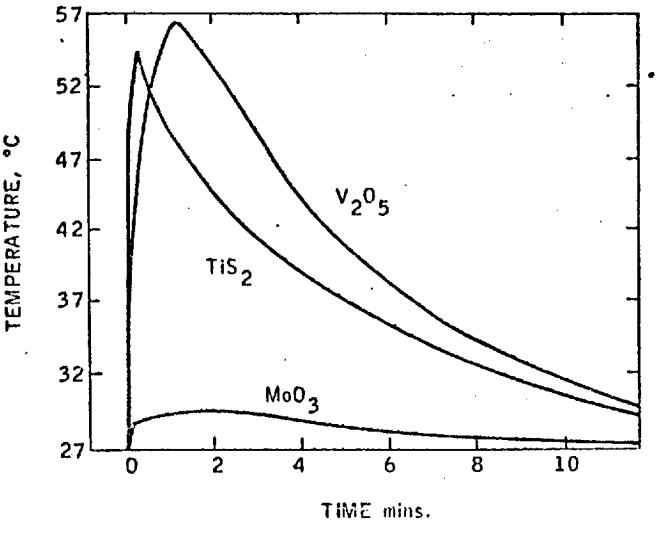


Figure 2: Effect of the Addition of Excess n-BuLi to Equivolent Slurries of V_2O_5, TiS_2 and MoO_3.(Ref.24)

quantity of heat released should also give a rough estimate of the free energy available from the system if the entropy contribution is known or limited.

Along a similar line, it is better to examine the change in the properties of the materials upon lithium intercalation. It has been demonstrated that when lithium atoms intercalate into TiS_2, electrons are donated to the host layers and change the conduction band structure (11). The conductivity of the specimen is then changed with lithium dissolution. This property should be useful for the investigations of compounds with lower electronic conductivity.

IV. Experimental:

The solid hosts used were TiS_2 single crystals, grown by iodine vapour transport of TiS_2 powder (10); V_2O_5, single crystals pulled from the melt at 700°C supplied by the Crystal Growth Laboratory, Imperial College; VO_2, purchased from Alfa Products. All solid phases were dried at over 100°C and under vacuum before use. n-BuLi solution in n-hexane of concentration 2.4 M was obtained from Alfa Products. n-Hexane and n-octane, bought from BDH Chemicals, were purified by distillation and stored with molecular sieves. The standardisations of hydrochloric acid and sodium hydroxide (both AnalaR) solutions were calibrated against AnalaR potassium hydrogen phthalate which was dried at ~100°C before use.

Since n-BuLi is sensitive to oxygen and moisture, all the reactions were carried out in a Gallenkamp manipulation glove box filled with dried Ar gas. To determined the concentration of the n-BuLi solution, 2 ml of stock solution was put into a conical flask. Absolute alcohol was added drop-wise until the violent reaction ceased. The flask was then removed from the dry box. Water and a known amount of standardized HCl were added to the flask. The solution was then heated to evaporate the organic phase. A few drops of phenolphthalein were added as indicator and the solution was titrated with NaOH solution to determine the

excess amount of HCl. In the double titration, 1,2-dibromoethane was added drop-wise to n-BuLi solution. The solution was swirled gently and allowed to stand for a few minutes. After the violent reaction stopped, absolute alcohol was added and the procedures described above were followed.

When lithiation of the solid was studied, excess n-BuLi solution was brought into contact with the weighed sample. After several days, the solid phase was separated from the liquid phase by filtration through a sintered glass funnel. The solid sample was washed with n-hexane and dried for further studies. The combined filtrate was analysed by acid-base titration for remaining n-BuLi. The up-take of lithium by the host was inferred from the difference between initial and residual reagent. The double titration was not used in the residual analysis because of insufficient volume of reagent. The solids separated after the reaction were examined with a Phillips x-ray diffractometer using CuKα radiation. Special care was taken to prevent the interference of moisture by covering the sample with a polythene film under inert atmosphere.

The kinetic study of the lithiation of the substance was done in a series of reaction vessels containing the same volume of n-BuLi solution and a similar amount of solid sample. At certain time intervals, one vessel was analysed by acid-base titration to determine the reacted n-BuLi.

The development of an UV spectrophotometric technique was carried out at room temperature with a Uvispek Photoelectric spectrophotometer. The absorption of the solution was studied in a 10 mm quartz photocell with a teflon stopper. Vacuum grease was used around the stopper to make the system gas-tight. The wavelength of the radiation was calibrated by a Holium filter to less than 0.5 nm deviation. A series of n-octane solutions in n-hexane was prepared and examined over the range of wavelengths from 190 to 300 nm. No appreciable absorption of radiation energy was observed up to 1 M octane solution within the range of 205 to 208 nm. n-BuLi solutions were thus analysed in this range and the concentrations were calibrated by the double titration method.

In the study of V_2O_5, a single crystal, with 2 tungsten wires attached to it, was placed in a n-BuLi solution. The

resistance of the sample was monitored as a function of time with a Solartron 7040 voltmeter. Due to the irregular shape of the single crystal, it is not possible to derive the conductivity of the specimen from the experimental data.

In the electrochemical study of VO_2, a pellet of VO_2 (as purchased) was cold-pressed at a pressure of 4.4×10^7 Nm^{-2} and then sintered at 500°C under vacuum (~ 35 micron Hg) overnight. The electrochemical cell used was a standard 3-electrode assembly. Lumps of lithium metal (Koch-Light, 99.8%) were cut and trimmed off the oxidised surface. The lithium was attached to a tungsten or molybdenum wire and incorporated into the cell immediately. The electrolyte was lithium perchlorate (Alfa) dissolved in propylene carbonate (BDH). Propylene carbonate (PC) was first dried by P_2O_5 and then fractionally distilled under reduced pressure with nitrogen gas bubbling through. The salt was dried under vacuum at 300°C overnight. The dried salt was then transferred to the dry box and dissolved in distilled PC to a concentration of about 1 M and the solution was stored with dried molecular sieves (BDH, type 3A).

V. Results and Discussion:

1. Vanadium Pentoxide:

It is known that vanadium pentoxide is a layer-like compound. Because the open structure enables ready insertion of other species, it has been extensively studied as a cathode depolariser in non-aqueous lithium cells. Whittingham demonstrated that the open-circuit voltage (O.C.V.) on the Li/V_2O_5 cell is almost constant for one lithium intercalation per mole of V_2O_5 at 3.4 V and then falls abruptly to 2.5 V for a second lithium (28). This compound was chosen for the development of n-BuLi reaction for its established reaction with lithium.

The stoichiometry of the chemical reaction between n-BuLi and vanadium pentoxide single crystal was determined to be 3.1 after 8 days reaction. Another single crystal was monitored by resistance measurement (fig. 3) which showed the reaction was complete after

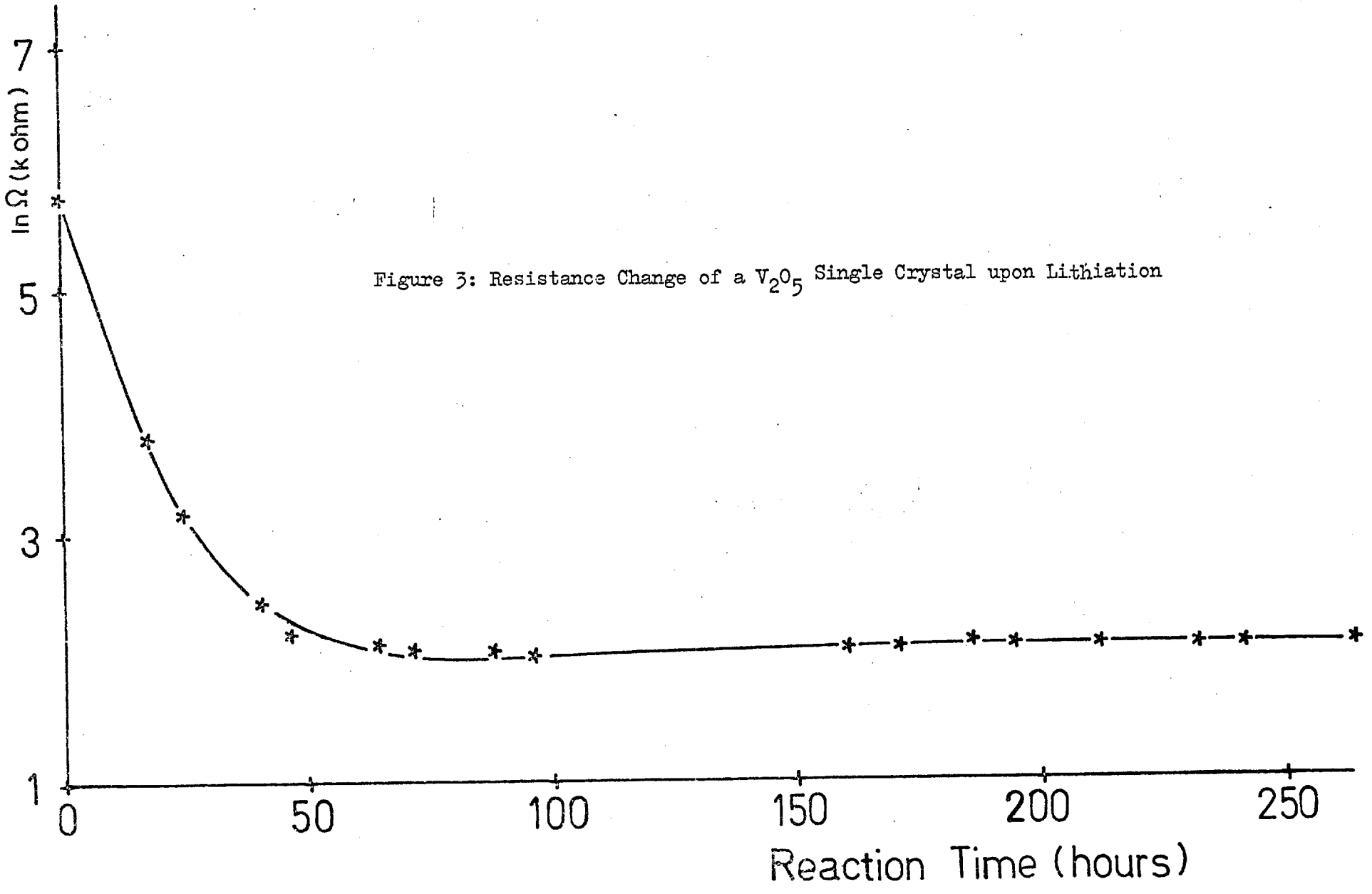


Figure 3: Resistance Change of a V_2O_5 Single Crystal upon Lithiation

50 hours. However a kinetic study of the similar reactions on V_2O_5 powder was less successful as variable values of x(in $Li_xV_2O_5$) between 4 and 4.5 were recorded for the reaction time from 0.5 hour to 72 hours. This indicates a rapid reaction which is almost instantaneous when the reactants are brought together and the reaction of the powder sample extends further than those of the single crystal. The same investigation performed at Exxon (24) showed 2 equivalent moles of n-BuLi reacted with V_2O_5 even when excess reagent was present. When a large excess of n-BuLi reagent is used (as in the present case where it is 8-16 times excess), reaction is likely to proceed beyond simple lithium insertion into the lattice, i.e. other side reactions would have happened. The extent of this interference is expected to be larger in powder samples than single crystals which have small surface area. These probably account for the high chemical stoichiometry of the reaction.

An attempt to study the kinetics of lithiation by x-ray diffraction of the reaction products was also carried out. However the result is not as informative as expected. Apart from the disappearance of 2 lines, the x-ray pattern is hardly changed for reaction time from 0.5 hour to 265 hours. This is further evidence of extremely fast reaction. As can be seen in fig. 4, the pattern is very simple and completely different from the Exxon result (9). There is no diffraction corresponding to the Li_2O phase which was originally suspected as the product of the possible side reaction. The product has not been indexed or identified as any known compound.

The kinetics of the reaction are very fast. Reaction starts within the first minute when reactants are brought together (fig. 2). The estimated reaction time is 20-25 minutes. This is probably the reason why no change has been measured by titration and x-ray methods. The recommended reaction time, however, is a few days which is required for proper chemical equilibrium. In the resistance experiment, a stable value is reached after 50 hours (fig. 3) indicating the long equilibrium time needed for a large sample in which the diffusion length is considerably longer than the powder analogue.

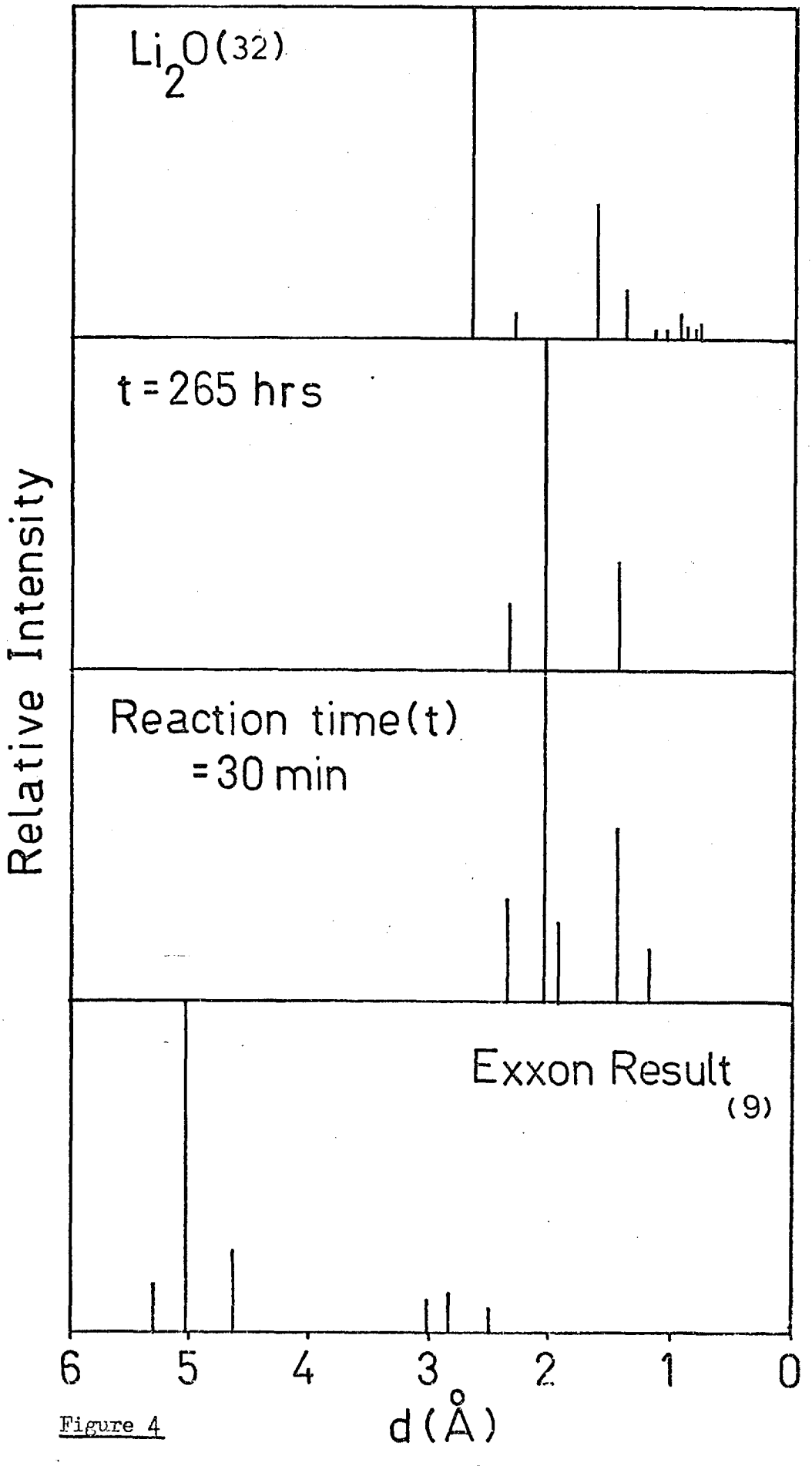

Li_2O(32)
t = 265 hrs
Reaction time(t)
= 30 min
Exxon Result
(9)
Relative Intensity
6
5
4
3
2
1
0
d(Å)

Figure 4

2. Vanadium Dioxide:

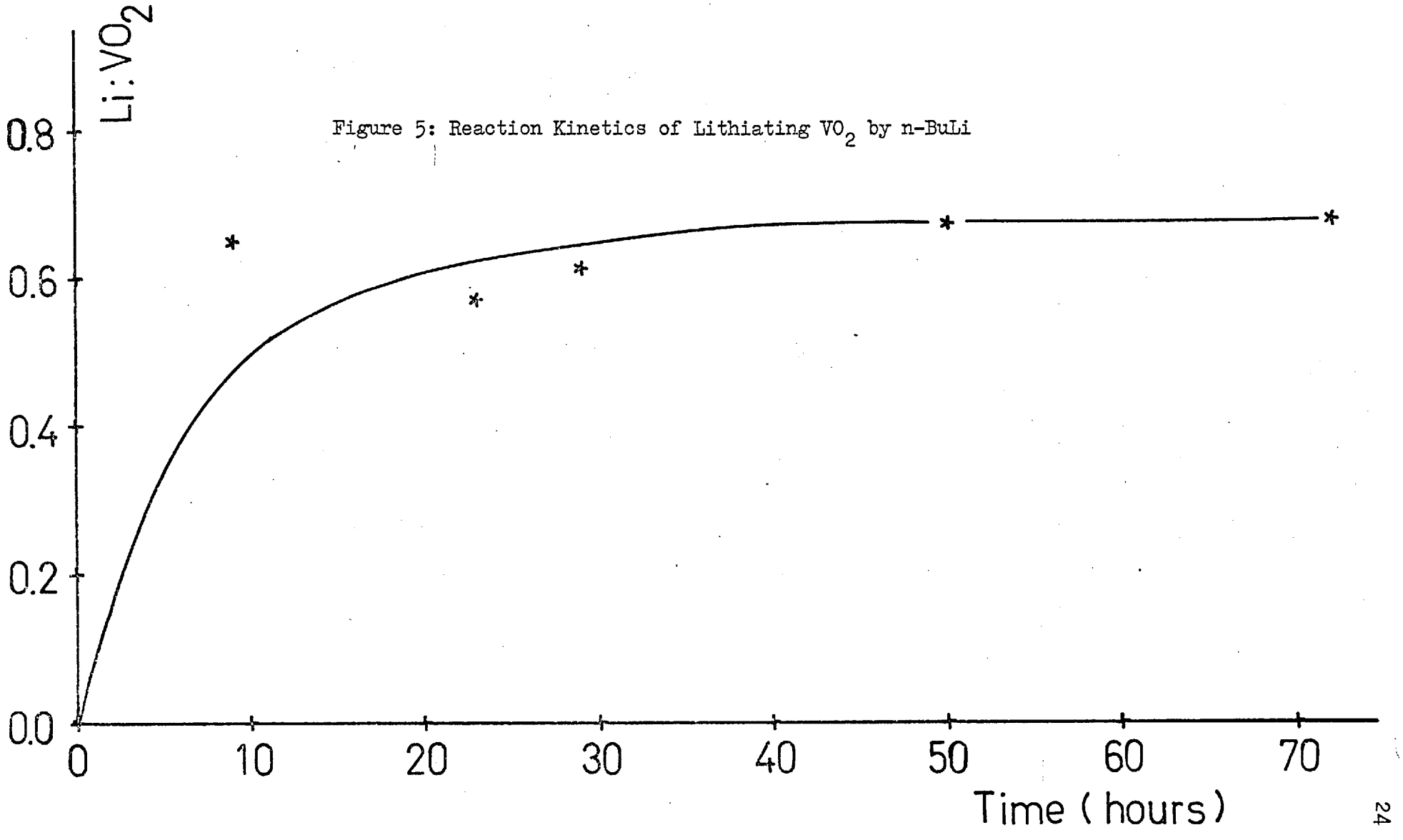
It is known that lithium ions diffuse rapidly in rutile, TiO_2 (29). Recent results also confirm that TiO_2 has a high lithium solubility (Li: TiO_2 = 0.6) and an exceptionally high lithium diffusion coefficient $\tilde{D} = 5.73 \times 10^{-6}$ cm^2/s at 80°C (24). Vanadium dioxide also adopts the same structure at temperatures above 70°C. The structure is distorted below the transition temperature due to vanadium-vanadium bonding. The similarity of these two compounds led us to evaluate VO_2 as a SSE material.

Each mole of vanadium dioxide can accept about 0.65 gm atom of lithium and this value was reached after 9 hours (fig. 5). These kinetic results were obtained by chemical analysis of the n-BuLi by titration. The solid samples after the kinetic run were examined by x-ray powder diffraction. As figure 6 shows, the reaction product consisted of Li_2O and new phase(s). The new phase(s) was/were not identified. No extra new phase was formed at the later stage of the reaction. The crystallinity of the sample decreased as the reaction proceeded. At the end of the run, some original peaks had disappeared and most of them were ill-defined. The peaks could not be indexed as $CaFe_2O_4$ lattice (30) to which the lithium vanadium bronze $Li_xV_2O_4$ was expected to be isostructural.

The kinetics of the lithiation reaction of VO_2 are not so fast as V_2O_5. The distorted structure, perhaps, is the major factor which impedes the motion of lithium in the solid phase. It will then be reasonable to expect the oxide in its rutile structure to have a faster reaction. However, it is practically difficult to use n-BuLi at 70°C. To stabilise the rutile polymorph at room temperature by doping with rutile forming compounds, $W_{0.052}V_{0.948}O_2$ (31) for instance, is a possible way to obtain the information.

When VO_2 is studied in an electrochemical cell, its behaviour (fig. 7) is not that expected on the basis of the screening results. Lithium is easily introduced into VO_2 up to 0.24 gm atom per mole, after this value, lithium intercalation is difficult and it starts to plate on the electrode. If the current

Figure 5: Reaction Kinetics of Lithiating VO_2 by n-BuLi



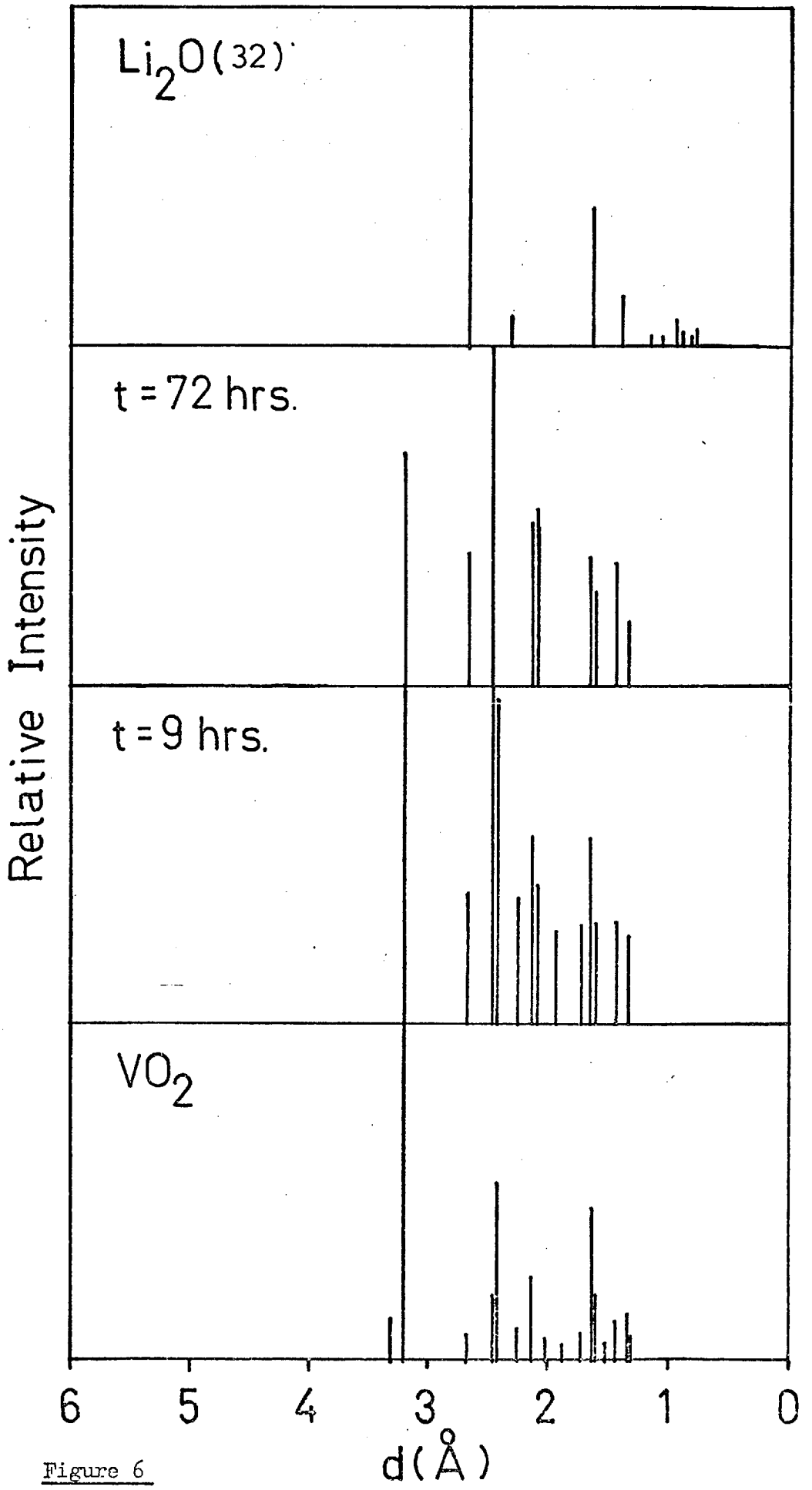


Figure 6

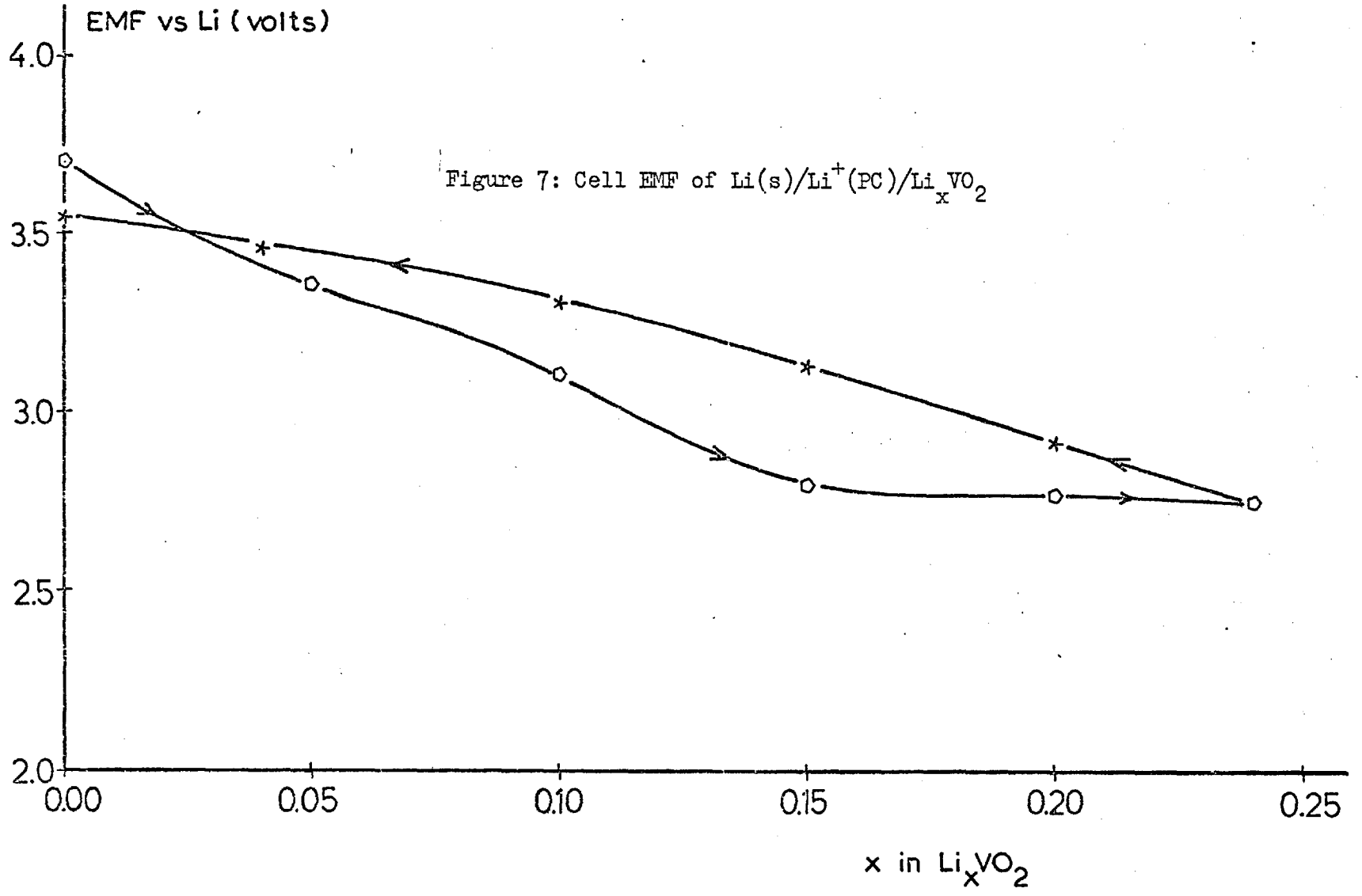


Figure 7: Cell EMF of $Li(s)/Li^+(PC)/Li_xVO_2$

is cut off at this stage, the deposited lithium dissolves into the solid indicating a slow diffusion process which impedes the dissolution. This finding is also consistent with that found in the screening test.

3. UV Spectrophotometry Analysis:

The wave length 285 nm is not used in this work because at this wavelength the absorbance by n-BuLi was found to be unstable. Moreover, the radiation at this wavelength apparently has a certain effect on the solutions as the absorbances at shorter wavelengths decrease after the same solutions have been irradiated at wavelengths from 282 to 286 nm. The absorbances of n-BuLi and n-BuOLi are found to be in linear relationship with concentration at 208 and 205 nm respectively (fig. 8 and 9). Both straight lines do not pass through the origin indicating a background absorption although the interference due to solvent has been eliminated by the choice of wavelengths. The parameters of Beer's law obtained in this work and by Urwin and Reed (27) are given in table 1. The discrepancy in the results is due to the different concentration ranges in which the absorbances are measured. The previous investigation was carried out in the range from 6×10^{-3} to 3.1×10^{-2} M, while in the present case the concentrations studied are much higher, ranging from 1.2 to 2.3 M.

The decomposition rate of n-BuLi solution due to the reaction with air/water vapour leaking into the photocell, was monitored (fig. 10) by this technique. An exponential decrease of absorbance at 208 nm with time is observed which suggests that n-BuLi concentration decreases when the photocell is left in air for a long period. The chemical (photochemical ?) reactions involved are not clear at the moment. It can be seen, though, that the contribution of the reaction between oxygen and n-BuLi is not great because the absorbance at 205 nm corresponding to the butoxide concentration does not show any significant correlation with the change of n-BuLi concentration.

The lithiation of titanium disulphide single crystal by

Figure 8: Optical Absorbances (A) of n-BuLi Solutions

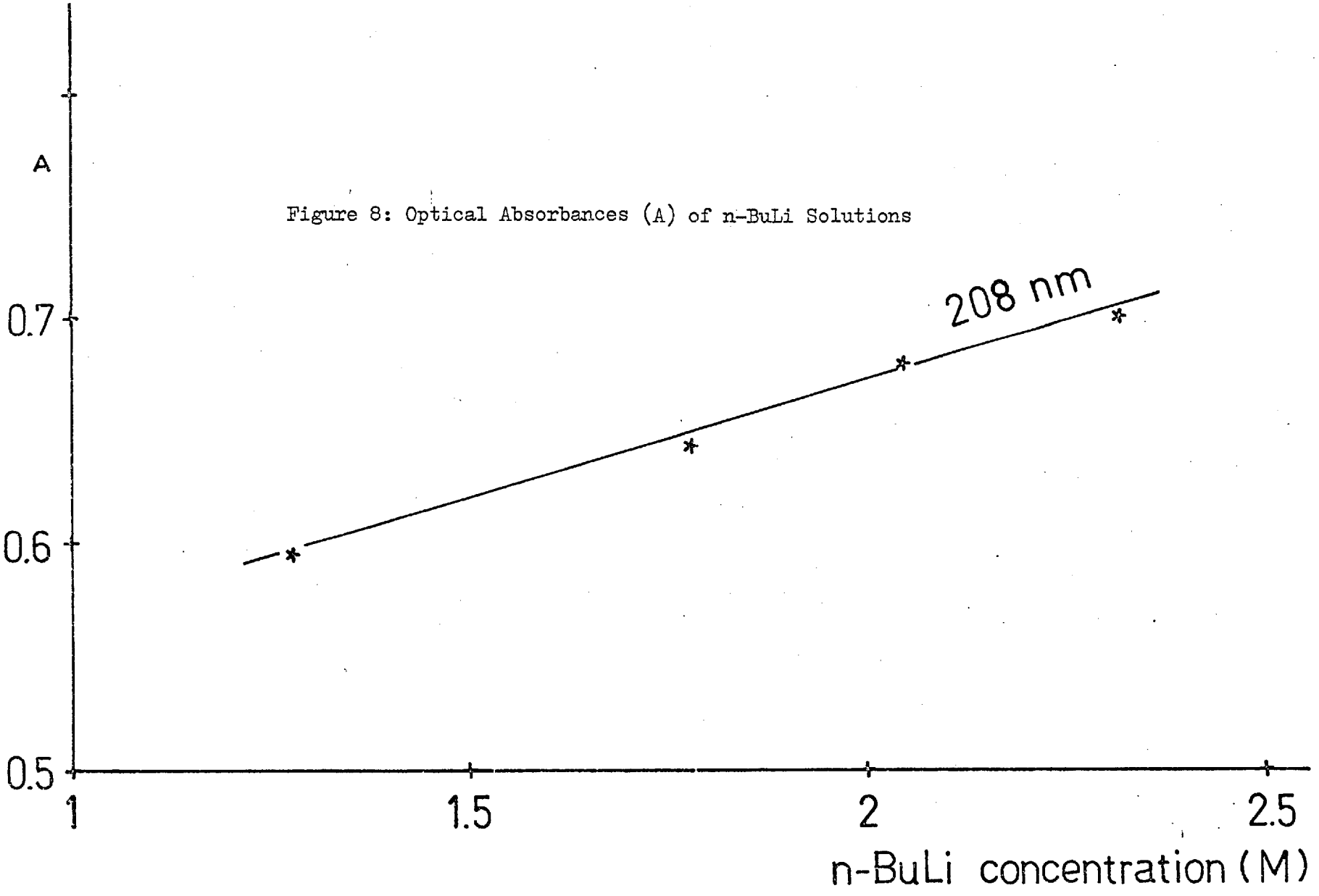


Figure 9: Optical Absorbances(A) of n-BuOLi Solutions

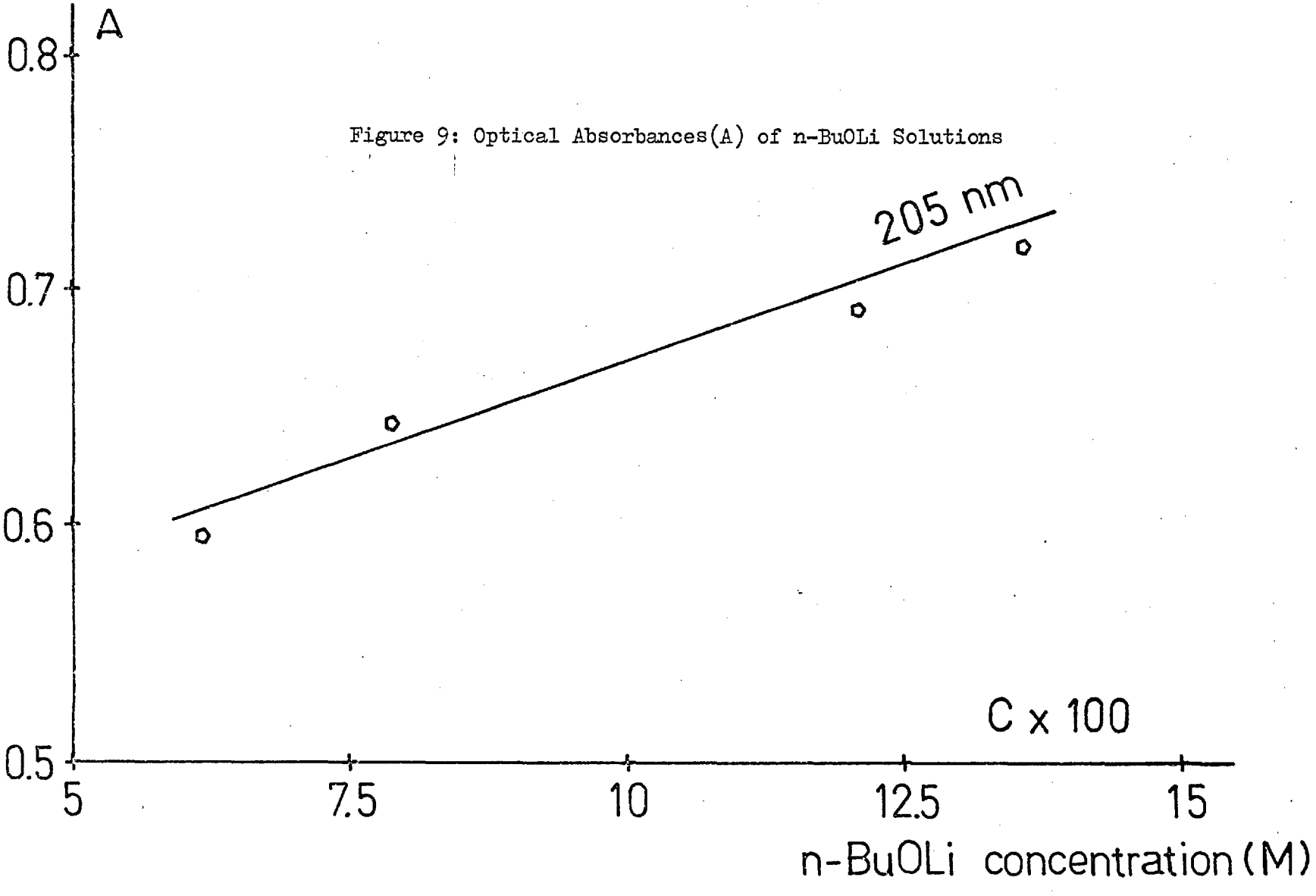


Table 1 : The Parameters of Beer's Law Obtained in UV Spectrophotometry Studies

Beer's Law : $A = A_0 + a\,b\,C$

where A: absorbance,

A_0: absorbance at zero concentration,

a: absorptivity,

b: the length of the photocell,

C: concentration of the absorbing species.

	This Work	Urwin & Reed(27)
λ (nm)	208	285
A_0	0.4622	---
a (l/mole.cm)	0.1035*	91
C Range (M)	1.2 - 2.3	6×10^{-3} - 3.1×10^{-2}

*obtained by least square method.

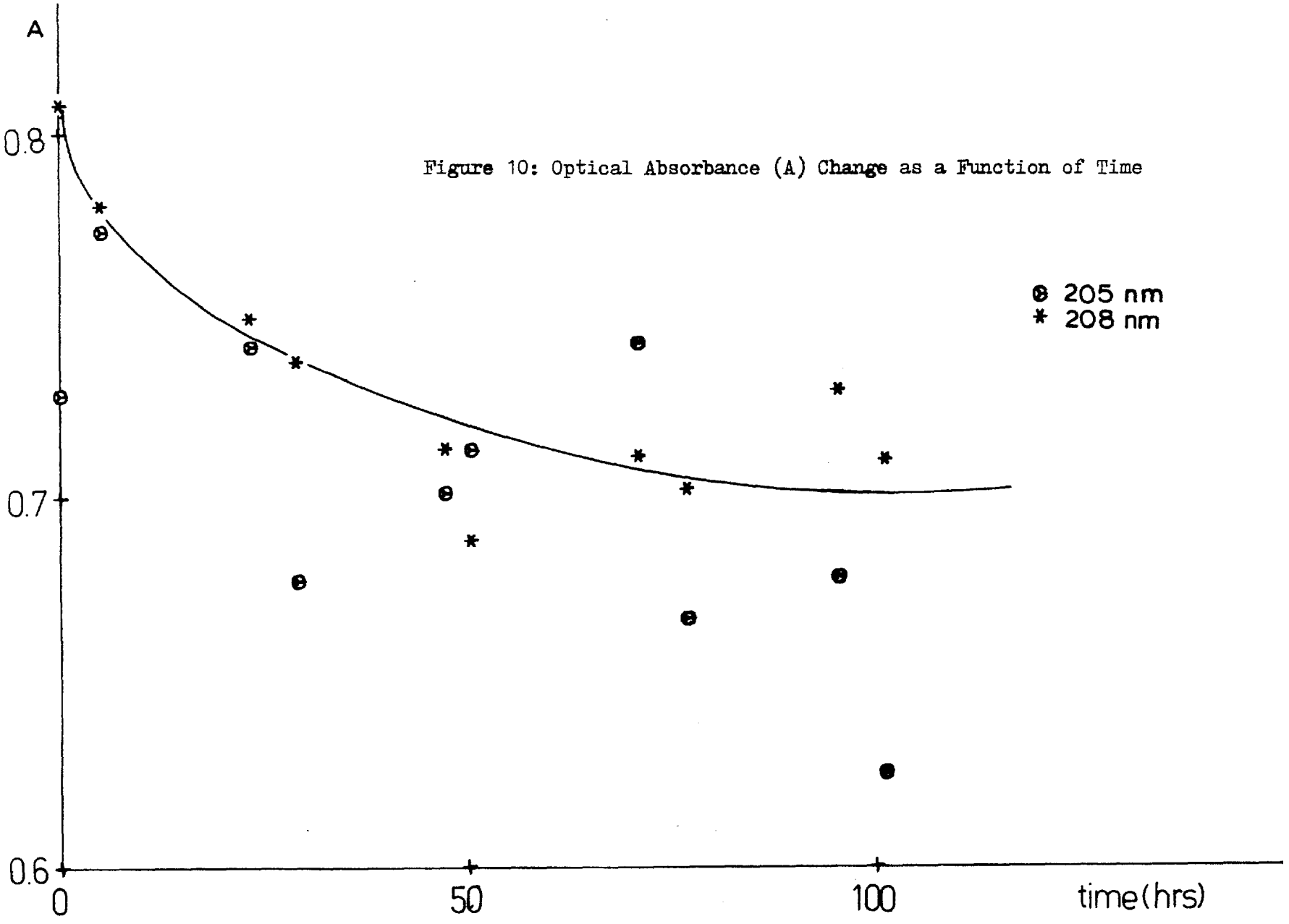


Figure 10: Optical Absorbance (A) Change as a Function of Time

n-BuLi was followed by this technique. The rapid incorporation of lithium is displayed as a corresponding decay of absorbance at 208 nm (fig. 11). Although the points are scattered, a clear drop in absorbance in the first 5 hours is an obvious indication that the lithiation proceeds at a rapid rate.

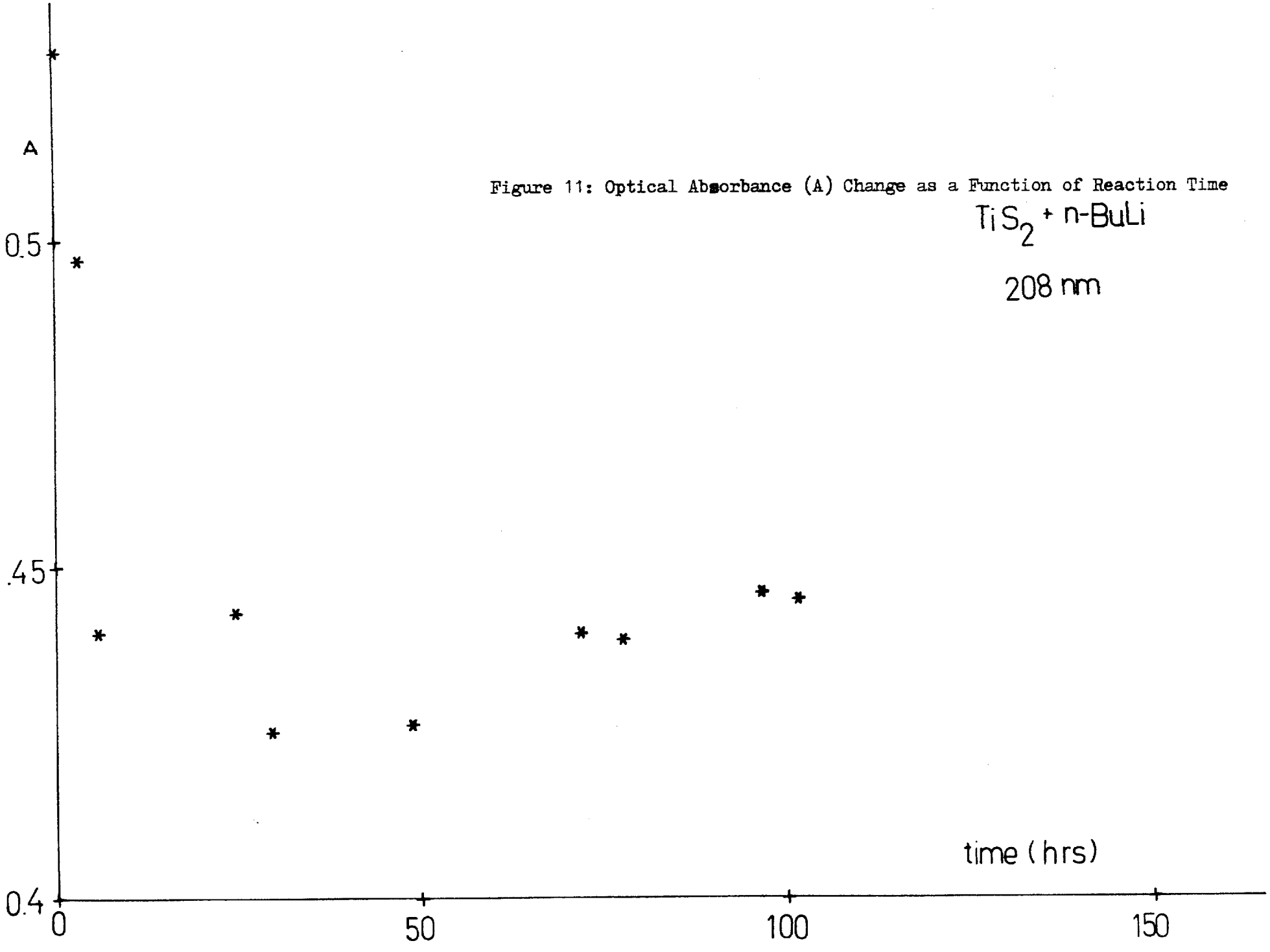
On the whole, the UV spectrophotometric technique is promising as a tracing method for n-BuLi reaction. Accurate quantitative measurements are still difficult to make. A better photocell design to minimise leakage of gaseous molecules into the measuring apparatus is undoubtably needed. It should also be emphasised that the precision of calibration of the n-BuLi concentration determines the overall accuracy of the measuring technique. In this work, double titration was used and its precision is believed worse than the in-situ NMR calibration used in a previous study (27). Unfortunately, such an instrument was not available to modify the analytical technique.

For further development, a wide range of concentrations ought to be re-examined for a wide spectrum of wavelengths. In conjunction with this, a reliable accurate calibration method must be used to give any significant meaning to the results.

VI. Conclusion and Suggestions for Further Work:

It has been proved that the n-BuLi reaction is a general one and the results are usually in good agreement with the available electrochemical data. However, the work described above has indicated that unless the experiment is carefully performed, the results are probably misleading. When the amount of Li dissolved in the material is high, its activity increases correspondingly and other reactions with the solid matrix may take place leading to the decomposition of the intercalated phase. It is therefore not sensible to use a large excess of reagent. In the case of strong oxidising agents, the results should be interpreted with great care. It is better to interpret the n-BuLi reaction results as the amount of lithium reacted with the substance of interest. Before any firm evidence of lithium intercalation is available, jumping to the same conclusion on

Figure 11: Optical Absorbance (A) Change as a Function of Reaction Time



the basis of n-BuLi reaction would be premature.

As a screening agent n-BuLi is effective and generally applicable. However, the information gained from this agent is incompete. It is the lithium dissolution and the formation of the solid solution which are the main interests. To get evidence of the new phase thus formed, x-ray inspection on the lithiated sample is a necessary auxiliary method to be used in the screening test. Although, in the present work x-ray diffraction has not provided much information, it is certain that new phases are formed from the reaction.

The development of the kinetic study of the reaction is still in its preliminary stages. The spectroscopic method should be superior to the conventional titration technique. It enables not only rapid in-situ analysis, but also the possibility of separating the interference of other species which is hard to eliminate in titration. In addition to these factors, the non-destructive analysis limits the errors introduced in repeated sampling and handling of the reactive n-BuLi.

The analysis of the n-BuLi concentration has been widely accepted as the indicator of the extent of the reaction. It is believed that the change in the properties of the material being studied is the more reliable source of information about the extent and rate of the lithiation. Further development should be guided along this direction.

CHAPTER 3

COPPER MOLYBDENUM SULPHIDES

I. Introduction:

Ternary molybdenum sulphides of general formula $M_xMo_6S_{8-y}$ were first reported by Chevrel et al. (33). These compounds have been extensively investigated because of their superconducting properties. Another interesting feature of these so-called Chevrel compounds is their open structure which consists of channels running through the crystal in a 3-dimensional arrangement. Among the wide range of possible M ions (table 2), copper and lithium Chevrel compounds are the two chosen for study as possible 3-dimensional SSE materials.

II. Aspects of Ternary Molybdenum Sulphides, Literature Survey and Deduction:

1. The Crystal Structure of the Chevrel Phases:

The Chevrel compounds marked r in table 2 crystallise in a similar structure which can best be illustrated by reference to lead molybdenum sulphides. Marezio et al. (36) determined the structure of $Pb_{0.92}Mo_6S_{7.5}$ which can be described as being built up of a distorted sulphur-cube network with every four cubes occupied once by Pb atom and once by 6 Mo atoms. The 6 Mo atoms are situated approximately at the face centres of the sulphur cube and arrange themselves in an octahedron. The average Mo-Mo distance inside the octahedron is 2.704Å which is comparable with the Mo-Mo distance in $MoCl_2$, a compound which also contains Mo_6 octahedra, with the value of 2.61Å corresponding to a Mo-Mo single bond (37). Figure 12 illustrates the idealised structure of $PbMo_6S_8$. It can be seen that the structure comprises 'Mo_6S_8' clusters with cavities centred at (0, 0, 0) and (0, $\frac{1}{2}$, 0). The lead atom resides in the central cavity being connected by other empty cavities to form channels along the rhombohedral axes.

H																
Li r	Be											B	C	N	O	F
Na r	Mg t,r											Al	Si	P	S	Cl
K ?	Ca r	Sc t	Ti	V	Cr t	Mn t,r	Fe t,r	Co t,r	Ni t,r	Cu r	Zn r	Ga x	Ge x	As x	Se x	Br s
Rb ?	Sr r	Y t	Zr	Nb	Mo x	Tc	Ru x	Rh x	Pd r	Ag r	Cd r	In r	Sn r	Sb x	Te x	I s
Cs x	Ba r	La r	Hf	Ta	W	Re	Os	Ir	Pt	Au x	Hg	Tl r	Pb r	Bi x	Po	At
Fr	Ra	Ac														

Table 2: Members of the Series $M_xMo_6S_8$ (36)

r: rhombohedral; t: triclinic; x: proper phase did not form;

?: reports subject to verification(60,59); s: substitutional solid solution $Mo_6S_6X_2$(34).

N.B. Some lanthanide and actinide Chevrel phases and their solid solutions with the lead phase are also reported(48,35).

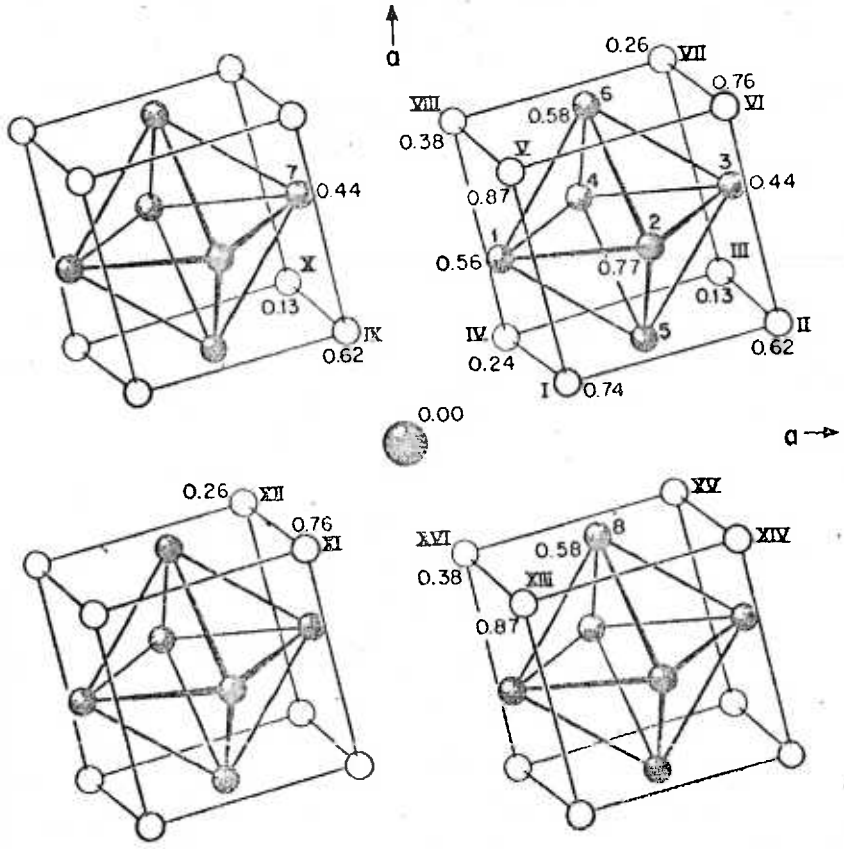


Figure 12: The Idealised Structure of $PbMo_6S_8$ (Ref. 33). Project along the rhombohedral a axis. The heights of the enumerated atoms are given as functions of the unit cell parameter. The open circles represent sulphur atoms, shaded spheres are molybdenum, and the black sphere at the origin is lead.

The space group of $Pb_{0.92}Mo_6S_{7.5}$ is $R\bar{3}$ with one formula per unit cell. The lattice parameters are a = 6.551Å and $\alpha = 89.33^{\circ}$. The Pb and six Mo atoms are assigned to the origin and the 6f positions respectively. Six of the sulphur atoms are in 6f positions and the other two are in special 2c positions which are marked IV and XI in figure 12. The $\bar{3}$ axis goes through the sulphur atoms at 2c sites and the origin.

The Mo_6S_8 clusters are held together by 2 types of bonding:

(a) Mo-S intercluster interaction, and

(b) Pb-S interaction.

In this structure, every Mo atom is surrounded by 4 sulphur atoms of the same cluster and one sulphur atom of the adjacent cube. The arrangement of these sulphur atoms is a tetragonal pyramid. This spatial configuration results when the Mo_6S_8 clusters are tilted w.r.t. the rhombohedral axis. This shortens the Mo-S intercluster distance and produces a significant interaction. The tilting angle of $Pb_{0.92}Mo_6S_{7.5}$ is about 15°. It is worth mentioning that the sulphur atoms at 2c positions do not participate in this type of interaction. The surroundings of this type of sulphur atoms are 3 Mo atoms and one Pb atom in a distorted tetrahedral arrangement. Apart from these Mo-S bonds, the clusters are also held together through the Pb-S bonding. If Pb atoms are missing from the channels, this type of interaction also vanishes and the stability of the lattice is then expected to be low. Indeed, Mo_3S_4 cannot be prepared directly from the elements at high temperature indicating that the Pb-S interaction is an important force to stabilise the structure. On the other hand, Mo_3Se_4 can be prepared at high temperature and crystallises in the same structure (38). The Se-Se intercluster bonds are believed to be responsible for the stability of the phase.

Although Mo_3S_4 is not stable at high temperature, this phase can be obtained by removing the small M ions from the ternary compounds with HCl (39). The main feature of this phase is the retention of the 'Mo_6S_8' cluster unit after the removal of M ions. The structural data for Mo_3S_4 are compared here with those of $PbMo_6S_8$, a compound with a large M atom and $NiMo_3S_4$, a compound with a small M atom.

Table 3: Comparison of Crystallographic Data of Three Selected Chevrel Phases:

	Mo_3S_4	$NiMo_3S_4$	$PbMo_6S_8$
Intercluster Mo-Mo (Å)	3.084	3.185	3.267
Intercluster Mo-S (Å)	2.425	2.460	2.566
Diagonal S_{2c}-S_{2c} (Å)	6.155	6.143	5.906
Intracluster Mo-Mo (Å)	2.780	2.732 (40)	2.704 (36)
Mo-Mo-Mo Angles (°)	56.25	58.38 (40)	58.42 (36)
of Mo_6 octahedron	60.00	60.00	60.00
	61.88	60.81	60.79

(N.B. Data from reference no.39 unless mentioned otherwise)

The longer diagonal S_{2c}-S_{2c} distance in Mo_3S_4 than in the ternary phases indicates that the M atom in the channel binds the clusters together and shortens this distance in ternary phases. When these atoms are absent in the MO_3S_4 lattice, stability of the lattice is gained by intercluster Mo-S bonding which is expected to be stronger as revealed by the shorter bond distance, and Mo-Mo intercluster interaction. This latter bond distance is much longer than the Mo-Mo distance in $MoCl_2$ (2.61Å). It should also be noted that the intracluster Mo-Mo distance decreases and the Mo_6 octahedron becomes regular when the third element (M) is present in the phase. These observations are believed to be caused by the Mo-Mo intercluster interaction stabilising the phase and the effect is 2-fold. Firstly, the cluster is distorted to favour the orientation for significant Mo-Mo interaction. Secondly, part of the valence electrons of Mo atoms is no longer available for the intracluster bonding. This weakens the Mo-Mo bonding within the Mo_6 octahedron as the bond distance is elongated and the octahedron becomes less regular. The presence of the third element (M) not only stabilises the lattice through M-S bonding but also provides electrons (from ionisation of the atom) for the bonding within the octahedron.

Another interesting feature about the $Pb_{0.92}Mo_6S_{7.5}$ structure is the occupancy of the special sulphur 2c sites. Marezio et al. (36) found that the occupancy factor of these sites is less than 100%, from which the nonstoichiometry of sulphur is deduced. Since the sulphur atoms at these positions interact with Pb atoms, the thermal displacement of Pb atoms along the bonding direction is expected to be low. However, the crystallographic results show otherwise. Whether this is because the large thermal displacement reduces the occupancy factor of these sites, or the weak force constant between the partially occupied sites and Pb atom causes the large thermal displacement, is not clear.

2. The Electronic Structure of the Chevrel Phases:

It is known that the amount of M in the phase can vary, with x value (in $M_xMo_6S_8$) ranging from zero to one for large M atoms and from zero to four for small M atoms. The effect of this variation on the $Cu_xMo_6S_8$ structure has been studied (41) and will be discussed in a later section. One of these results is that the Mo_6 octahedron becomes more regular when the copper content increases. This result agrees with the discussion about the crystallographic effect of the third element M on the Mo_6 octahedron given in the last section.

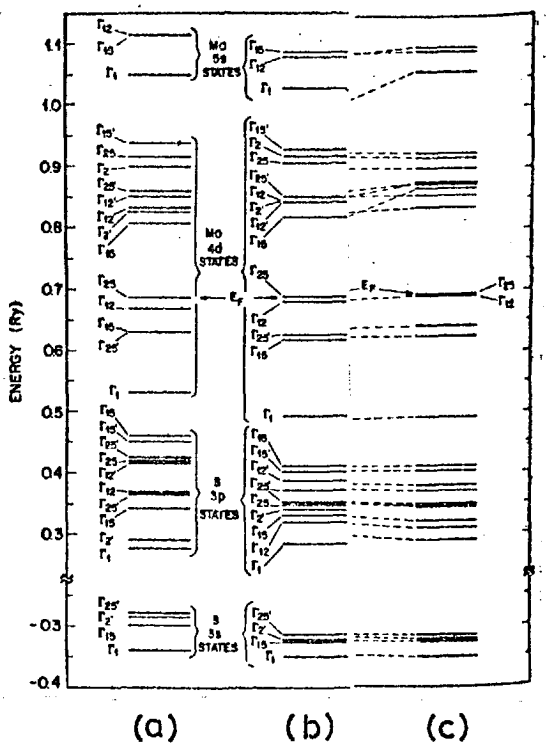
To understand this effect, it is easier to start with a better-known compound $MoCl_2$. The ionic formula can be rewritten as $(Mo_6^{2+}Cl_8^{-1})^{4+}Cl_4^{-1}$ and the Mo_6 unit is an almost perfect octahedron. There are 12 Mo-Mo bonds between 6 Mo atoms arranged in an octahedral form and 24 electrons are required for these 12 single bonds. The total number of valence electrons available per $(Mo_6Cl_8)^{4+}$ unit is exactly 24. In other words, when the electrons required for the 12 Mo-Mo single bonds are provided, the regular Mo_6 octahedron results.

By analogy, the stability of Chevrel phases can be considered in terms of the number of valence electrons available for Mo-Mo bonding. (Strictly speaking the applicability of this argument to covalently bonded compounds is doubtful and the concept

can only be treated as an approximation.) Assigning the formal charge of +2 to Mo and -2 to S, the formula $Cu_4^+[Mo_6^{2+}S_8^{2-}]^{4-}$ is deduced. When the third element is absent, the deficit of electrons is highest (4 electrons). The Mo_6 octahedron is therefore distorted most. When the third element is introduced into the phase, the electrons from the ionisation of the M atom increase the number of electrons available for bonding and the stability of the phase gradually improves. This simple '24 electrons' principle, first proposed by Yvon and Paoli (42), is found successful in describing some of the properties of Chevrel phases, for example, the drop of T_c (the superconducting transition temperature) value when 24 valence electrons are available for Mo_6 bondings (43); the instability of Mo_3S_4 and the low maximum M content in Mo_3Se_4, in which selenium has a formal charge lower than -2 (44).

More detailed molecular orbital (MO) calculations have been performed on $PbMo_6S_8$ by Mattheiss and Fong (45). To simplify the calculation, these authors assumed perfectly cubic Mo_6S_8 units and the absence of the tilting of the cubes. The results show 30 MO energy levels including 13 Mo 4d levels (fig. 13). When these levels are filled with available electrons (84 valence electrons altogether), the last two electrons are accommodated in a triply-degenerate Γ_{25} state. This partially occupied state gives rise to the metallic conductivity (electronic) of the phases. The Pb 6s level lies well below E_f and the 6p band is placed well above the E_f. In this situation, the two 6p electrons are donated to the Mo 4d bands and the +2 valency on Pb results. Another interesting feature of the energy levels is the presence of an energy gap between the E_f and the lowest unoccupied state. This separation, of value 1.5-1.8 eV, prevents the filling of the higher states when the Γ_{25} state is filled by the electrons from the third element. This restricts the maximum solubility of copper in Mo_6S_8 to 4 atoms if monovalency of copper is assumed.

There are 12 4d Mo energy levels below E_f and 24 electrons are required to fill them. This agrees with the deduction of the principle based on the ionic bonding scheme, in which the formal charge on sulphur atoms is assumed to be -2. This assumption can be ratified in two ways. If one compares the intracluster S-S



State	Energy (Ry)	$\{S\}$	$\{d_{xy}\}$	$\{d_{yz}, d_{zx}\}$	$\{d_{x^2-y^2}\}$	$\{d_{3z^2-r^2}\}$
$\Gamma_{15'}$	0.929	...	...	0.970	...	...
Γ_2	0.918	...	...	...	1.000	...
Γ_{25}	0.907	...	...	0.698	0.256	...
$\Gamma_{25'}$	0.850	...	0.833	0.021	...	...
Γ_{12}	0.844	0.001	...	...	0.016	0.970
$\Gamma_{2'}$	0.842	...	0.677	...	...	...
$\Gamma_{12'}$	0.841	...	0.917	...	...	...
Γ_{15}	0.818	0.000	...	0.192	...	0.737
Γ_{25}	0.689(E_F)	...	...	0.289	0.690	...
Γ_{12}	0.681	0.014	...	...	0.825	0.004
$\Gamma_{25'}$	0.627	...	0.000	0.886	...	...
Γ_{15}	0.618	0.101	...	0.657	...	0.210
Γ_1	0.495	0.247	...	...	...	0.698

Figure 13: Energy Levels for the Mo_6S_8 Cluster (Ref. 45)
(a) LCOAO energy levels for the Mo_6S_8 cluster;
(b) corresponding results for the LCAO model; and
(c) the effect of tilting on the energy levels.

Table lists the fractional orbital content of the wave functions near E_f.

distance (1.73Å) in $PbMo_6S_8$ with the ionic radii of sulphur (1.70Å) (46), the values are close enough to justify the assumption. The other approach is based on the energy levels proposed above. The sulphur 3s and 3p states are far below the E_f and therefore they are filled. The -2 valency of sulphur atom not only justifies the assumption of '24 electrons' principle, but also implies the central cavity is highly ionic and the M ions will be held mainly by Coulombic interaction.

It is important to note that the energy levels are calculated on the ground that tilting is absent and Mo_6S_8 cubes are perfect. When these two factors are included, although it is closer to reality, the symmetry of the compound decreases and the calculation becomes laborious. Mattheiss and Fong (45) allowed the tilting effect and estimated the distortion on the energy levels. Their results show that little effect has been exerted on the MO states (fig. 13). The two states near E_f, however, are brought close and can be considered as a whole. calculation also shows that these states involve primarily the non-bonding $\{d_{x^2-y^2}\}$ orbitals (designating the equivalent orbitals: $d_{x^2-y^2}$, $d_{y^2-z^2}$ and $d_{z^2-x^2}$). Assuming no intercluster coupling of $\{d_{x^2-y^2}\}$ orbitals, the band width at E_f is narrow, which in turn gives a high density of states at E_f. As discussed in Chapter 1, a material with this electronic structure is likely to exhibit only a small contribution to the change of the electrochemical potential of electrons as the concentration of M atom is increased.

3. <u>The Delocalisation of M Ions</u>:

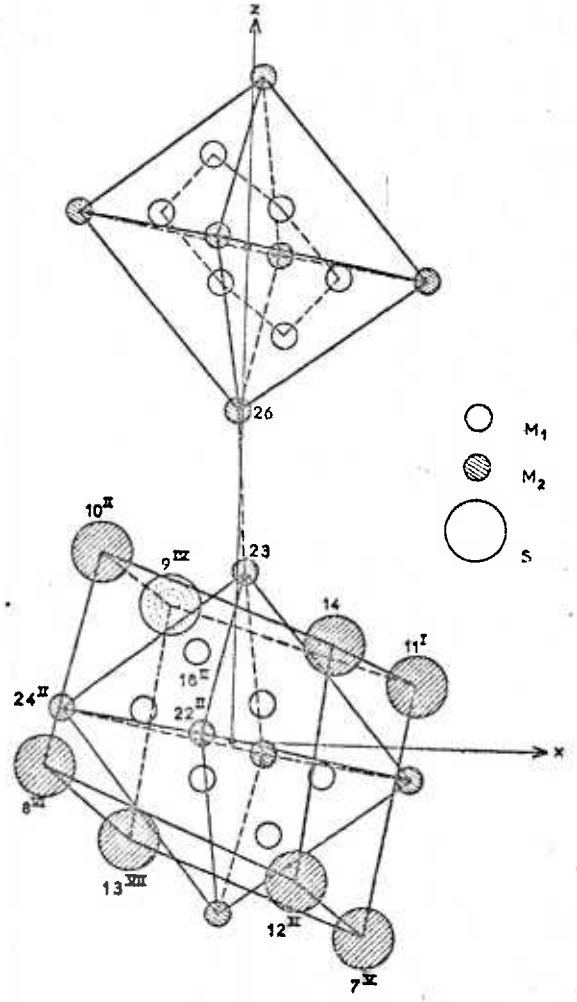
As illustrated in the last section, there are four vacant electronic states per Mo_6S_8 formula. They can be filled by the electrons donated by the M atoms. Therefore, the amount of M which can be accommodated in the phase depends on the valency of M atom. The maximum dissolution of mono-valent copper atoms is 4 per Mo_6S_8 while the limit for divalent lead atoms stands at one, despite the availability of two more vacant electron states. This suggests that the crystallographic parameters are also important

in determining the dissolution of the third element.

This aspect of the Chevrel phases has been studied. Guillevic et al. (40, 47) studied $NiMo_3S_4$, $Ni_{0.7}Mo_3S_4$, $Co_{0.8}Mo_3S_4$ and $Fe_{0.66}Mo_3S_4$ and found these ions distributed statistically over 12 possible sites in the channel. More detailed crystallographic study has been carried out on $Cu_{2-z}Mo_3S_4$ (41). From these investigations, it can be seen that these sites are formed when the sulphur cube surrounding the cavity at (0, 0, 0) is compressed along the ternary axis. This produces six equivalent tetrahedral sites (M_1) in a hexagonal shape centred at the ternary axis with the plane perpendicular to the axis. The distances between the M_1 sites, as determined from the copper phases, are between 1.26 to 1.31Å depending on the population of these sites. Another six tetrahedral sites (M_2) are situated slightly above and off the face centre of the S_8 cube and reside in the cavities centred at (0, $\frac{1}{2}$, 0). Each M_1 site has one M_2 site attached to it and since M_2 sites are not coplanar, they form an octahedron like the Mo_6 unit in the Mo_6S_8 cluster (fig. 14). Separations between M_1 and the interconnected M_2 sites in $Cu_{2-z}Mo_3S_4$ range from 1.12 to 1.43Å as a function of z. Each M_2 site is also linked to another M_2 site from the adjacent cube and a string of M sites spreads in 3 dimensions through the lattice.

Because of their close proximity, the adjacent sites (M_1-M_1 or M_1-M_2) cannot be occupied simultaneously. The distribution of copper ions over these sites clearly depends on the overall concentration of copper. Figure 15 shows the occupancies of two sites as copper content in the phase increases. As the amount of copper is building up inside the phase, some of them are forces towards the peripheral sites (M_2) and reside there. Gradually increasing population on M_2 sites, however, enhances the repulsive interaction between the M_2 sites of 2 neighbouring cubes. This force acts in opposition to the occupancy of M_2 sites and consequently a tendency of re-occupying M_1 sites is seen.

It appears that the delocalisation effect occurs to different extents for different ions. As suggests by Yvon (48), the size of ion is not the determining factor. Examining the structural properties of the Chevrel phases with mobile ions



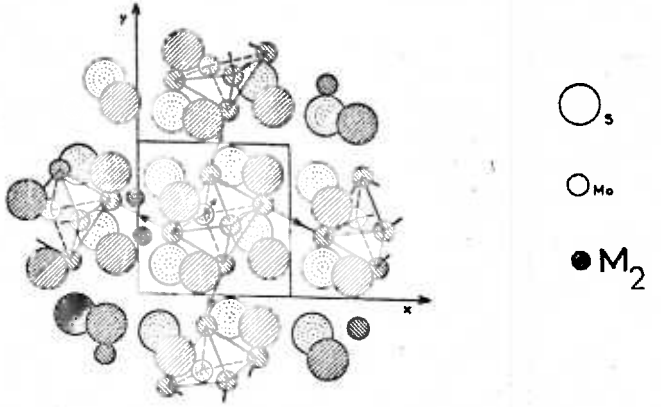


Figure 14: The Crystallographic Positions of M_1 and M_2 Sites (Ref. 40)

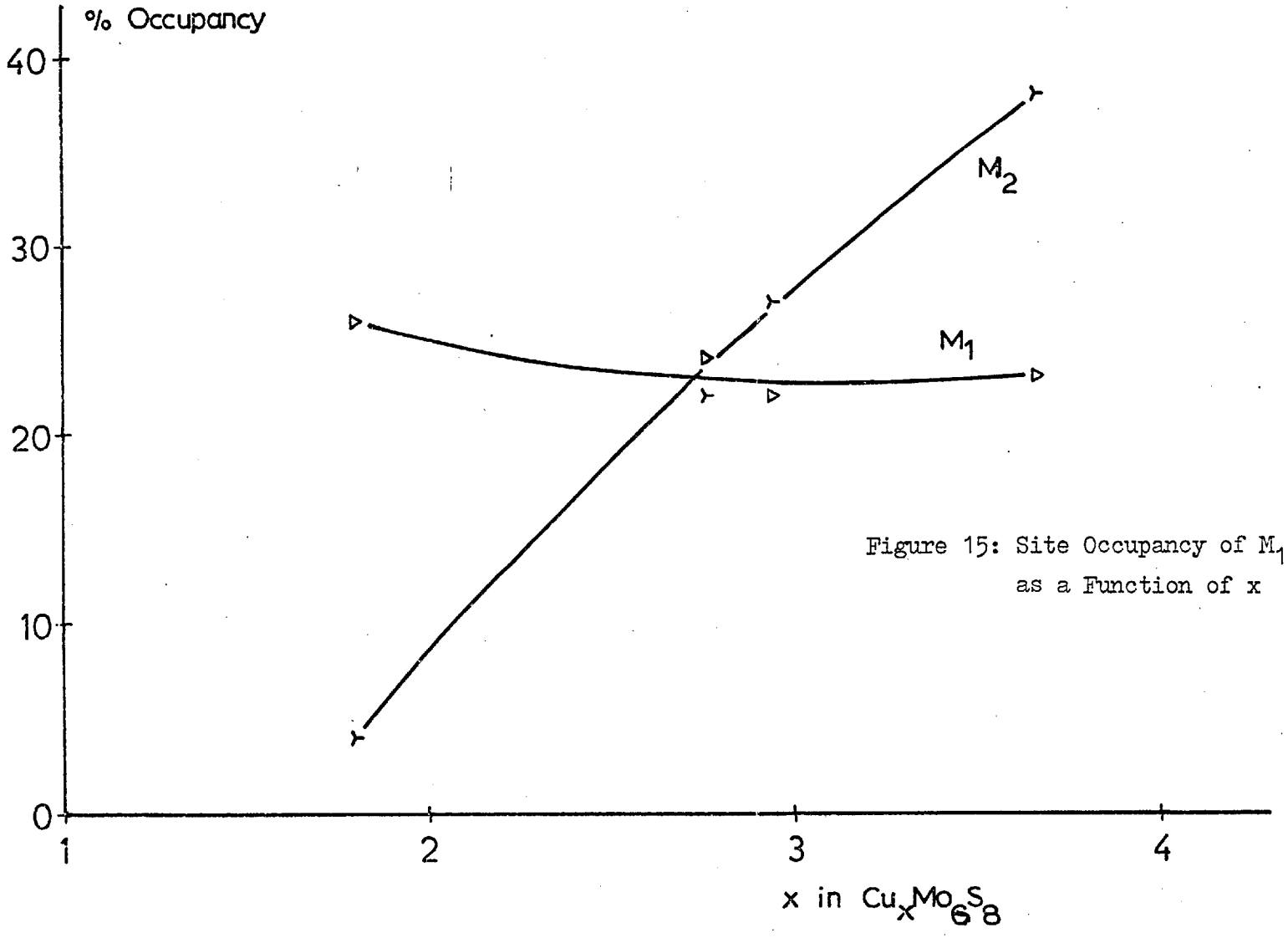


Figure 15: Site Occupancy of M_1 and M_2 Sites as a Function of x (Ref. 41)

(table 4), there is a trend that only those ions preferring tetrahedral coordination and with an effective ionic radius (46) at that coordination equal to or less than 0.63Å form phases with high α_R values. It is important, for the delocalisation to occur, that the ions favour the tetrahedral sites, otherwise the ions would take the high coordination central site in this highly ionic environment. Ions with d^{10} configuration would suit the condition. Co(II) and Ni(II) are often found in tetrahedral configurations (49). Although Fe(II) prefers octahedral to tetrahedral sites, it does not exclude the possibility of occupying the tetrahedral site rather than the 8-coordinated central site. The argument also explains the localisation of La(III), Gd(III), Pb(II) and Sn(II) in their corresponding Chevrel phases. The size effect of the ion comes into consideration when the tetrahedral sites have been favoured. As the crystallographic results show (41), the tetrahedral sites are very close to each other. Large ions would not easily occupy these sites. Therefore, the large Ag(I) ion, though it likes to take the tetrahedral sites, finds the constraint of doing so is too great and a relatively small α_R for a delocalised ion results. The mentioned r_{eff} 0.63Å is only a value at which extensive delocalisation registers. Full investigation is required for the better location of the critical value. Another interesting point is the mobility of the doubly-charged ions. The leaching study (39) has shown the mobility of Fe(II), Zn(II), Co(II) and Ni(II) in the Chevrel lattice, despite the strong Coulombic interaction between the mobile ions and the lattice.

4. Ionic Conductivity in the Chevrel Compounds:

The ionic conductivity of M in the Mo_6S_8 lattice is the result of the delocalisation of the ions between M_1 and M_2 sites. That delocalised ions are mobile has been demonstrated by the early leaching work (39). A correlation of α_R, the angle of the rhombohedral cell, with the delocalisation of M ions was reported recently (48) (fig. 16). The principle is, that the closer on the ternary axis the Mo_6S_8 units come, the larger the α_R angle will be.

Table 4: Structural Parameters of Delocalised Ions in Chevrel Phases:

Ions	Ag(I)	In(III)	Fe(II)	Zn(II)	Ni(II)	Cu(I)	Co(II)
d^n	10	10	6	10	8	10	7
r_{eff} (Å)*	1.0	0.62	0.63	0.60	0.55	0.60	0.58
α_R (°)**	91.9	93.2	94.7	94.7+	94.8 (x = 2)	94.9 (x = 1.8)	95.2

* Ref. (46); ** Ref. (48); + Ref. (33).

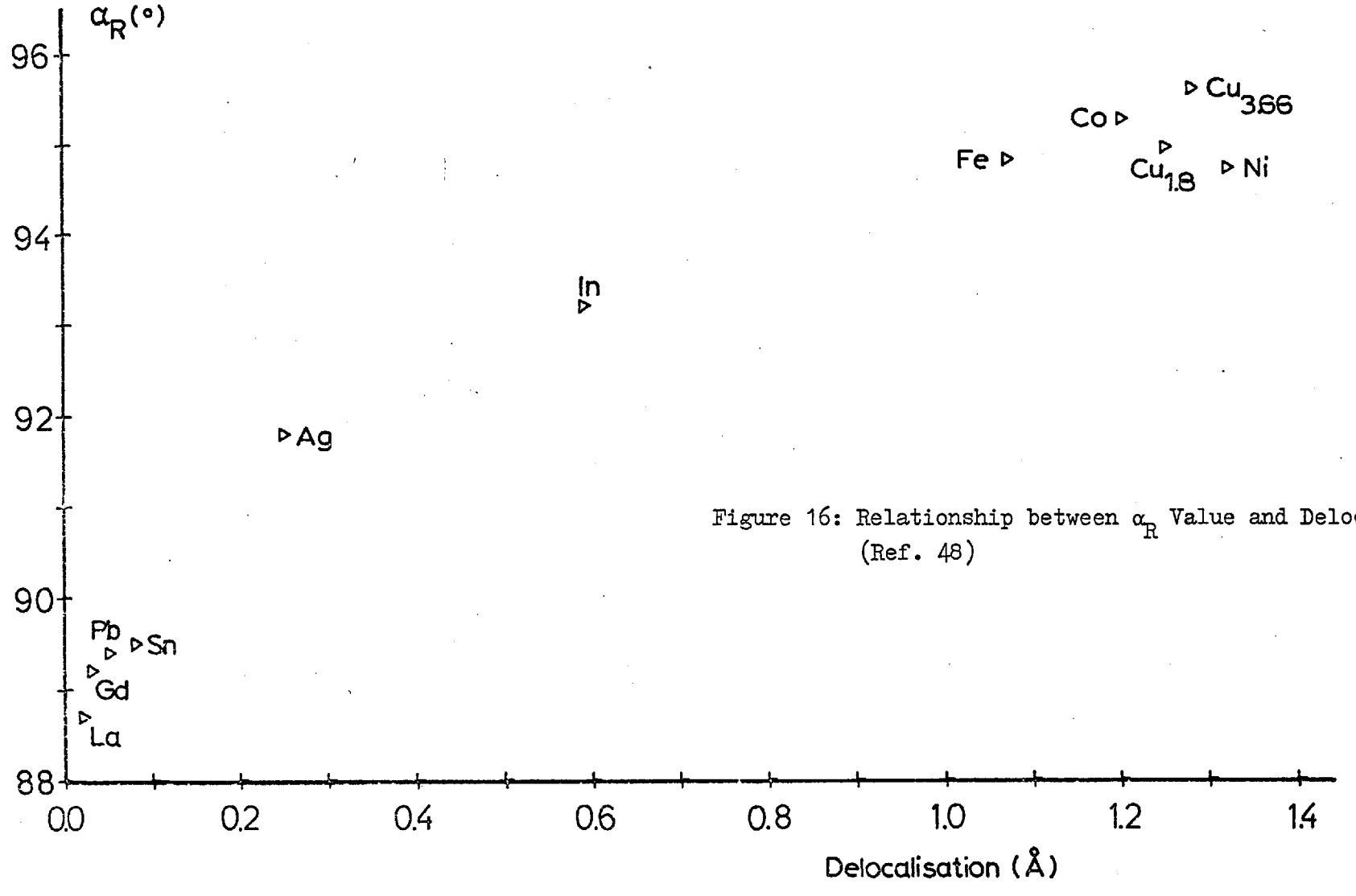


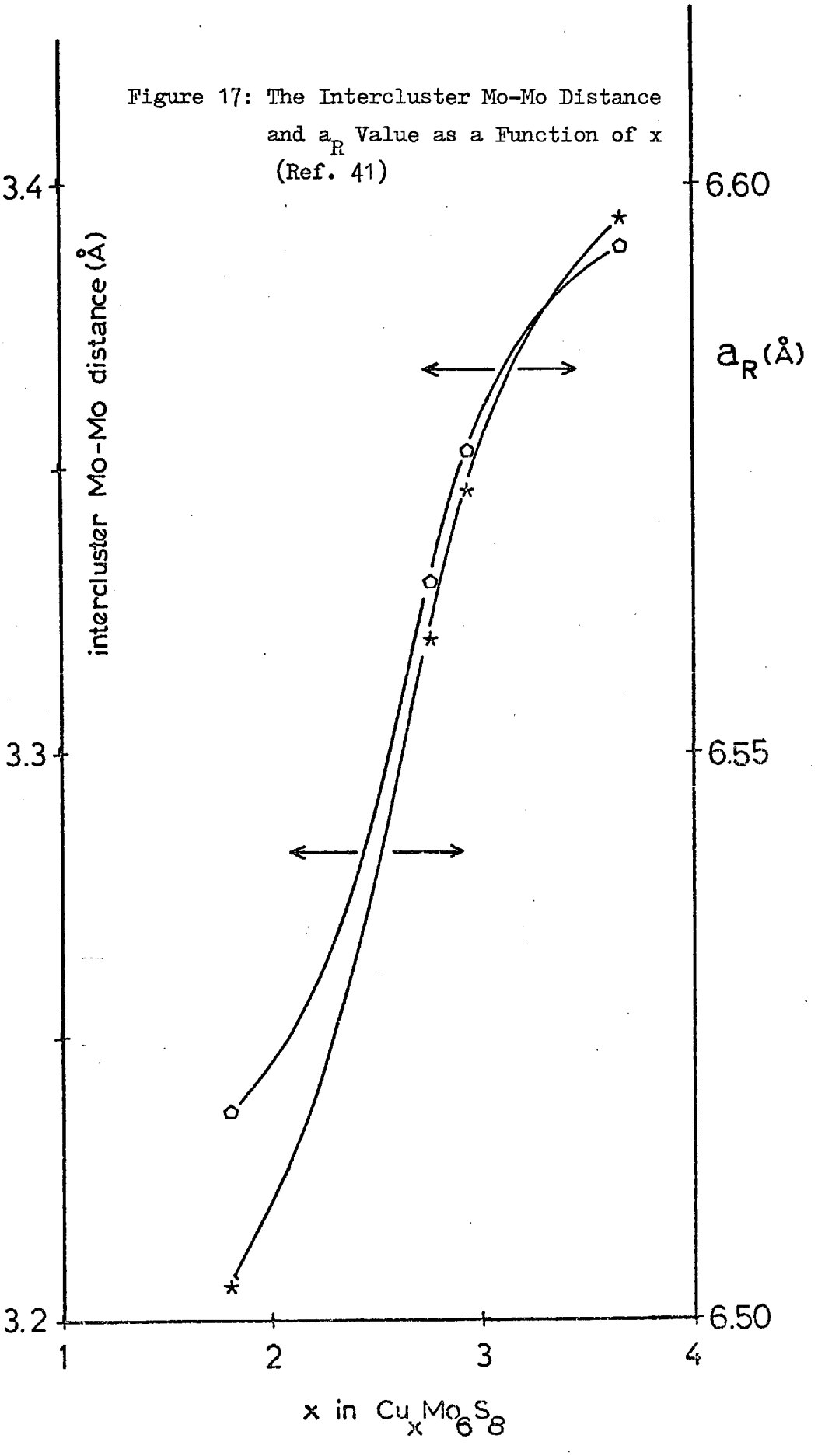
Figure 16: Relationship between α_R Value and Delocalisation (Ref. 48)

The M ions will then be squeezed from the central position to the tetrahedral sites. Since the delocalisation of M ions is important for a fast ionic motion inside the phase, the α_R angle can be a measure of this property. Silver Chevrel compound has an α_R angle of ~92°, and a delocalisation (defined as the difference of the rms vibrational amplitude perpendicular to the ternary axis and a constant) of only 20% of that of the copper phase. This suggests that the mobility of silver ions in the Chevrel lattice may be low.

It has been suggested that the copper ions are moving freely between M_1 and M_2 sites at r.t. (41). This comment, based on the analysis of the thermal vibration of the x-ray diffraction work, probably was reached on a high copper content phase, in which M_1 and M_2 sites are both populated. The ionic conductivity measurement (to be discussed in a later section) shows that the energy difference between the two sites is about 10 kJ/mole, which corresponds to the thermal energy at 930°C. This implies that the population of M_2 sites will be fairly low at the temperature range of present study until the M_1 sites are nearly full. This does not, however, imply that the bottleneck of the diffusion passage is between the M_1 and M_2 sites. As the x-ray diffraction work on copper (41) and nickel (47) compounds indicated, the long range motion between neighbouring cubes through M_2-M_2 passages is restricted. The diffusion bottleneck will then be on M_2-M_2 passages and the M_1-M_2 passage will be taken into consideration only when the M_2 sites occupancy is very low.

Examining the cavity at (0, $\frac{1}{2}$, 0) along the y direction (fig. 14), the ionic transport from one M_2 site to the neighbouring M_2 site passes through the line joining S_V and S_X atoms. Because this separation is substantially larger than the distance between Mo_1 and Mo_7 atoms, the latter value will be a better indication of the size of the bottleneck. Figure 17 plots this distance and the a_R value as a function of copper content. Both values increase with the x value and moreover the relationship between a_R and d_{Mo-Mo} is linear (fig. 18). This suggests that the high population on M_2 sites is acting to expand the lattice and a larger a_R value will give a wider separation between the Mo_6S_8 units. The value of the Mo_1-Mo_7 distance is around 3.3Å which is wide enough for Cu(I)

Figure 17: The Intercluster Mo-Mo Distance and a_R Value as a Function of x (Ref. 41)



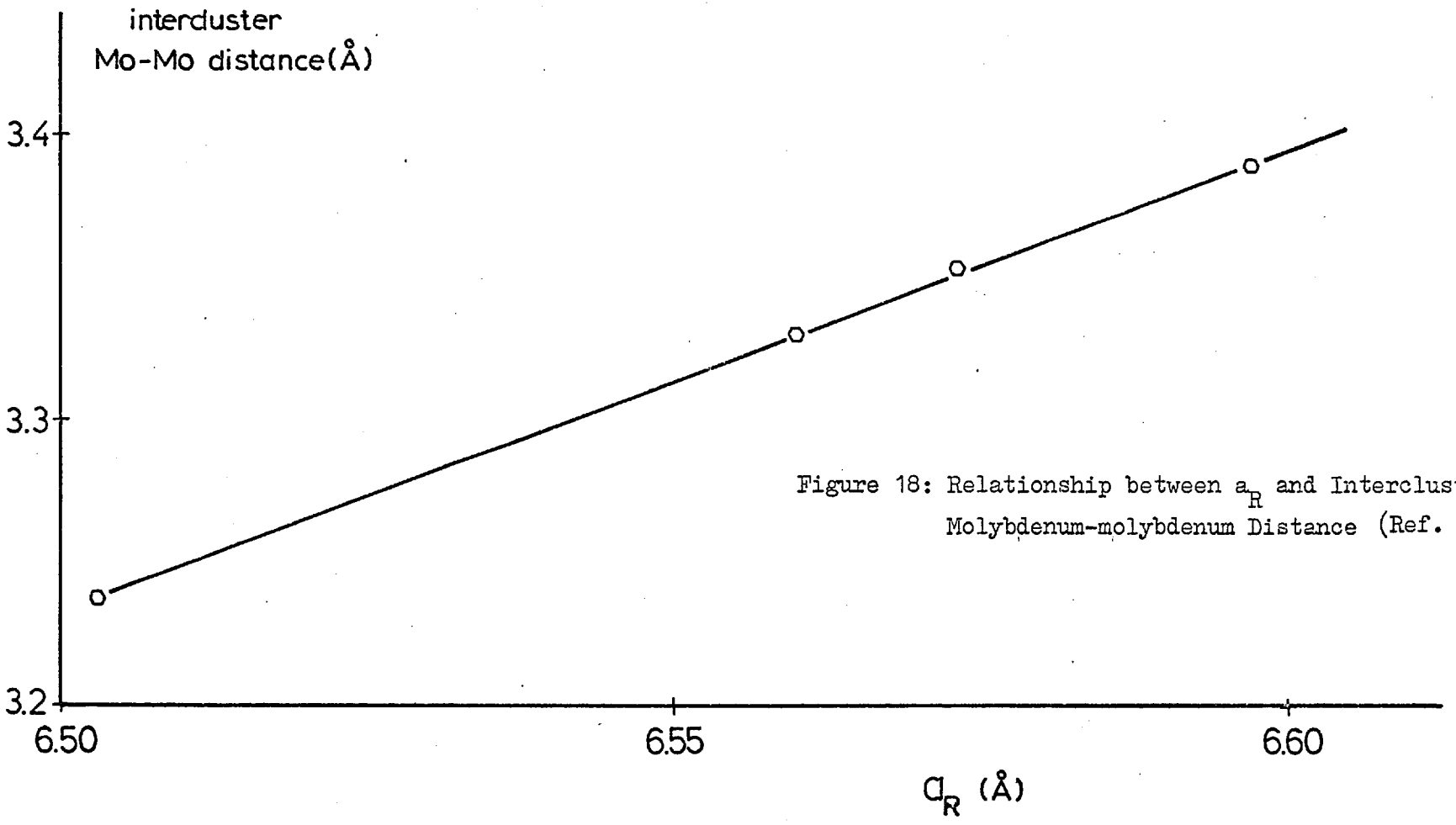


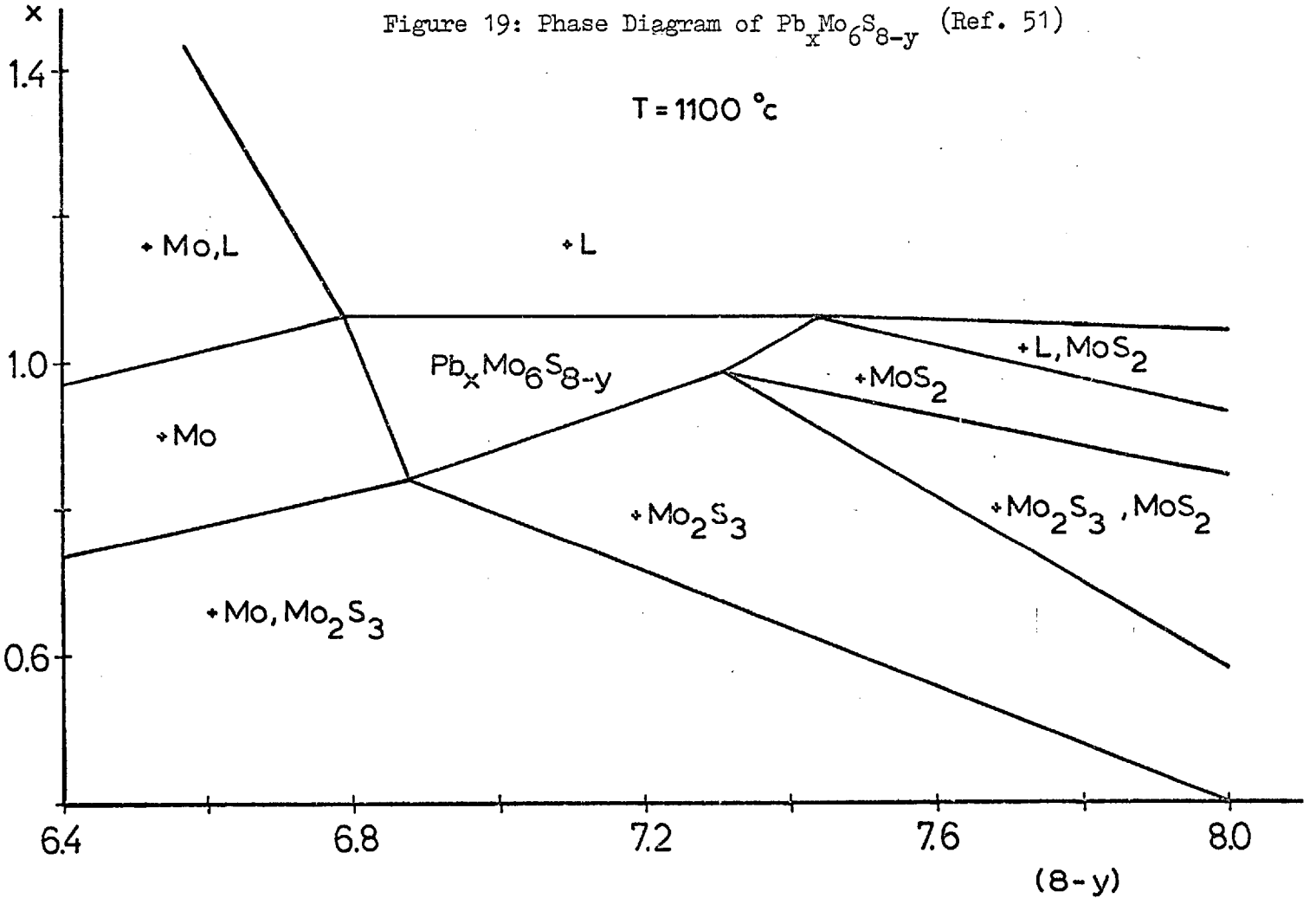
Figure 18: Relationship between a_R and Intercluster Molybdenum-molybdenum Distance (Ref. 41)

diffusion. The lattice constraint should not be a serious hindrance to diffusion. One possible obstruction to ionic motion through neighbouring M_2-M_2 sites is the strong bonding on the ions at M_2 sites. When an ion occupies a M_2 site, it is situated within the Mo-S intercluster bonding region. Putting a copper ion at this position may not produce direct bonding with Mo atoms. (Only a very limited solubility of Cu ~1.5% in Mo at 950°C has been reported in the literature (50) indicating the bonding between these two atoms is unfavourable.) The establishment of Cu-S bondings between copper ions and the surrounding sulphur ions will certainly interfere with the Mo-S intercluster interaction. The Cu-S bonds extend between the Mo_6S_8 clusters thus stabilising the lattice and also binding the copper ions at M_2 sites. Ionic mobility between M_2 sites will then require activation energy to overcome the binding energy on the ions.

5. The Non-stoichiometry of Chevrel Phases:

It has been known that non-stoichiometry exists in Chevrel phases, $M_xMo_6S_{8-y}$. The early work on the ternary molybdenum sulphides shows that impurity phases like MoS_2, Mo_2S_3 and Mo coexist with the ternary compound if the sulphur content is not carefully controlled. The first phase study was carried out on lead phase (51) and the phase diagram is given in figure 19. One can see that when the sulphur content is close to stoichiometry, MoS_2 and Mo_2S_3 phases are formed. If the y value is large, molybdenum metal is found as an impurity phase. These impurity phases can be converted to the ternary phase by increasing the Pb content. It looks as if the combined effect of two variables x and y alters the valency of molybdenum. When it is higher than a certain value, other molybdenum sulphides form. If it is reduced to a low value, molybdenum metal precipitates. Based on the '24 electrons' principle outlined in the previous section, a Chevrel phase can be written as $Cu_2^+Mo_6^{++}S_8^=$. The formal charge on the molybdenum in this phase is +2.33. High temperature preparation of this phase always produces a ternary phase contaminated by MoS_2.

Figure 19: Phase Diagram of $Pb_xMo_6S_{8-y}$ (Ref. 51)



It can be deduced, therefore, that the valency of the molybdenum has to be less than this value in order to avoid the formation of the impurity phase. By the same principle, the greater influence on phase stability of sulphur non-stoichiometry than M content can be deduced. Assuming 6 m/o sulphur deficient, an increase of one electron per Mo_6 unit results. This corresponds to 0.17 electron per Mo atom, which is an order of magnitude more than what can be gained by analogous increase of the M content.

Another interesting deduction from the '24 electrons' model is the dependence of copper solubility on sulphur non-stoichiometry. If the total number of electrons of the system, obtained by summing Mo 4d electrons and the ionised electrons from copper (+1 oxidation state) minus the electrons required for the octet of sulphur atoms, is set equal to 24, the amount of copper allowed in the phase will be restricted by the sulphur non-stoichiometry. Higher sulphur content will give higher copper solubility and vice versa. This can be seen by the fact that more electrons are required from M atoms to compensate the electrons removed by the higher sulphur content to maintain sufficient electrons for Mo-Mo bondings.

Thermal studies (39) on the binary phase Mo_6S_8 reveal that this phase decomposes at 468°C to an intermediate phase which proceeds to form MoS_2 and Mo. Further reaction between these two compounds at 1000°C gives Mo_2S_3 and Mo. Apparently, all the mystery about the separation of MoS_2 from the ternary phase depends on structural information about the intermediate phase. This is unfortunately not available at the moment. Nevertheless, one can still argue that the Mo_6S_8 is not thermodynamically stable and when sufficient activation energy is supplied, decomposition of the phase takes place. The sulphur sub-lattice of Mo_6S_8 is distinctly different from MoS_2, which has a close-packed one. Therefore, the decomposition will involve rearrangement of the sulphur sub-lattice.

It is controversial whether sulphur vacancies or molybdenum inclusions in the channels are the means to accommodate the sulphur deficiency. Bars et al. (38) were in favour of the inclusion of excess molybdenum in the channels to describe $Mo_{3+x}Se_4$. Through density measurements on $PbMo_6S_8$ and its solid solution of

other M ions, Sergent et al. (35) believe that excess molybdenum accounts for the non-stoichiometry and S_8 units should be used instead of Mo_6 units. Flükiger et al. (52) also reported the absence of sulphur vacancies. Crystallographic study of $Pb_{0.92}Mo_6S_{7.5}$ (36), however, provides strong evidence supporting the Mo_6 unit. No molybdenum was found in the empty cavities and a partial occupancy at S(2c) sites was measured. Another piece of evidence is acquired from the study of lead Chevrel phase (51). Hauck found that the α_R angle increases with the sulphur content. The gradual filling of the S(2c) sites increases the Pb-S interaction and the α_R angle will increase as the clusters are pulled closer by the stronger force. As the picture is not clarified, the Mo_6 unit will be used in this article as in the majority of the literature.

The effect of non-stoichiometry on the transport properties is also subject to this controversy. If the excess molybdenum ions are indeed inside the channels, this, without any doubt, will impede the ionic conduction. If it is the sulphur vacancy which is accommodating the non-stoichiometry, the partially filled S(2c) sites probably discourage the occupation of M_2 sites. This will also impede the ionic conduction. Therefore, sulphur deficiency may give worse conductivity properties, regardless of which defect is accommodating the non-stoichiometry.

In summary, the single phase of ternary molybdenum sulphide can be controlled by two variables, namely, amount of M (x value) and the non-stoichiometry of sulphur (y value). The effect of the variation seems to fix the valency on molybdenum at a value estimated to be less than +2.33. The impurity phase MoS_2 can be eliminated by either decreasing the sulphur content or increasing the M content. A larger effect is anticipated by the former alteration. A large deficit of sulphur will precipitate molybdenum as metal. Similar effects can be expected if a high M content is introduced, which reduces the valency of the molybdenum.

III. Preparation, Specimen Fabrication and Characterisation of Copper Molybdenum Sulphide

1. Experimental Procedures:

Copper molybdenum sulphide $Cu_xMo_6S_{8-y}$ was prepared by direct combination of elements at high temperature. The starting materials were copper powder (99.3%) obtained from Koch-Light, recrystallised sulphur (Specpure) purchased from Johnson Matthey and molybdenum powder (99.99%) also bought from Koch-Light. Another molybdenum powder batch was also used in early preparations. This batch was subsequently analysed by x-ray fluorescence by the Analytical Service Laboratory at Imperial College and less than 500 ppm of K and Ca were found. Before use, molybdenum powder was dried at 150°C under vacuum, copper was dried at r.t. under vacuum and sulphur was placed under an IR lump to dry and cooled down inside a desiccator. The appropriate amounts of 3 elements were weighed and ground together with an agate pestle and mortar. The mixture was loaded inside a silica tube which had been washed with chromic acid, water and acetone and dried thoroughly inside an oven. The tube was then evacuated with an ice-bath surrounding the loaded end and was sealed off. The vacuum inside the tube at sealing-off was about 4.5×10^{-2} torr. The tube was heated to 400°C and held at that temperature overnight to ensure reaction without excessive heat being released. The temperature was brought up to 1000°C slowly and held for 2 days. Slightly longer reaction time, 3 days, was given to larger batches. Before the tube was quenched to r.t. in air, the temperature was brought to 1100°C and held for 3 hours.

The product thus obtained was examined by x-ray powder diffraction. A Guinier camera with Co Kα radiation was used for phase identification. For more precise measurements, a Phillips diffractometer with Cu Kα radiation was employed. Potassium bromide (AnalaR, Hopkins and Williams) was selected as an internal standard.

The hot-pressing technique was used for fabrication of specimens. The copper molybdenum sulphide was first cold-pressed in an 8 mm steel die. The pellets were encapsulated with Pt foil,

placed in a $\frac{1}{2}$" graphite die and surrounded by boron nitride powder. A RF set was used to generate the heat and the temperature was measured with an optical pyrometer. On a few occasions, when a lower temperature was required, an alumina die and a resistance furnace were employed. The system was first evacuated and hot-pressed at temperature between 1000°C and 1450°C and under pressures ranging from 5×10^7 Nm^{-2} for graphite dies to 9×10^7 Nm^{-2} for alumina dies. The pressing time was 2 hours. The sample obtained was checked by x-ray powder diffraction. A rectangular bar specimen was cut from the sample with a high speed diamond saw and paraffin lubrication. The density was then inferred by measuring the dimensions and the weight of the specimen.

The compositions of the samples as prepared and hot-pressed were analysed by atomic absorption (AA) spectroscopy by the Hydrometallurgy Group at Imperial College. The sample was dissolved in nitric acid and bromine/carbon tetrachloride solution. The concentrations of copper and molybdenum were determined directly with the corresponding standard solution. To determine the sulphur content, a measured amount of barium chloride solution was introduced into the solution. By determining the barium concentration in the solution by AA method the concentration of sulphur (in sulphate form) could be measured.

2. Results and Discussions:

2-1. Phase Study of $Cu_2Mo_6S_{8-y}$:

The product as prepared was a dull dark grey powder. In the large scale preparations, small crystals were found in the interior of the chunk. Under an optical microscope, rectangular platelets less than 1 mm long were clearly seen. No difference between the x-ray diffraction patterns of the powder and the crystalline material was observed.

The results of the chemical analysis disagreed with the values derived from the weights of the elements used in the preparation (table 5). In view of the large analytical error (10%), it was decided to use the preparation formula with some

Table 5: Analytical Results of $Cu_2Mo_6S_{8-y}$

Prepared Composition	Calculated w/o			Experimental w/o		
	Cu	Mo	S	Cu	Mo	S
$Cu_2Mo_6S_{7.9}$	13.29	60.21	26.5	14.00	60.61	25.44
$Cu_2Mo_6S_{7.85}$	13.31	60.31	26.37	14.37	59.87	20.60
$Cu_2Mo_6S_{7.8}$	13.34	60.41	26.25	13.94	60.64	23.50
$Cu_2Mo_6S_{7.7}$	13.38	60.62	26.	13.14	60.38	25.79
$Cu_2Mo_6S_{7.65}$	13.40	60.72	25.87	13.08	59.56	25.79
$Cu_2Mo_6S_{7.59}$	13.43	60.84	25.72	13.57	57.96	25.83

uncertainty in the sulphur content which is the element most susceptible to loss during the processes.

Table 6 shows the phase study results of the copper Chevrel phases at 1100°C.

Table 6: Results of Phase Studies of $Cu_2Mo_6S_{8-y}$

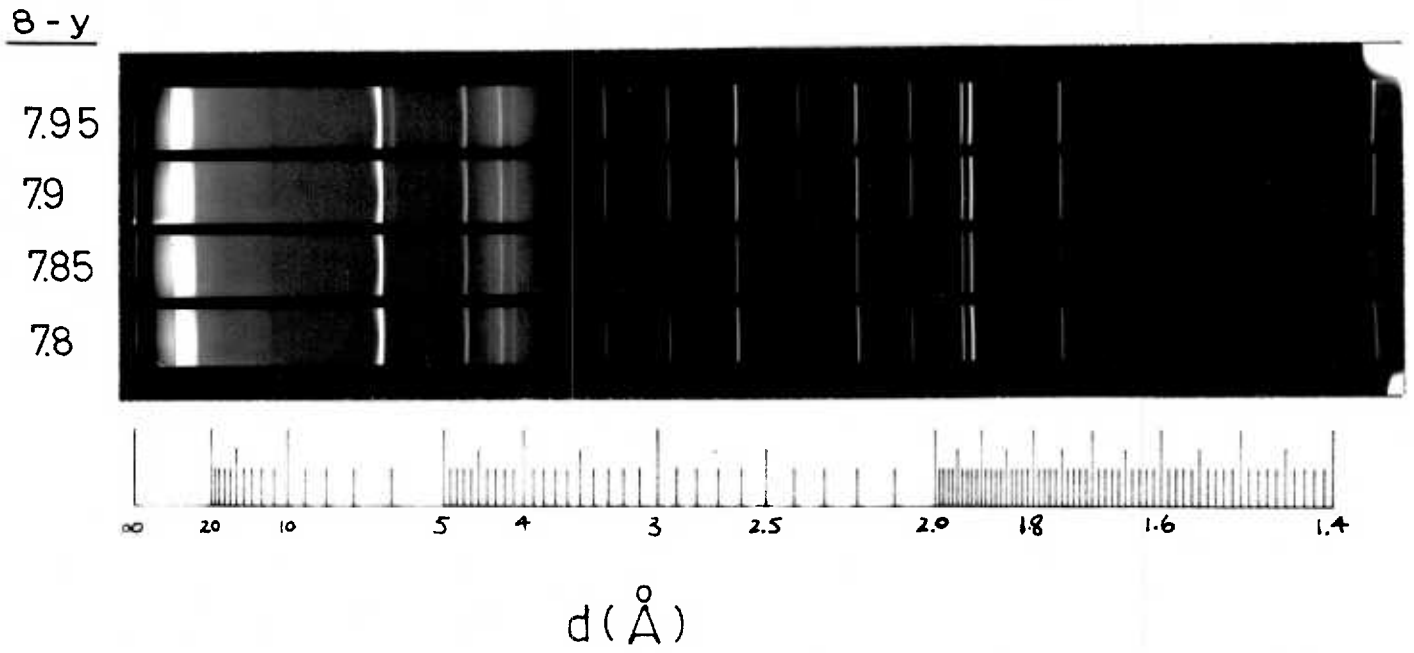
(8-y)	Phases Found
8	TP* + MoS_2
7.9	TP + MoS_2
7.85	TP
7.8	TP
7.7	TP
7.65	TP + Mo
7.59	TP + Mo

* TP: ternary phase

The MoS_2 phase was identified by its 100 diffraction line at d = 6.145Å and the presence of Mo metal was indicated by the existence of its 100 line at d = 2.225 Å. Figure 20 shows the gradual disappearance of the line at d = 6.145 Å as the sulphur content decreases. The line at d = 2.225 Å is more difficult to find because it lies very near to a broad 131 line of the ternary phase. Direct preparation of the phase $CuMo_6S_{7.65}$ was also attempted. The result showed a mixture of the ternary phase and MoS_2. This indicates that the copper content is not high enough to stabilise the ternary phase at high temperature. The lattice parameters of the phases, obtained by a computer program based on the least-square principle, are given in figure 21. For the phases with MoS_2 and Mo present, only the lines of the ternary phase are used ignoring the impurity phases.

The most interesting result is that depicted on figure 21. As the sulphur content increases from 7.59, gradual decreases of a_R and α_R values are seen. These two parameters go through their minimum at about 7.7 and ascend within the single phase. Having reached their peak values at the threshold sulphur content of the MoS_2 appearance, they descend again. The α_R value rebounds to a

Figure 20: Formation of MoS_2 as a Function of Sulphur Content



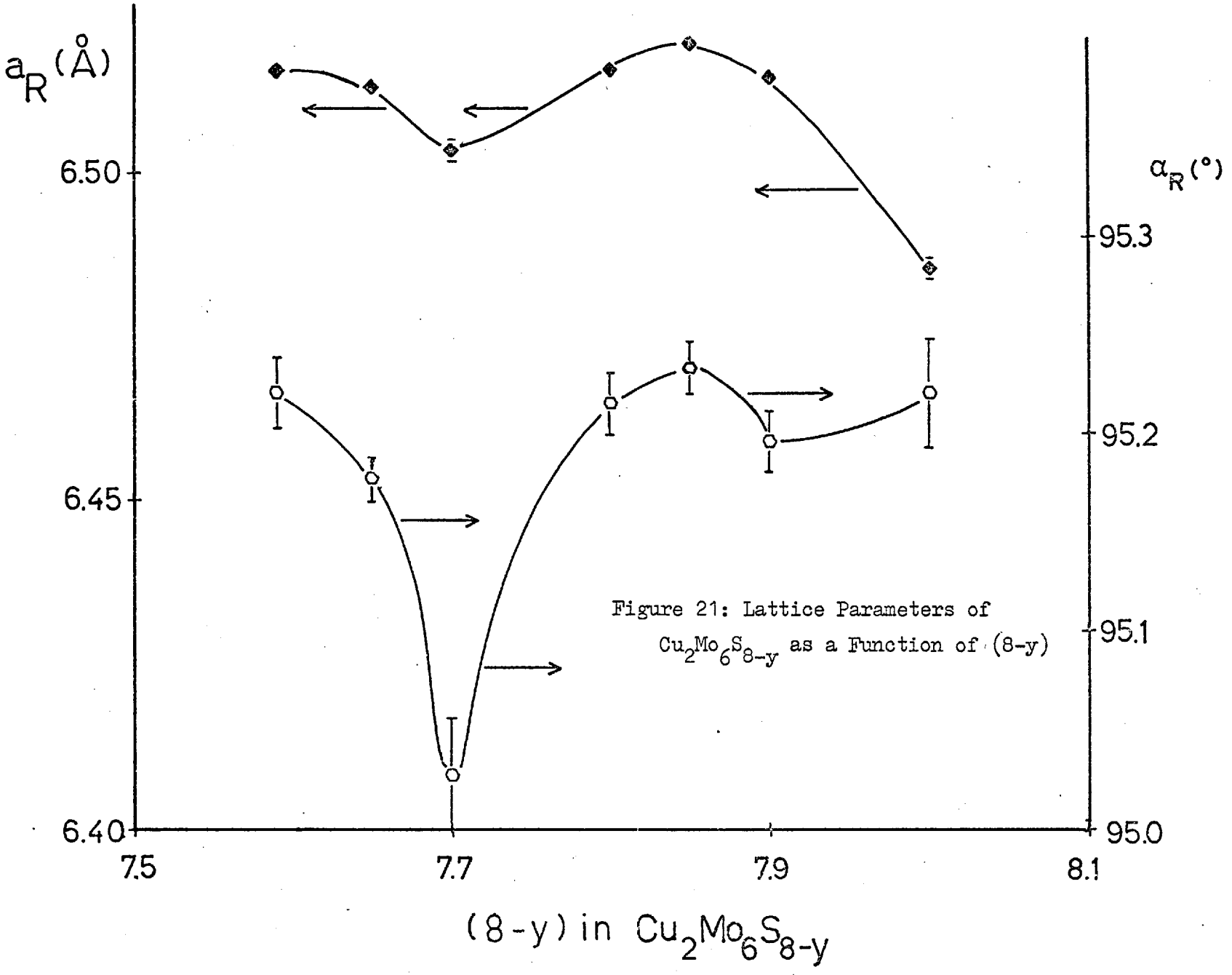


Figure 21: Lattice Parameters of $Cu_2Mo_6S_{8-y}$ as a Function of (8-y)

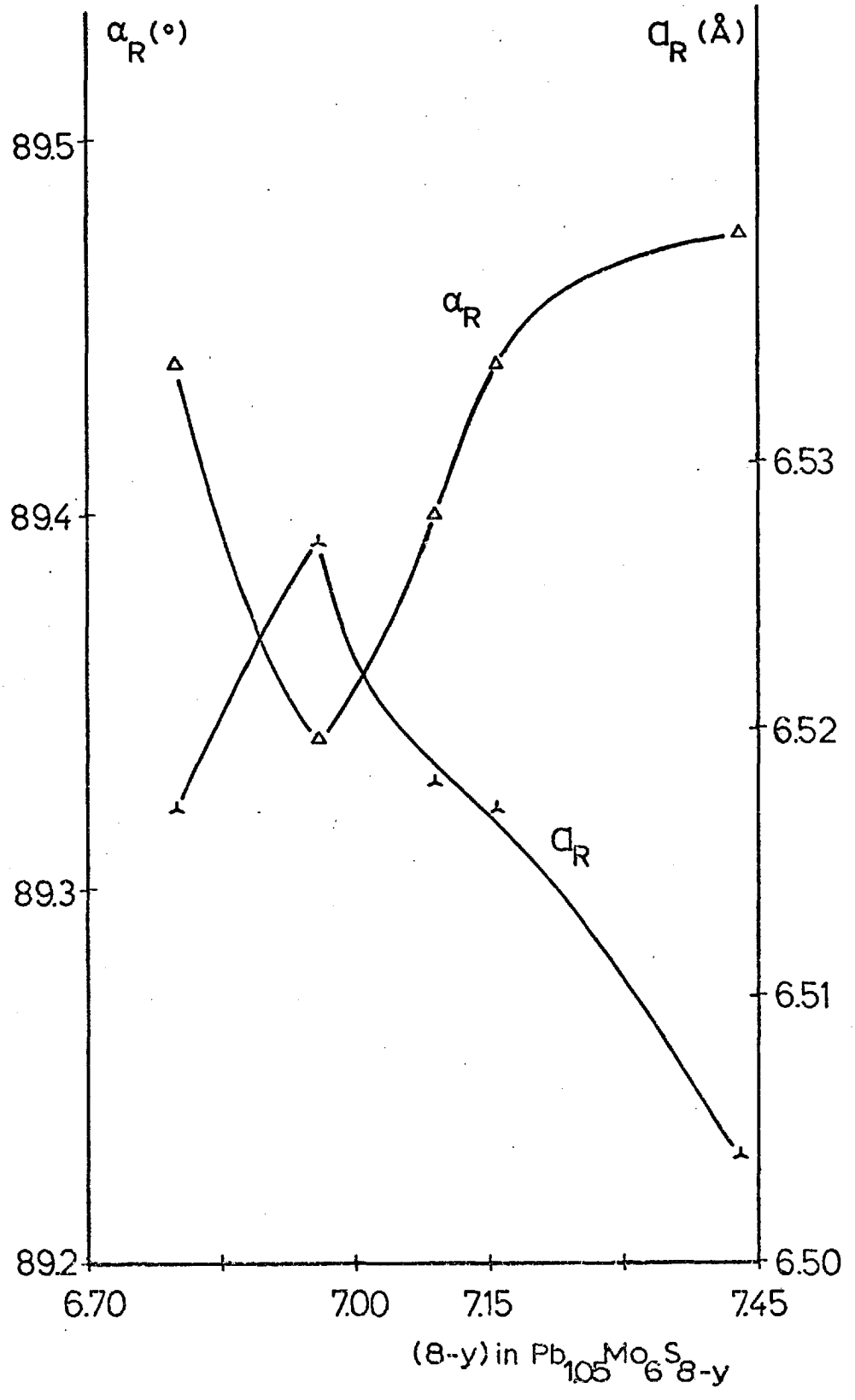
slightly higher value at 8, while a_R value decreases montonically.

Inside the single phase region, α_R angle increases with sulphur content. This can be argued that the gradually increasing occupancy of S(2c) sites enhances the attractive interaction between the clusters. The closer these clusters are, the larger the α_R value should be. The a_R distance also increases with (8-y) value. Apart from the contracting force between the clusters, there is a repulsive force generated at the cavity centred at $(0, \frac{1}{2}, 0)$ when the M_2 sites are occupied. When a high percentage of S(2c) sites is occupied, the tetrahedral M_2 sites thus formed are favoured by the copper atom. This not only gives a stronger repulsion force, but also reduces the contracting interaction. As the result of larger separation between clusters, a_R is larger. In lead Chevrel phases, the a_R value behaves in an opposite way (fig. 22). This is probably because the M_2 sites cannot be occupied by lead atoms and the contracting force dominates the variation of the a_R value.

Outside the single phase region, the variation of the lattice parameters w.r.t. sulphur content is not easy to explain. If the impurity phase is not interfering with the ternary phase, the lattice parameters would have remained at the same values as at the phase boundary. This type of change is, however, not seen which may suggest that some sort of interference by the impurity phase is occurring. The fact that copper can be intercalated into TiS_2 (53), may indicate that the layered MoS_2 phase could serve as a host for copper ions. Therefore, on the sulphur rich side, the re-distribution of copper ions between the ternary phase and the emerged MoS_2 phase can lead to a decrease of copper content in the Chevrel phase. As a result of this decrease, both parameters decrease, which is a consistent observation with the later study on the effect of copper content on lattice changes (section IV-2). On the sulphur poor side, Mo metal is rejected. The changes of the parameters are significant, especially the α_R angle. It is not certain which type of interference is operating here.

In summary, the single phase region of $Cu_2Mo_6S_{8-y}$ seems to occur at an (8-y) value from 7.7 to 7.85. This corresponds to a molybdenum valency between 2.23 and 2.28. When more sulphur is

Figure 22: Lattice Parameters of $Pb_{1.05}Mo_6S_{8-y}$ as a Function of (8-y). (Ref. 51)



present, MoS_2 forms. If the sulphur content is lower than 7.7, Mo metal co-exists with the ternary phase. The variation of the rhombohedral lattice parameters within the single phase region can be described in terms of the occupancy of M_2 sites as the non-stoichiometry of sulphur changes. The defect structure based on sulphur deficiency is adopted in the argument.

2-2. Hot-pressing of $Cu_2Mo_6S_{8-y}$ Phases:

It has been difficult to obtain single crystals of Chevrel compounds. Small crystals just large enough for x-ray work can be grown. For analytical purposes and diffusion measurements, these crystals are not suitable. In order to obtain samples of density close to the unit cell density for diffusion measurements, the hot-pressing technique was chosen. (Since this part of the present investigation had started, there were reports about the preparation of large single crystals by fusion of the pre-reacted Chevrel compounds in a high-pressure argon furnace (41, 52). Single crystals of $Cu_{1.8}Mo_6S_8$ of size 3 cm^3 could be obtained by this method.)

The results of several attempts are listed in table 7. Apparently, the temperature is an important factor in achieving high density. However, an excessively high temperature can create MoS_2 as on the x-ray Guinier film a faint diffraction line at $d = 6.1\text{Å}$ from a sample hot-pressed at 1450°C is visible. This further supports the point that the Mo_6S_8 unit is a metastable phase which decomposes at high temperature. An exceptionally high density is measured on sample no. 2 despite the occurrence of grain growth. A rather coarse powder starting material probably caused the grain growth. The reason for the resulting high density is perhaps contamination with high density material, like Mo metal ($d = 10.28$ g/cm^3). The temperature of 1325°C seems to produce best results and this temperature was used for fabrication of the dense specimen.

The x-ray diffraction patterns of the sample before and after hot-pressing are compared. The overall pattern remains

Table 7: Hot-press Results of $Cu_2Mo_6S_{8-y}$

No.	Compound	Temp.(°C)	Pressure(Nm^{-2})	Press time	Resultant density	% theoretical
1	$Cu_2Mo_6S_{7.65}$ (I)	1050	9×10^7	4 hours	4.669	80.4
2	$Cu_2Mo_6S_{7.65}$ (I)	1325	5×10^7	2 hours	5.786	99.7
3	$Cu_2Mo_6S_{7.65}$ (II)	1235	5×10^7	20 mins	4.87	83.7
4	$Cu_2Mo_6S_{7.65}$ (II)	1450	5×10^7	5 mins	4.975	85.6
5	$Cu_2Mo_6S_{7.65}$ (II)	1325	5×10^7	2 hours	5.408	93.0
6	$Cu_2Mo_6S_{7.59}$	1325	5×10^7	2 hours	5.692	98.4

identical. In table 8, the lattice parameters changes of the samples on hot-pressing are tabulated. The differences are small but significant. The trend of change indicates an increase of the Mo/S ratio. This increase can be reached by either losing sulphur or gaining Mo during hot-pressing. If the sample suffers from a substantial sulphur loss, Mo metal should be seen. This occurred in the sample $Cu_2Mo_6S_{7.65}$ but in $Cu_2Mo_6S_{7.59}$, the Mo peak of the original powder disappeared after hot-pressing. Apparently, the higher sulphur content sample has a larger capacity for Mo dissolution. When the sample is hot-pressed at a temperature higher than the preparation temperature, Mo dissolution takes place. An increase of Mo/S ratio varies the lattice parameters. In the case of the other sample, the sulphur loss at the high temperature has a larger effect on the already low sulphur content. Mo metal is thus deposited. The finding of the former case indicates that the sulphur loss under these conditions is not heavy. Otherwise, Mo deposition rather than dissolution would have happened.

The small sulphur loss is not a problem for the fusion of Chevrel phase at high vapour pressure. The decomposition of the phase through sulphur loss will be retarded by the high argon pressure. It is the thermal stability of the Mo_6S_8 lattice at high temperature (1550-1750°C) which is doubtful. Based on the result of the present investigation, the MoS_2 separation in these samples might have happened at the fusion temperature. But there is no mention about the phase-purity of the single crystals prepared by high pressure fusion and the solid produced from the congruent melt of $Cu_{1.8}Mo_6S_{8-y}$ from 1680°C (51).

IV. The Phase Study of $Cu_xMo_6S_{7.59}$:

The phase relationship between copper molybdenum sulphide and the sulphur content has been discussed. It is also known that the copper content in the compound is another parameter that determines the phases. It is important to acquire this information in order to test the applicability of this compound as SSE material. This aspect of the compound was reported on the specimens prepared

Table 8: Comparison of Lattice Parameter Changes on Hot-pressing at 1325°C

Sample	a_R	α_R	a_H	c_H
$Cu_2Mo_6S_{7.65}$ (II)	6.51442	95.174	9.61922	10.21522
$Cu_2Mo_6S_{7.65}$ (II) RF	6.49626	95.1153	9.58791	10.1994
$Cu_2Mo_6S_{7.59}$ (III)	6.51544	95.2212	9.62435	10.20659
$Cu_2Mo_6S_{7.59}$ (III) RF	6.50434	95.1201	9.60021	10.21108

at high temperature (41) but in that study, no sulphur non-stoichiometry was specified. In this section, phase study of a compound with a defined sulphur non-stoichiometry $Cu_xMo_6S_{7.59}$ will be reported. The coulometric titration method is used to alter the x value of the compound in place of high temperature preparation.

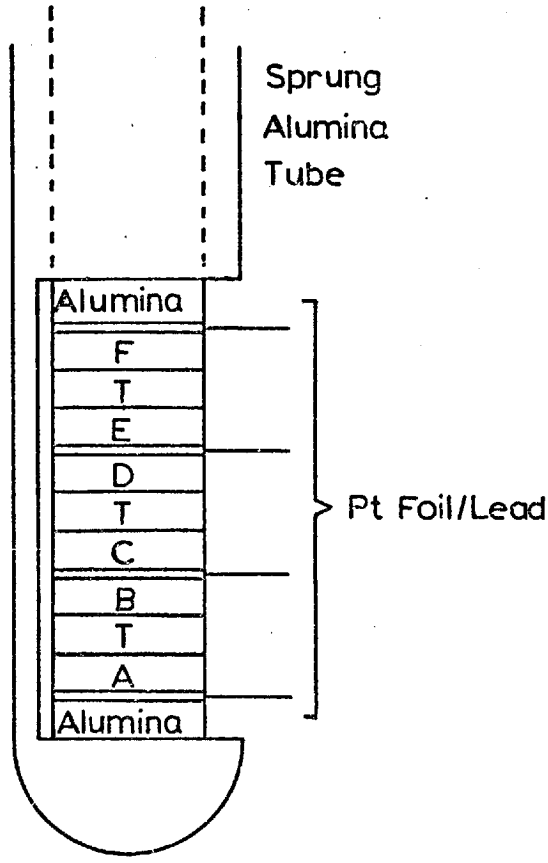
1. Experimental Procedures:

$Cu_2Mo_6S_{7.59}$ was prepared from the elements and hot-pressed at 1325°C with the same detail as previous described. A shoulder corresponding to Mo metal was seen on the x-ray diffractometer results of the hot-pressed sample.

The electrochemical cell is shown in figure 23. Because of the convenient starting composition, $Cu_2Mo_6S_{7.59}$ was used as a source and 'sink' of copper. The solid electrolyte used was so-called Takahashi compound, 94 $CuBr \cdot 6(CH_3)_2 C_6H_{12}N_2Br_2$, with the highest copper ionic conductivity of 3.5×10^{-2} $(ohm.cm)^{-1}$ at 20°C (4). The organic constituent was prepared by bubbling MeBr (Koch-Light) through a methanol solution of 1,4-diazobicyclo (2, 2, 2) octane (Koch-Light) at 0°C, followed by 2 re-crystallisations of the precipitate from methanol. Cuprous bromide (puriss. grade, Koch-Light) was re-crystallised from 10% hydrobromic acid under a nitrogen atmosphere. The constituents in the right proportions were ground together with methanol in an agate mortar and pestle. Having evaporated the solvent under vacuum, the mixture was re-ground and pressed in a 8 mm steel die with a 'G' clamp. The pellets were then loaded in a 8 mm graphite die with graphite spacers between the pellets, and hot-pressed at 170°C and 6×10^7 Nm^{-2} under vacuum for 20 hours. After the graphite at the surface was polished off, the pellets were used in the electrochemical cell. A typical ionic conductivity value of the pellet thus formed is 1.2×10^{-2} $(ohm.cm)^{-1}$ at 23°C. (More detail of this investigation can be found in reference (54).)

The electrochemical cell was operated at 95°C. By controlling the number of coulombs passing through the pair of

Figure 23: The Electrochemical Set-up for $Cu_xMo_6S_{7.59}$ Sample Preparation



A to F : $Cu_xMo_6S_{7.59}$

T: $94CuBr \cdot 6C_8H_{18}N_2Br_2$

samples, six specimens with different x values were prepared. A binary sample $Mo_6S_{7.59}$ was prepared by leaching a $Cu_2Mo_6S_{7.59}$ sample with half-diluted concentrated HCl solution in air for 10 days. These samples, together with the starting material, were examined by a Phillips x-ray diffractometer with Cu Kα radiation. AnalaR potassium bromide was used as an internal standard. The diffraction patterns were indexed and the lattice parameters were obtained by means of a least-square refinement computer program.

2. Results and Discussions:

The x values of samples A, B, C, D, E and F are 1.49, 2.51, 0.29, 3.36, 1.05 and 3.13 respectively. The final voltages between A & B, C & D and E & F are 128.6, -400 and 245.6 mV respectively. These values are in good agreement with the thermodynamic data obtained at 127°C which read 147.5 and 255 mV for A & B and E & F respectively.

The overall patterns of the samples remain similar. The 003 and 131 peaks are most shifted by changing the x value. Two weak peaks originally buried by these peaks are revealed as the result of the shift. One is at d = 3.42 Å and the other at d = 2.23 Å. The latter peak is identified to be the 110 peak of Mo metal. The relative intensity of this peak to 131 reflection of the ternary phase does not show any apparent relationship to x value. This eliminates the possibility of the precipitation of Mo metal when more copper is present in the phase. This also indicates that Mo metal is present in the compounds of high Mo/S ratio. The reason why it is not seen previously by x-ray is the presence of the broad 131 peak of the ternary phase. The density of the hot-pressed sample should therefore be considered lower than the figures suggest because of the contamination of the high density (10.2 gm/cm^3) Mo metal. It is interesting to note that the Mo peak is absent from the binary compound. This is probably because the long acid leaching removes not only the copper atom from the ternary phase but also the contaminating Mo metal.

The peak at d = 3.42 Å has not been identified. No

correlation of its abundance (measured by the intensity ratio of the peak and 003 peak) with the x value is visible. It shows that it is not generated by the copper removal but is seen because of the shift of 003 peak.

The MoS_2 phase is not seen throughout the whole range of x value. This means that this phase is not created even at very low copper content. The low operating temperature is probably inhibiting the growth of the phase.

The lattice parameters of the samples are plotted w.r.t. x value in figure 24. The values are in good agreement with other investigation (41) except at the high copper side. Both lattice parameters of the rhombohedral cell increase with x value. After the sharp increase when changing from the binary to the ternary phase, the parameters remain almost constant up to an x value of 1. The M_1 sites are populated at a low level in this range of x value. Together with the low percentage occupancy of S(2c) sites, the intercluster interaction along the ternary axis is not expected to be affected as the x value increases. Beyond this range, further filling of the M_1 sites by copper atoms brings in the contracting effect which is shown by the ascending α_R angle. An increase is also found in a_R value. The actual reason of this increase is not known. One possible cause of the expansion of the lattice is the weakened intercluster Mo-Mo interaction when copper content is building up in the phase. The increasing intracluster bondings at higher x value indicates that the non-bonding orbitals of Mo atoms may have been used in these bondings and thus their contribution to the intercluster interaction is reduced. When the M_2 sites begin to be occupied, an increase of a_R value is seen. The α_R angle also increases but at a moderate gradient after the saturation of M_1 sites. The already high occupancy on M_1 sites may restrain the contracting force. The slight drop of both parameters at the high copper content brings the previous results (41) off the curve. Although it is possible to interpret this drop in terms of the M_2-M_2 interaction between the adjacent cubes, the argument does not agree with the deductions of the thermodynamic results (see the following section). Had the M_2-M_2 repulsion caused the decrease of M_2 and increase of M_1 population, the $\Delta\bar{H}$ value should have decreased

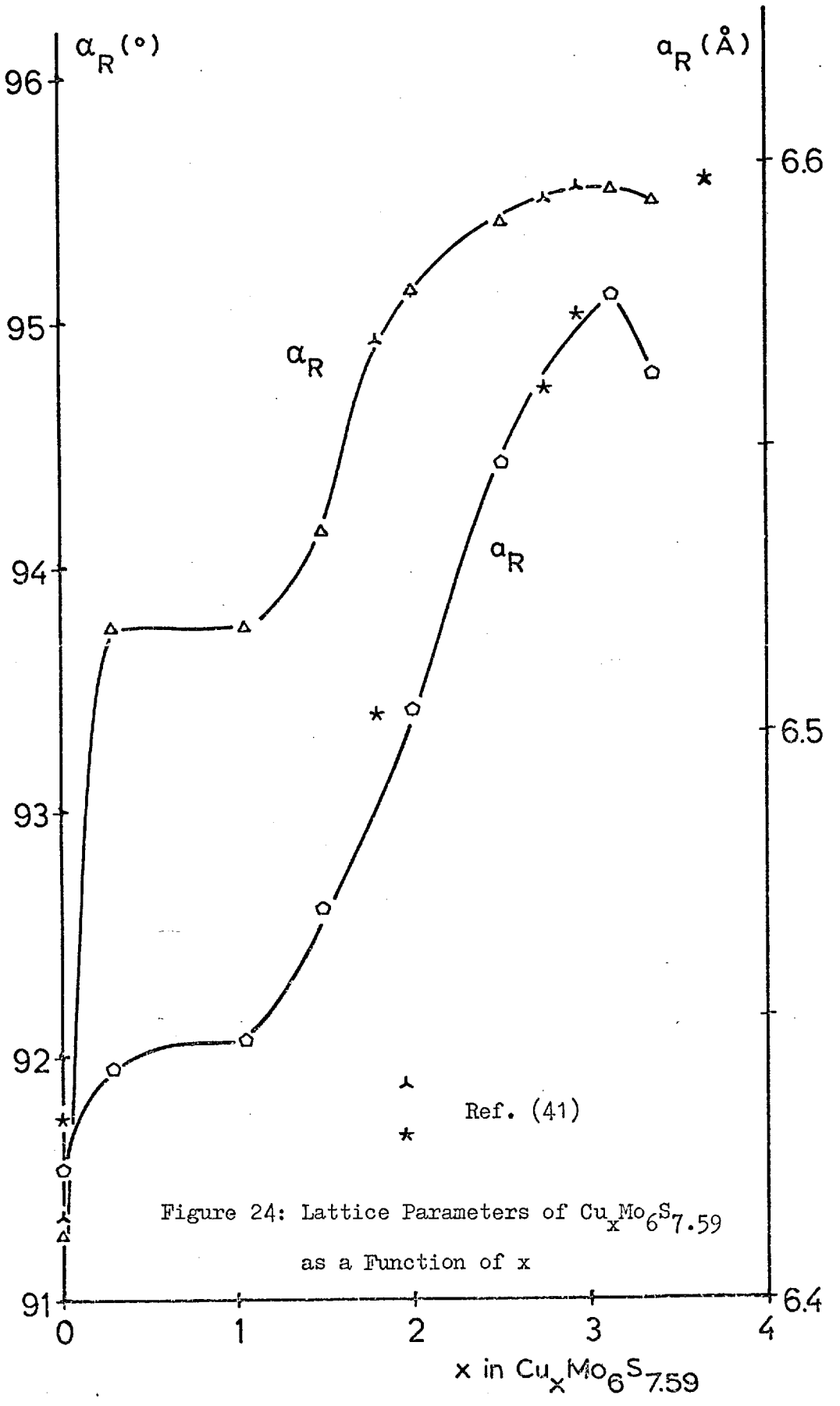


Figure 24: Lattice Parameters of $Cu_xMo_6S_{7.59}$ as a Function of x

at the composition (x = 3.13), which is not seen experimentally (fig. 27).

The volume of the hexagonal cell increases by 5.8% from x = 0 to 3.13, at which the largest change of lattice is recorded. The a_R and α_R values change by +2.4% and +4.7% for same range of x value. These values are smaller than the 10% c-axis increase in TiS_2 when lithium is intercalated into the phase to form $LiTiS_2$. This puts copper molybdenum sulphide in a good position to be a 3-dimensional ionic conductor.

V. Solid State Electrochemical Study of Copper Molybdenum Sulphide:

1. Experimental:

The copper molybdenum sulphide $Cu_2Mo_6S_{7.59}$ was prepared directly from elements at 1100°C in an evacuated silica tube. A bar of the size 5.5 x 1.2 x 1.2 mm^3 was cut with a high speed diamond saw from a specimen hot-pressed at 1325°C. The density of the specimen was 98.4% of thecretical value. Chalcocite (Cu_2S) was used as source and sink of copper. This material was prepared by heating sulphur and copper rod (both Specpure grade) in separate compartments of an evacuated silica tube. The tube was heated to 500°C and the temperature was maintained until the sulphur was no longer visible. The temperature was then raised to 900°C and held for a week. The sample thus prepared, after being ground to fine powder, was hot-pressed under vacuum in an 8 mm graphite die at 950°C for 2 hours with a pressure of 3×10^{-7} Nm^{-2}. Specimens were machined with a high speed diamond saw with paraffin lubricant. (For more details about chalcocite, see ref. (54).) The solid electrolyte, 94 CuBr.6 $(CH_3)_2$ $C_6H_{12}N_2Br$ (T), was prepared according to the procedures given in the last section. The hot-pressed pellets were polished inside the dry box to the appropriate size. For use as an ionic probe, a layer of copper metal was vacuum-evaporated on one flat surface of the specimen.

The solid state electrochemical cell assembly was shown in figure 25. The copper content of the sample was changed by coulometric titration. After a constant current had been passed

S: $Cu_xMo_6S_{7.59}$

T: 94 CuBr·
$6\,C_8H_{18}N_2Br_2$

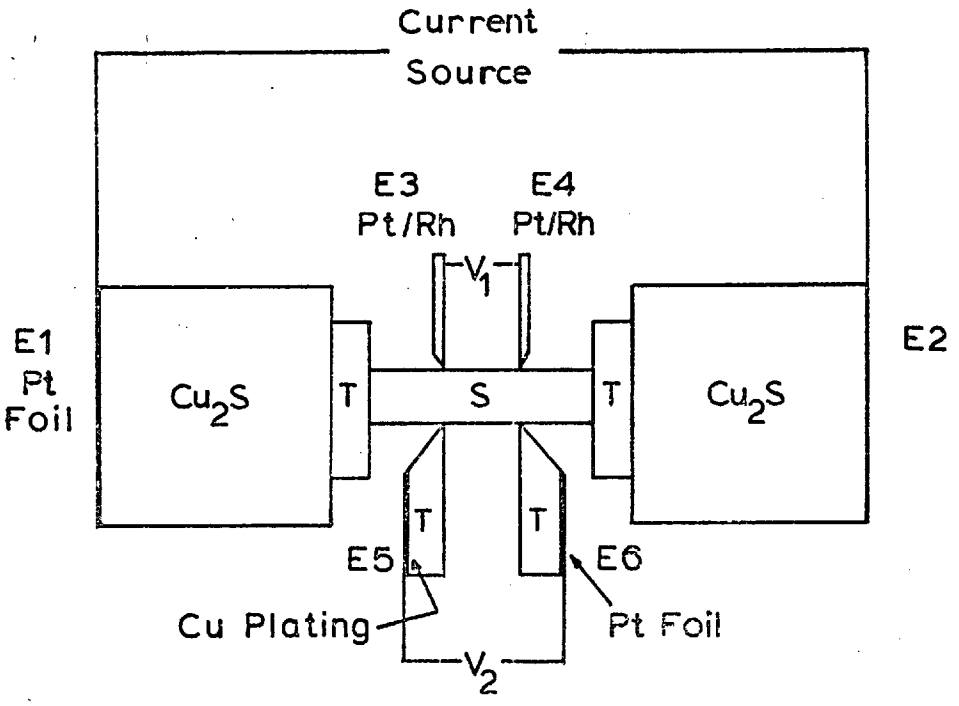


Figure 25: Experimental Set-up for 6-point Conductivity Measurement on $Cu_xMo_6S_{7.59}$

between E2 and E3 for a period of time, the voltage between the sample (E4) and the ionic probe (E6) was monitored until an equilibrium value was reached. The temperature was then varied and the equilibrium voltage change was recorded. From these, the thermodynamic data were inferred. To measure the ionic transport data, a constant ionic flux was passed through the bar (from E1 to E2 or reverse), the voltage across the ionic probes (E5 & E6) was monitored until the value was steady. The current was then switched off and the voltage between the ionic probes decayed to a steady value. The value of $\tilde{D}$ was then calculated with equations [A22] and [A16] (see the Appendix). The ionic conductivity was determined by equation [A20b]. The activation energy of chemical diffusion (ionic conductivity) was calculated by measuring the chemical diffusion coefficient (ionic conductivity) at different temperatures. The thermodynamic and ionic transport data as a function of copper content in the sample were acquired by repeating the experiment at different compositions. The temperature range used in these studies was between 396°K and 443°K. The voltage changes were monitored with a pre-programmed computer (Commodore 2001 Model).

2. Results and Discussions:

2-1. Thermodynamic Studies:

The EMF curve (fig. 26) of the cell is highly reproducible. Certain hysteresis was found in earlier studies (not shown) probably due to the experimental error of manual operation. There are 2 inflection points on the EMF curve, one at $x = 1.86$ and the other at $x = 2.63$. The first inflection point is very close to the concentration at the saturation of M_1 sites ($x = 2$). The deviation from $x = 2$ may be accounted for by the sulphur deficiency which can reduce the maximum copper content and hence change the populations of M_1 and M_2 sites. The second inflection point is not as obvious as the first one. On the whole, the EMF of the cell linearly increases towards copper unit activity as the copper content builds up in the phase. The $(\Delta E/\Delta X)$ is about

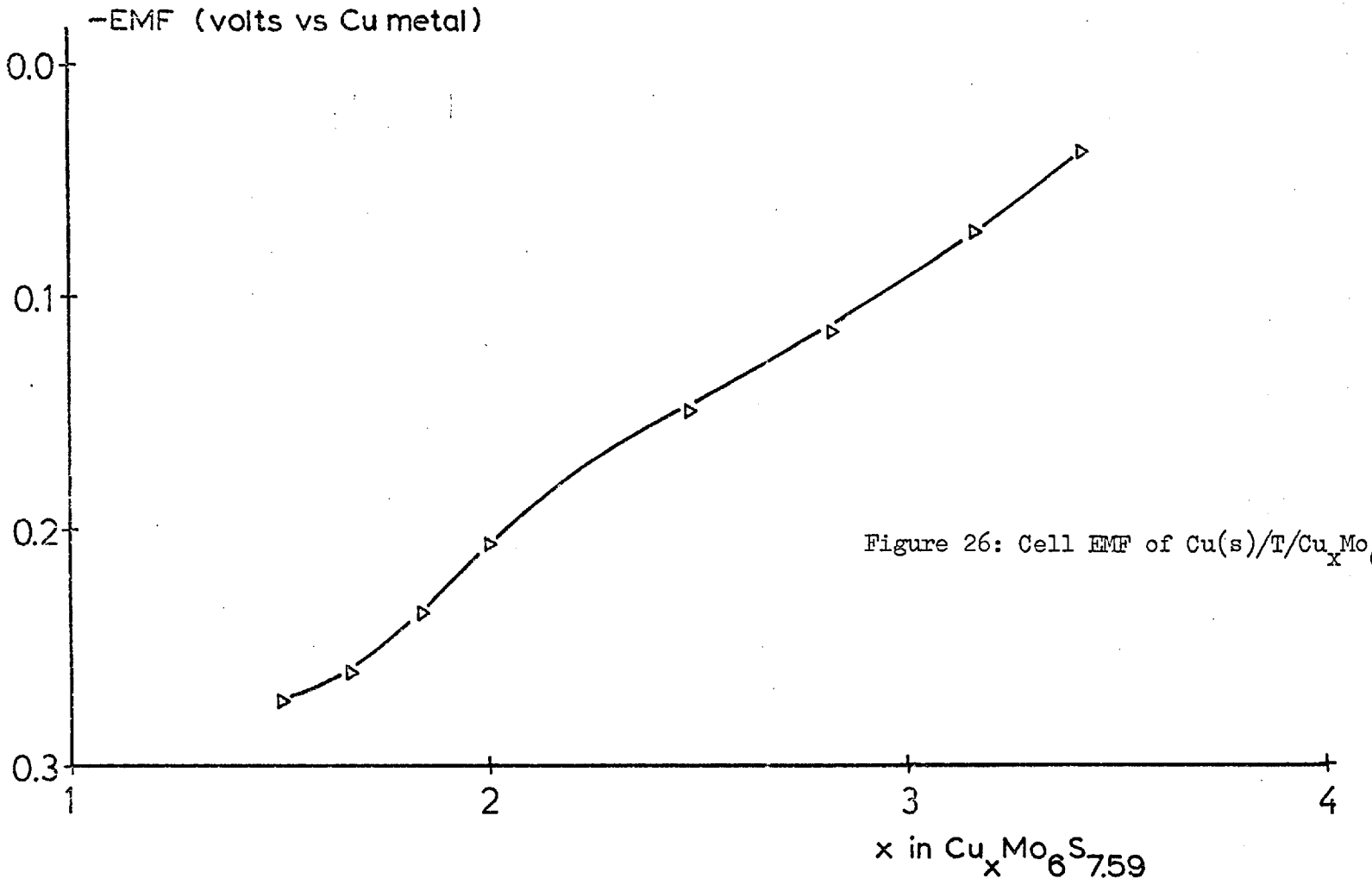


Figure 26: Cell EMF of Cu(s)/T/$Cu_xMo_6S_{7.59}$

115 mV/unit. No characteristic plateau of the 2-phase region can be seen on the curve.

Figures 27 and 28 show respectively the partial molar enthalpy and entropy of copper in $Cu_xMo_6S_{7.6}$. The $\Delta\bar{H}$ curve goes through a minimum point at x ~ 1.70 which coincides with the minimum on the $\Delta\bar{S}$ curve which occurs at x ~ 1.75. The configurational entropy change of mixing can be given as

$$\Delta S_{conf} = -R\ (X_A \log X_A + X_B \log X_B)$$

where X_i is the mole fraction of the i species, and A & B are designated as ions and vacancies respectively. In the case of perfect Chevrel phase and assuming M_1 and M_2 sites are degenerate, a maximum point on the $\Delta\bar{S}$ curve would occur at x = 2, where the concentrations of ions and vacancies are equal. However, M_1 is the more favourable site. When the x value is less than the M_1 saturation composition, the entropy change will result from the occupation of these sites only. When M_2 sites begin to be populated, the extra configurational arrangement lifts the entropy and an increase results. With further increase of M_2 occupancy, however, the situation becomes similar to the one where M_1 and M_2 sites are degenerate. A maximum point at x = 2.07 followed by a steady decrease in $\Delta\bar{S}$ are then observed. The electronic contribution to the entropy term is limited because the high density of states at the Fermi level should have little effect on the entropy change when the copper content increases.

The partial molar enthalpy of copper ions can be expressed as

$$\Delta\bar{H} = n_1E_1 + n_2E_2$$

where n_i is the number of copper ions at the M_i site with energy E_i. The sharp increase of enthalpy after x = 1.70 may be due to the starting of M_2 occupation. The change of slope at x = 2.63 coincides with the second inflection point on the EMF curve. The nature of this change is not clear yet.

Dudley and Steele (55) have developed a statistical model

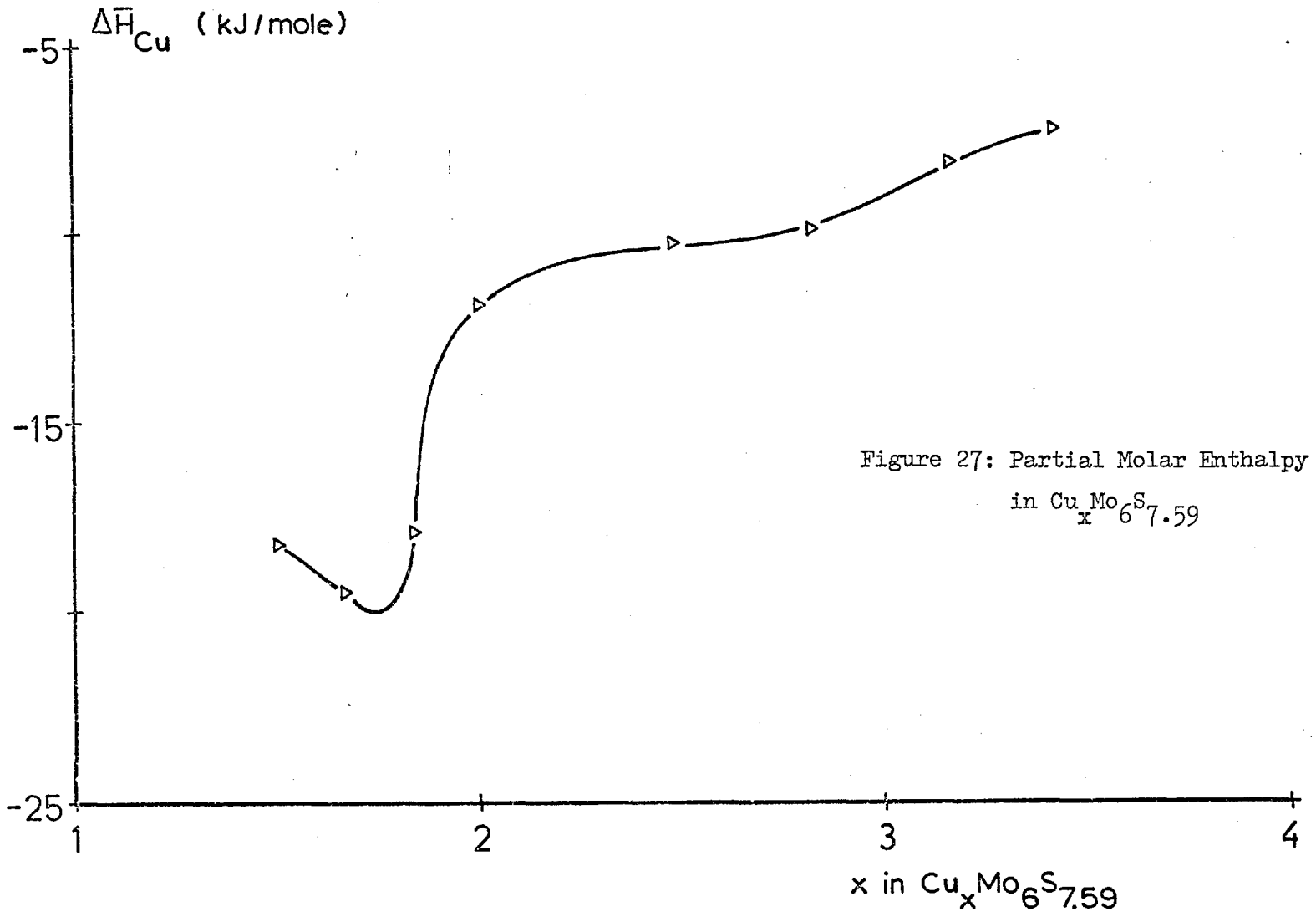


Figure 27: Partial Molar Enthalpy of Copper in $Cu_xMo_6S_{7.59}$

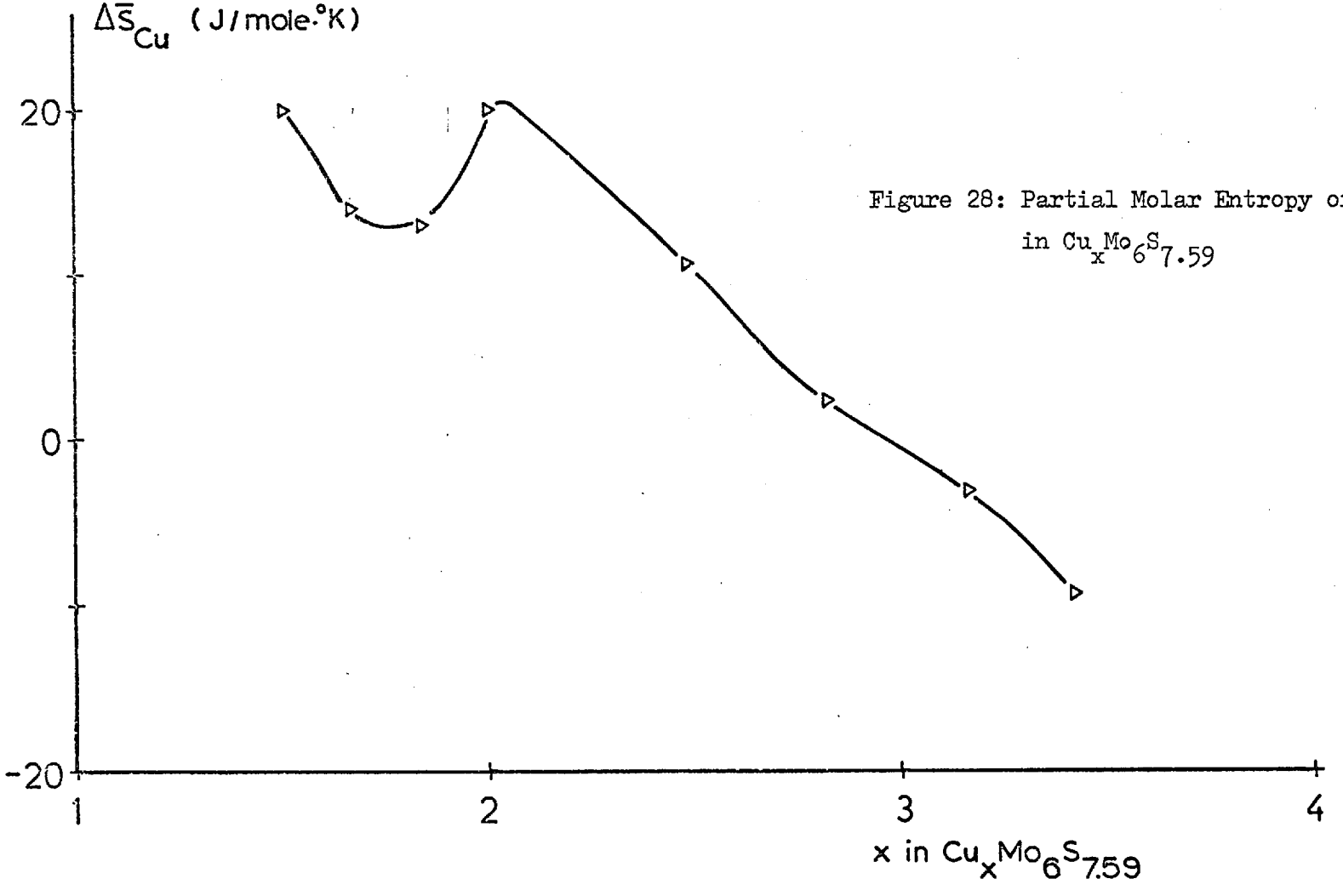


Figure 28: Partial Molar Entropy of Copper in $Cu_xMo_6S_{7.59}$

for the distribution of ions over two different sites. Despite the neglect of the cation-cation interaction, the experimental results agree well with the description of the model.

2-2. Ionic Transport

Because of the high electronic conductivity of Chevrel compounds, the electronic probes did not respond to the ionic flux and no effort was made to measure the electronic conductivity at general copper contents. (Electronic conductivity will be significant until the sample is saturated with copper, when there is an energy gap between the occupied and empty energy levels. This property has been studied by Dudley (56).)

The ionic conductivities together with its activation energy and the chemical diffusion coefficients are given as a function of copper contents in figures 29 and 30 respectively. The high $\tilde{D}$ value of the order of 10^{-5} cm^2/s can be achieved at $3.3 \geq x \geq 2.5$ at $400^{\circ}K$ and a low activation energy of ~ 20 kJ/mole is also measured. The transport properties improve as the copper content increases. The reduced activation energy when the M_2 sites are populated is obviously displayed in figure 29. The difference of about 10 kJ/mole contributes to the energy difference between the copper ions at M_1 and M_2 sites. A small increase of E_a from $x = 2.50$ to 3.14 and a trend towards a smaller E_a value at high x values can be seen. This complicated behaviour is not fully understood. The binding energy on the copper ions at M_2 sites should not be affected significantly by the change of copper content. The variation of E_a as function of x value suggests that the activation energy of diffusion consists of more than just the energy to liberate the copper ion from M_2 site. Furthermore, the σ_i value is not simply proportional to the increase of the concentration of charge carriers, indicating the E_a term is a more influential factor in ionic conductivity. It can be said that the copper ionic mobility in the Chevrel lattice is dependent on the copper content. However, the factors influencing the mobility are not known and there is no obvious energy barrier on the copper ion

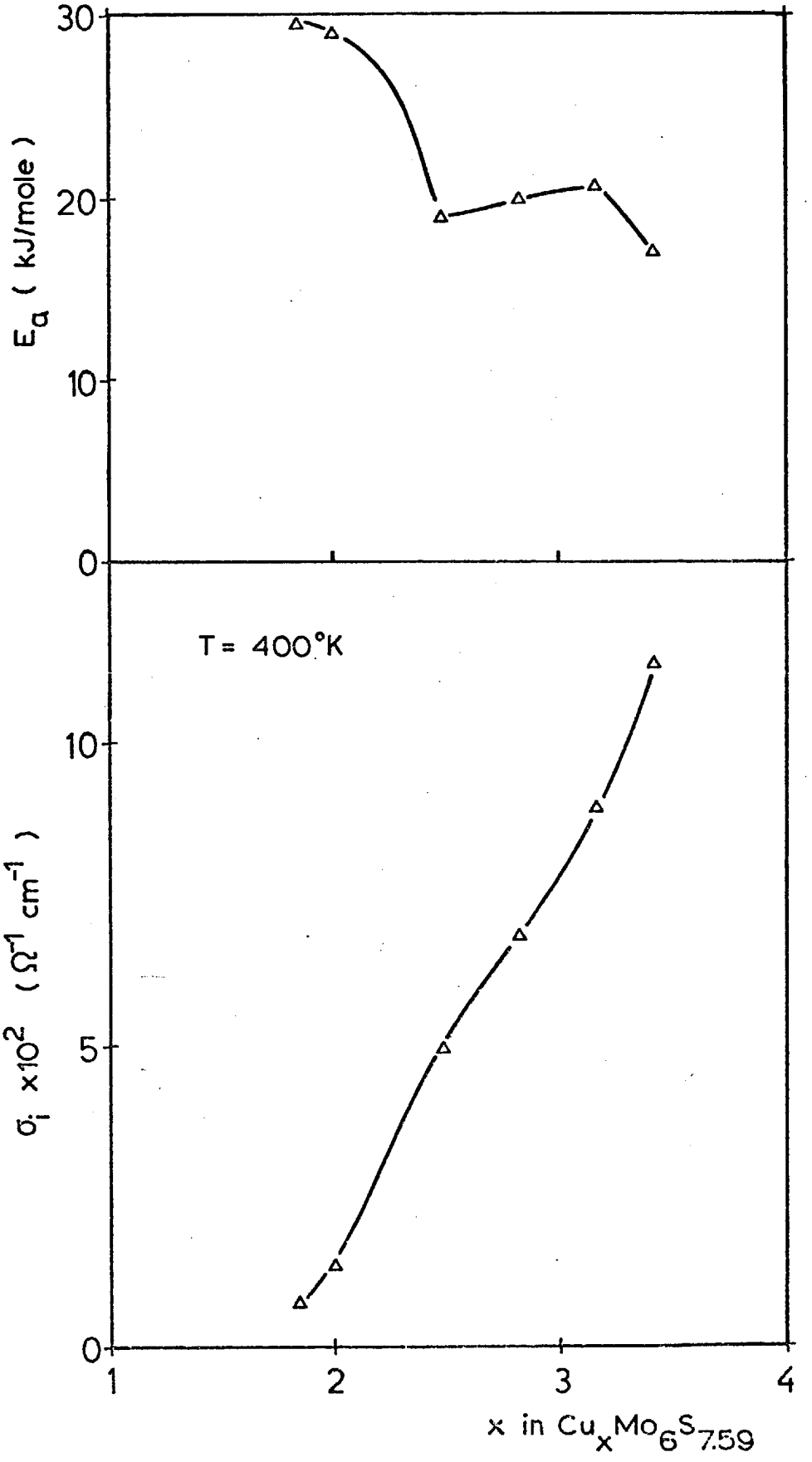


Figure 29: Ionic Conductivity and Activation Energy for Diffusion for Copper in $Cu_xMo_6S_{7.59}$

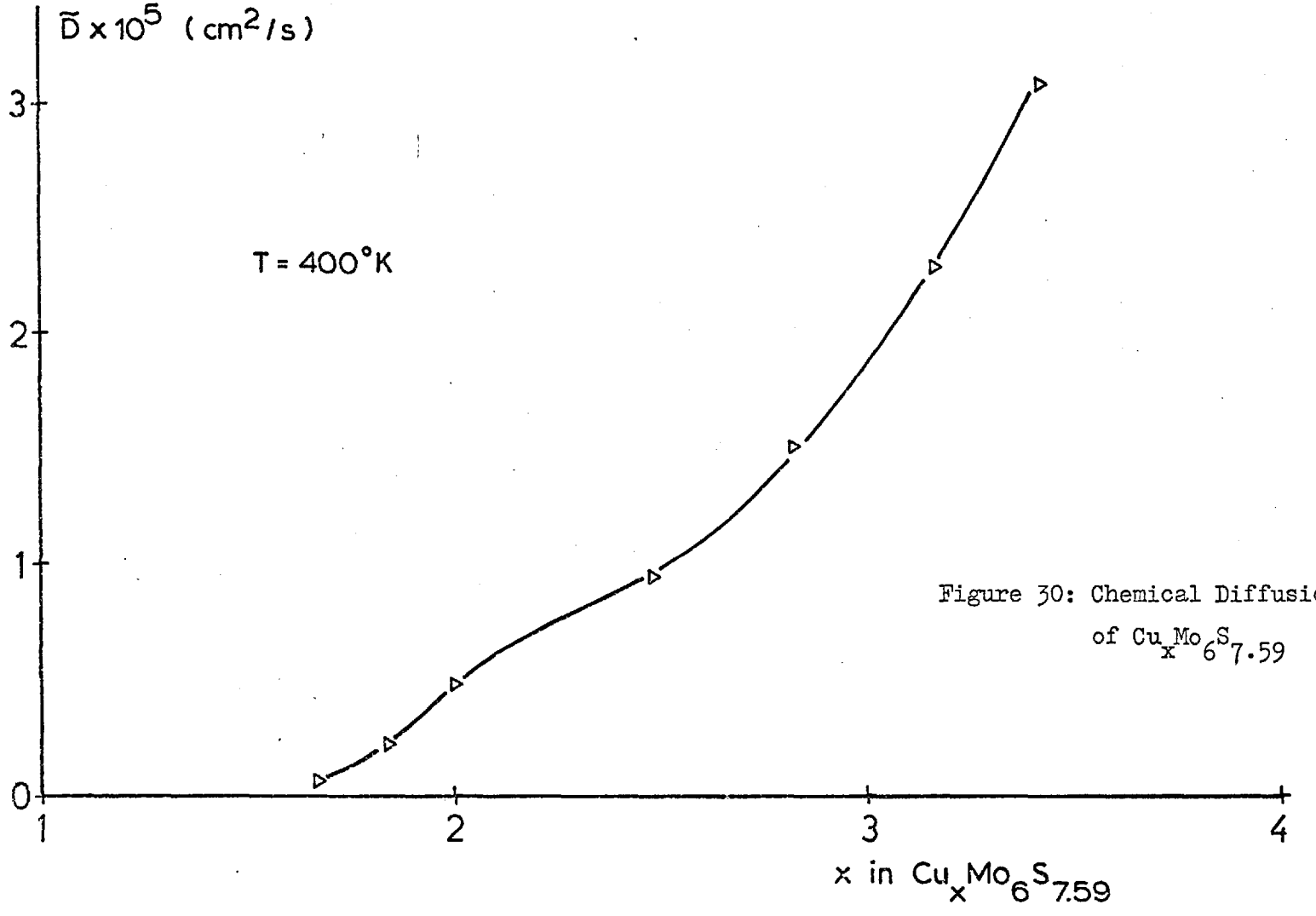


Figure 30: Chemical Diffusion Coefficient of $Cu_xMo_6S_{7.59}$

transport which may be responsible for the observed behaviour.

The ionic conductivity of $Cu_{3.31}Mo_6S_{7.59}$ is 0.105 $(ohm.cm)^{-1}$ at 400°K, which is better than the value 0.097 $(ohm.cm)^{-1}$ obtained on a sample of composition $Cu_{3.31}Mo_6S_{7.65}$. Whether this difference is the result of sulphur non-stoichiometry (it should give an opposite effect) or the density of sample (the high sulphur phase has a lower density of 93% theoretical value), is very hard to say when only 2 cases have been studied.

The very fast ionic conductivity in the Chevrel lattice may also suggest that the sulphur vacancy is probably a more reasonable choice than the molybdenum-in-the-channels to accommodate the non-stoichiometry of the phase.

The best ionic conductivity of copper Chevrel compound is compared in table 9 with other reported fast copper ionic conductors.

Table 9: Comparison of Fast Copper Ionic Conductors

Conductors	$\sigma_i (ohm.cm)^{-1}$	T (°K)	E_a (kJ/mole)	Reference
$Cu_{3.4}Mo_6S_{7.59}$	0.113	400	17.3	This work
$Cu_{5.41}Fe_{1.08}S_4$	0.11	443	-	(54)
$Cu_{1.75}Se$	0.1	400	5.5	(72)
T	3.5×10^{-2}	293	11.3	(4)
$RbCu_3Cl_4$	1.3×10^{-2}	413	13.5	(57)
$Rb_4Cu_{16}I_7Cl_{13}$	0.34	298	7.0	(58)

It is evident that copper Chevrel compound has a copper ionic conductivity comparable to the best copper ionic conductors.

VI. Summary and Conclusions:

Copper molybdenum sulphides $Cu_2Mo_6S_{8-y}$ have been prepared from the elements at 1100°C. The phase study indicates that the single phase region of the ternary compound is between $S_{7.7}$ to $S_{7.85}$. Higher sulphur content produces MoS_2 impurity phase while

Mo metal precipitation occurs in the sulphur-poor compounds. Samples of ~98% theoretical density can be obtained by hot-pressing the powder at 1325°C and 5×10^{-7} Nm^{-2} pressure. The changes of lattice parameters of the phase as a function of copper content are also studied. The results are not entirely understood especially at the extremes. The largest changes of α_R and a_R value of the rhombohedral cell are +4.7% and +2.4% respectively.

The thermodynamic and ionic transport data are collected by means of solid state electrochemical methods. The partial molar entropy change of copper ion can be described by the stepwise population of the two possible lattice sites, M_1 and M_2 sites, by copper ions. The same model does not, however, give a satisfactory description of the change of the partial molar enthalpy of the copper ion. The ionic transport is among the best for copper ionic conductors ever reported. The $\tilde{D}$ value of the order of 10^{-5} cm^2/s and σ_i value between 10^{-1} and 10^{-2} $(ohm.cm)^{-1}$ can be achieved with $3.3 \geq x \geq 2.5$ at 400°K. A low activation energy for diffusion of ~ 20 kJ/mole is also measured in the same range of x values. The long range ionic motion occurs through the M_2-M_2 passage linking the neighbouring cubes in 3-dimensions. The bottleneck of the passage can be represented by the intercluster Mo-Mo distance. For the sake of fast ionic conduction, M_2 sites have to be populated. This avoids the activation energy of transferring copper ions from M_1 to M_2 sites. The ionic transport properties continue to improve as the x value becomes larger. The increasing concentration of charge carriers affects the activation energy in some unknown ways.

For its rigidity of lattice, the absence of 2-phase equilibrium as copper is put into or removed from the phase and the fast ionic conductivity over a wide range of x values, the copper Chevrel phase promises to be a suitable 3-dimensional SSE material.

CHAPTER 4

LITHIUM MOLYBDENUM SULPHIDES

I. Introduction:

With the encouraging results on the copper molybdenum sulphide, it was very natural to try to study the lithium analogue. Although its existence was reported (33), lithium molybdenum sulphide has not been studied as thoroughly as other Chevrel compounds having interesting electronic superconductivity properties. Until recently, Schollhorn et al. (59) claimed that they could electrochemically introduce lithium into Mo_3S_4. The reaction seems to occur fairly fast and reversibly under dynamic conditions. No information was provided, however, about the dependence of the transport properties upon composition or structure. It was considered appropriate, therefore, to investigate these aspects of lithium molybdenum sulphide.

II. Preparation, Characterisation and Fabrication of Lithium Molybdenum Sulphide:

Chevrel et al. (33) first prepared lithium molybdenum sulphide by hydrogen reduction of $LiMoS_2$ at 950°C for 24 hours. The product was determined to be $Li_2Mo_2S_3$ with the rhombohedral cell parameters a_R = 6.622 Å and α_R = 94°32'. If this formula is converted to the general form (on Mo_6 unit), it is very tempting to express it as $Li_2S \cdot Li_4Mo_6S_8$. The co-existence of Li_2S is of course undesirable for interpretation of the results. Another disadvantage of this method is the lack of control of the sulphur stoichiometry which has been demonstrated to be a vital factor affecting the structure of the phase.

Another accidental preparation of Chevrel compounds was reported by Schollhorn et al. (60) in a recent publication. This was done by treating MoS_2 in sodium metal and NaCl at 900°C. The

solid residue was washed with water. One product, when examined by x-ray diffraction, showed a similar pattern to that of the binary Chevrel phase. The binary phase, instead of the ternary phase, was formed because the washing process had removed the sodium ions from the phase.

To prepare the lithium Chevrel compound, there are two possible routes. One is to lithiate the binary compound Mo_6S_8 which can be prepared by removing M from the ternary compound $M_xMo_6S_8$. Another route is using the ionic exchange method which has been used successfully with β-alumina. It is known that the crystal will break down when the third element is removed from the phase. If the ionic exchange can be performed, the equilibrium should maintain a situation whereby the lattice sites are occupied by one ion or the other. This is very important because the occupation of the sites will ensure the integrity of the sample. Ionic exchanging a hot-pressed specimen of copper molybdenum sulphide to a high density lithium Chevrel compound could become a very useful technique.

1. Ionic Exchange

1-1. Introduction

Molten nitrate salts have been employed successfully in β-alumina studies (61). The fast ionic diffusion in the solid state enables the ions to establish an equilibrium between the melt and the solid. With suitable control of the equilibrium, the desired ion can be introduced into the solid phase. The preparation of lithium beta-alumina illustrates this principle. Direct exchange of sodium β-alumina in lithium nitrate melt will only produce Li^+-Na^+ beta-alumina (62). To prepare lithium beta-alumina, silver beta-alumina is exchanged in a $LiCl/LiNO_3$ melt.

$$Li^+_{(m)} + Cl^-_{(m)} + Ag\text{-}\beta\text{-}Al_2O_3\ (s) \rightarrow$$

$$Li\text{-}\beta\text{-}Al_2O_3\ (s) + AgCl\ (solu.)\ \text{at } 350^\circ C.$$

The formation of the stable AgCl shifts the equilibrium in the desired direction and the lithium beta-alumina can be obtained.

The technique developed on the β-alumina system cannot be directly applied in this system though. Silver molybdenum sulphide is not a very suitable starting material because its relatively small α_R angle suggests a slower diffusion rate. Exchange was therefore carried out entirely on copper Chevrel compound. Apparently, the problem seems to be to find a suitable complexing agent to stabilise the copper ion either in a melt or in a solvent. Complexes of Cu(II) have been extensively studied in all sorts of media. However, very few Cu(I) complexes are known. Oxidation of Cu(I) to Cu(II), no doubt, will ease the choice of the complexing agent. However, redox reaction also complicates the situation on lithium and sulphur. As the expected product is a lithium compound, a medium of either an aprotic solvent or a molten salt under inert atmosphere is probably a reasonable choice.

1-2. Experimental:

Two solvents were used, namely, water and acetonitrile. The purification of the former was by standard distillation. GPR acetonitrile obtained from BDH was treated with P_2O_5 for 2 days, followed by fractional distillation under nitrogen gas flow. The first 10% (volume) and the last 15% of the original solvent were discarded and the collecting temperature was 80.5°C. In the receiving flask, dry molecular sieve (Hopkin & Williams, type 3A) was used to keep the solvent in an anhydrous state.

The lithium salts used were lithium chloride monohydrate (Koch-Light, pure A.R.), hydrous lithium thiocyanate (BDH, laboratory reagent) and ethylenediaminetetraacetic acid (EDTA) dilithium salt (Koch-Light, pure). In making the lithium chloride solution in acetonitrile, the salt was dried in an oven at 132°C for 1 day and then transferred to the dry box, in which the dissolution took place. The solubility of the salt was low and the saturated solution was stored over molecular sieve. When ethylenediaminetetraacetic acid dilithium salt (Li_2H_2Y) was used in aqueous solution, there was no pre-treatment.

The apparatus used in the molten-salt exchange is given in figure 31. A large excess of lithium salt was placed inside the alumina tube and dried under dynamic pumping at 200°C and 150°C for LiCl and LiSCN ($LiSCN/Li_2H_2Y$) melts respectively. After a few days, the system was cooled down and a specimen was loaded into the small alumina crucible with slots cut at the bottom to enable easy access of the melt. Prior to the immersion of the crucible into the melt, the whole system was further dried under the same conditions as the preliminary drying for another day. The temperature was raised to a value slightly over the melting point of the salt. Argon gas was then let through to fill the system before the alumina rod was lowered to bring the sample in contact with the melt. The specimen after exchange was washed with dried methanol in an extraction unit. It was then dried at 100°C under vacuum and weighed. The weight change after the exchange was used as a preliminary indication of the extent of the reaction.

When the occasion demanded, the sample was examined by a Phillips x-ray diffractometer with Cu Kα radiation. The powdered exchanged sample was mixed with silicone grease and spread onto a glass sample holder for x-ray diffraction. Only on one occasion was the composition of the exchange sample examined by atomic absorption (AA) spectroscopy by the Hydrometallurgy Group at Imperial College. The method used was similar to the one outlined in the previous chapter.

1-3. Results and Discussions:

Table 10 tabulates the results of ionic exchanges. The media LiSCN melt, CH_3CN and aqueous solution are obviously not suitable for the purpose. The two complexing agents SCN^- and CH_3CN are not strong enough to hold Cu(I) in the liquid phases. In Run No. 2, a weight gain was actually recorded indicating that lithium had entered the solid phase but no exchange had occurred. The different weight losses in the Li_2H_2Y aqueous solutions in different gas atmospheres have suggested that Cu(II) is a much easier ion to complex than Cu(I). The crumbling of the sample after

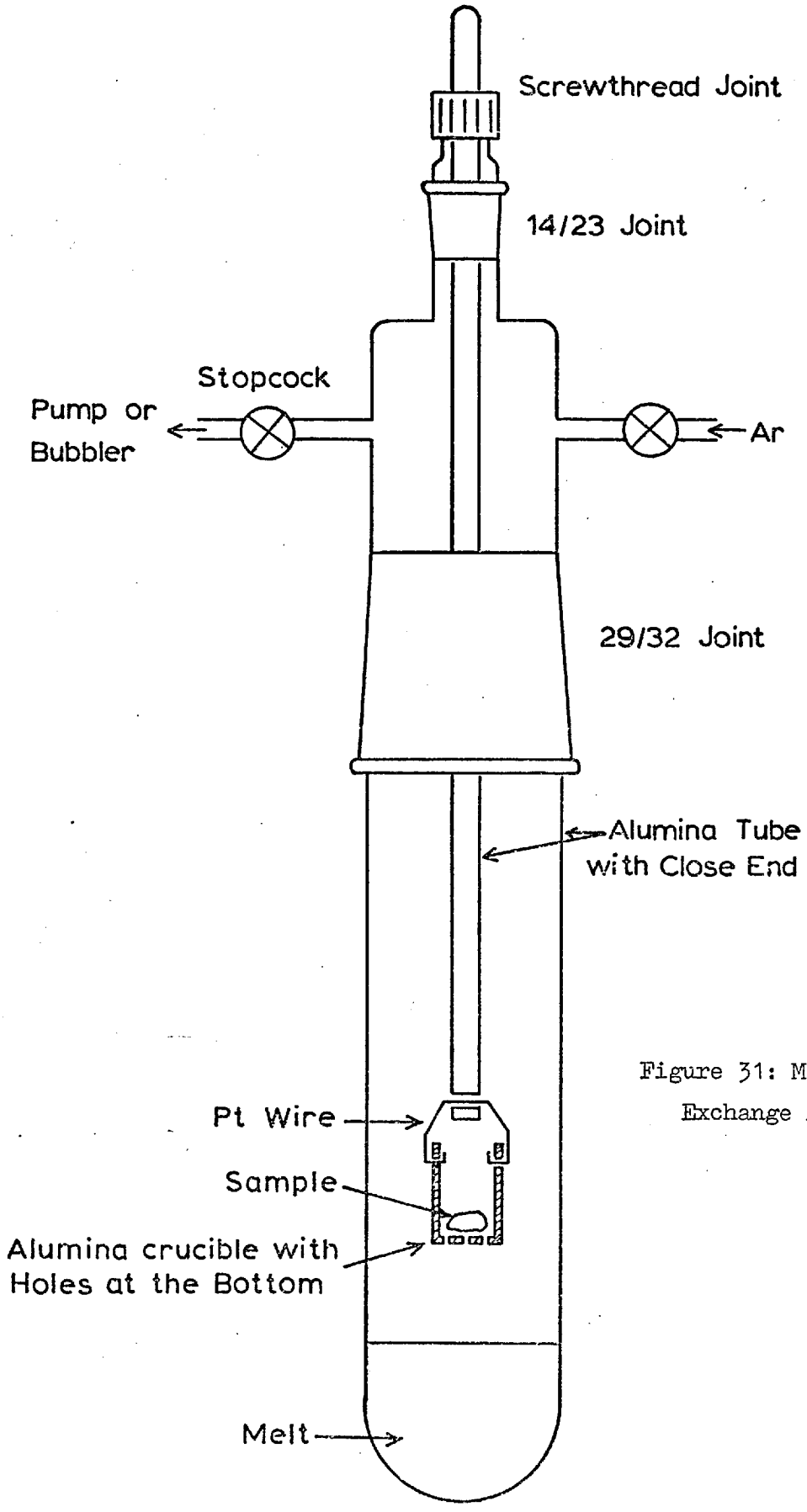


Figure 31: Molten Salt Exchange Apparatus

Table 10: Results of Ionic Exchange on Copper Chevrel Compounds

Run No.	Solid Phase	Liquid Phase	Temp. and gas atmosphere	Reaction Time (hours)	Weight Change (%)	Observation & Remark
1	$Cu_2Mo_6S_8$ (+ MoS_2)	LiSCN	200°C, N_2	24	0	-
2	Sample after Run 1	LiSCN	250°C, Ar	24	+ 1.74	
3	$Cu_2Mo_6S_8$ (+ MoS_2)	Li_2H_2Y, 0.05M aq. solu.	70°C, Ar	48	- 0.6	
4	$Cu_2Mo_6S_8$ (+ MoS_2)	Li_2H_2Y/LiSCN - 3 x 10^{-3}M	250°C, Ar	28	+ 2.19	Sulphur condensed on the cold part of the apparatus
5	$Cu_2Mo_6S_{7.65}$ (HP)	Sat'd Li_2H_2Y aq. solu.	r.t., N_2	77.5	- 0.24	Sample intact
6	Sample after Run 5	Sat'd Li_2H_2Y aq. solu.	r.t., air	76	- 0.71 (refer to the wt. before Run 5)	Sample intact
7	Sample after Run 6	Sat'd Li_2H_2Y aq. solu.	55°C, air	61	- 1.67 (refer to the wt. before Run 5)	Sample crumbled
8	$Cu_2Mo_6S_{7.65}$ (HP)	LiCl/CH_3CN	r.t., N_2	72	- 0.68	
9	$Cu_2Mo_6S_{7.65}$ (HP)	LiCl	630°C, Ar	48	-12.65	Sample retained but cracks were found later.

the removal of the third element was also confirmed experimentally.

In Li_2H_2Y/LiSCN melts, the observed sulphur loss is unlikely to come from the solid phase because of the measured weight gain. The source of sulphur would therefore be the thiocyanate ion which undergoes an oxidation reaction:

$$2\ SCN^- - 2e \rightarrow S_2 + (CN)_2$$

The most promising result is the exchange in the LiCl melt. On the assumption that the measured weight change is only dependent on the third element change, the products $Li_{1.03}Mo_6S_{7.65}$ and $Cu_{0.11}Mo_6S_{7.65}$ can give the measured weight loss of 12.65%. The x-ray diffraction result shows the formation of MoS_2 and a pattern of a ternary Chevrel phase. However, AA analytical results indicate no trace of lithium is present in the solid phase. Therefore, the weight loss is derived from the copper removal and/or sulphur evaporation from the solid sample. The sample after exchange appeared to be intact. It was later found broken into 2 pieces and when it was polished some fine cracks were seen. The substantial loss of copper probably causes the break-down of the sample.

The application of the ionic exchange technique in the Chevrel compounds is not feasible, at least under the conditions used in this investigation. There are always other alterations which can be made to improve the technique. It is known that the halide ions, CN^- and NH_3 can form complexes with cuprous ions. The formation of e.g. $CuCl_2^-$, $CuCl_3^{2-}$ and $CuCl_4^{3-}$ species is a possible reason for the results on Run no.9. On the other hand, the chemical activity of lithium is generally low in solution. In order to force the equilibrium to shift in the desired direction, very reactive lithium reagents like lithium metal and n-butyllithium may be used. A lithium metal solution in liquid ammonia, a reagent used for lithiation purposes, may also be suitable for the exchange process. A possible difficulty will be the low temperature (b.p. of NH_3 is -33.35°C), at which the ionic motions are likely to be slow, so much so that the establishment of an equilibrium becomes doubtful. This problem will be discussed later with the

ionic transport properties of the phase.

2. Lithiation of the Binary Chevrel Phase:

Since the attempts based on ionic exchange techniques failed to work, attention was then transferred to the other route, namely, the lithiation of the binary Chevrel phase. The binary phase can be obtained by removing the mobile third element from the ternary phase with HCl (39). Lithiation of the binary phase can be performed by either the electrochemical method or the lithium metal solution in liquid ammonia (59). For reasons of convenience, n-butyllithium was chosen as lithiation agent.

2-1. Experimental:

The copper molybdenum sulphides used were prepared as given in the last chapter. The reagents used to leach the ternary phase were hydrochloric acid and ferric solution. Concentrated hydrochloric acid (Hopkin & Williams, AnalaR) was diluted by half. The acid was then poured into a flask and purged with nitrogen gas overnight. Heat was also supplied to the system for this period if a high temperature was required. The solid sample, in powder form, was added to the flask and the leaching was assisted by a magnetic stirrer. To recover the solid, the mixture was filtered and the solid was washed thoroughly with distilled water and alcohol. The powder was dried below 100°C and under vacuum for a few days. Ferric solution was prepared by dissolving dried $Fe_2(SO_4)_3$ (Hopkin & Williams, GPR) in 0.1 M sulphuric acid. The concentration of ferric ion was 0.03 M. The leaching procedures were the same as in HCl. When an inert gas environment was not required, the leaching was carried out in air. X-ray diffraction was used to identify the phase in the same way as previously mentioned. The product of the Fe^{3+} solution leaching was analysed by x-ray fluorescence by the Analytical Service Laboratory, Imperial College.

The binary compound was studied by means of high

temperature x-ray diffraction. A Guinier-Lenne camera with Co Kα radiation was used. Dried helium gas was used to prevent oxidation of the sample at high temperature. The binary compound was also thermally decomposed in evacuated sealed quartz tubes at different temperatures. The products were examined by x-ray diffraction with a Guinier camera.

When the binary phase had been dried thoroughly, it was transferred to a dry box. The lithiation of the binary compound was carried out with a measured amount of 2.4 M n-butyllithium (Alfa Products) to give a lithium content of 2.3 per Mo_6S_8. The reaction time was two days. The separated liquid phase after the reaction was analysed by acid-base titration to estimate the amount of lithium in the solid phase. The technique of the quantitative analysis was that given in an earlier chapter.

The lithiated compound was analysed by AA spectroscopy to determine the lithium content in the solid phase, and examined by a Phillips x-ray diffractometer. Silicone grease was used to protect the powder sample. A thermal test on the lithiated compound was performed by heating the sample in an alumina crucible inside an evacuated Pyrex tube to 455°C for 17 hours and at 471°C for a further 22 hours. The heated sample was checked by x-ray diffraction.

2-2. Results and Discussions:

(a) The binary phase:

Leaching the ternary phase by hydrochloric acid in a nitrogen gas flow does not lead to the binary phase as the literature claimed (39). X-ray results reveal that the ternary phase is the only product of the leaching in such conditions, even at elevated temperatures. The proposed reaction was

$$Cu_xMo_3S_4\ (s) + 2H^+_{(aq.)} \rightarrow x\ Cu^{2+}_{(aq.)} + Mo_3S_4\ (s) + H_2\ (g)$$

However, no gas bubbles were seen during this treatment.

Electrochemical consideration leads to the conclusion

that such a reaction is highly unfavourable as the standard emf value (E°) is negative

$$Cu^{+}_{(aq.)} + H^{+}_{(aq.)} = \tfrac{1}{2}H_2\ (g) + Cu^{2+}_{(aq.)} \qquad E^{\circ}=-0.153V \text{ at } 25^{\circ}C$$

The reported results were probably obtained in the acid solution which had not been purged. The dissolved oxygen takes part in the redox reaction. The redox couple O_2/OH^- and Cu^+/Cu^{2+} gives an E° value 0.618 V and the reaction should occur spontaneously. In this circumstance, no hydrogen gas is formed and the carrier nitrogen gas is not needed. Should more controlled conditions be desired, using Fe^{3+}/Fe^{2+} in place of the oxygen gives an exactly identical E° value. This positive potential enables the leaching to be carried out in an inert gas atmosphere, which at the beginning was thought necessary to prevent any oxidation of the sulphide.

Both reagents produce the binary phase as confirmed by the x-ray results. No contamination by iron is found in the binary phase which is obtained by means of ferric solution leaching. No attempt has been made to study the kinetics of the leaching. Satisfactory results are obtained by using HCl acid in air and ferric solution in a nitrogen atmosphere. The solid residue after the leaching is often in a fine particle form indicating the break down of the lattice by the removal of the third element. This phenomenon is also seen when a piece of hot-pressed specimen is leached. Using the ferric solution in air for a long period, however, produces MoS_2 phase. The appearance of an MoS_2 x-ray diffraction line indicates that the low oxidation state Mo in the Chevrel phase is susceptible to oxidation when the third element has been removed. On the contrary, prolonged treatment of ternary compound with HCl in air does not produce any MoS_2 but seems to dissolve any excess Mo metal present. Due to the problems associated with the occasional formation of MoS_2 when using ferric solution, the acid leaching was considered a more reliable method of preparing the Mo_6S_8 compound.

The sulphur vapour pressure of the binary compound is quite high. A sample heated to 200°C under dynamic pumping has given off sufficient sulphur vapour to condense on the cooler part of the

apparatus. The α_R angle of the sulphur-lost sample decreases by 0.03% and the a_R value does not register any measurable change. Although the structure is only perturbed to a small extent in this case, extended heat treatment would not be advisable.

As discussed in chapter 3, there is no obvious crystallographic link between the Mo_6S_8 and MoS_2 phases. As the MoS_2 phase has been complicating the study of the Chevrel phases, understanding of this phase is very useful and an attempt was made to study the transition of Mo_6S_8 to MoS_2 by means of high temperature x-ray diffraction.

The sample studied was $Mo_6S_{7.7}$ which was prepared by HCl leaching in air. The temperature scan was from room temperature to 470°C over 60 hours. The results are depicted in figure 32. The first appearance of the MoS_2 line (d = 6.2 Å) is seen at 394°C, a much lower value than the reported 468°C (39). No sign of the reported metastable phase is seen. Some other lines, such as the one at d = 3.43 Å, a group of three around d = 2.43 Å and 3 strong lines covering d values of 1.70 to 1.73 Å, appear at a similar temperature as MoS_2 phase. These lines do not correspond to Mo and Mo_2S_3 phases and their identities are not known. The confused situation is made worse when the decomposition products at 485°C and 1000°C in the evacuated sealed tubes are found distinctly different from those indicated on the high-temperature x-ray film (fig. 32). The thermal decomposition of the Mo_6S_8 has taken place at 480°C but the typical diffraction pattern of Chevrel phase is still there. However, the previously mentioned lines are completely missing. Further heat treatment of the sample at 1000°C leads to yet another new pattern. Characteristic lines of Mo_2S_3 phase are spotted at d = 5.5, 2.82, 2.24 and 2.1 Å. The presence of Mo metal is supported by the line at d = 2.22 Å. Again, the strange lines picked up by the high-temperature x-ray camera are not seen.

To draw any clear-cut conclusion from this series of experiments seems very difficult. The appearance of MoS_2 happens at a lower temperature, namely 394°C. Whether this lower value is because of the ever-decreasing sulphur vapour pressure at the sample surface or is due to the stoichiometry of the phase, is not

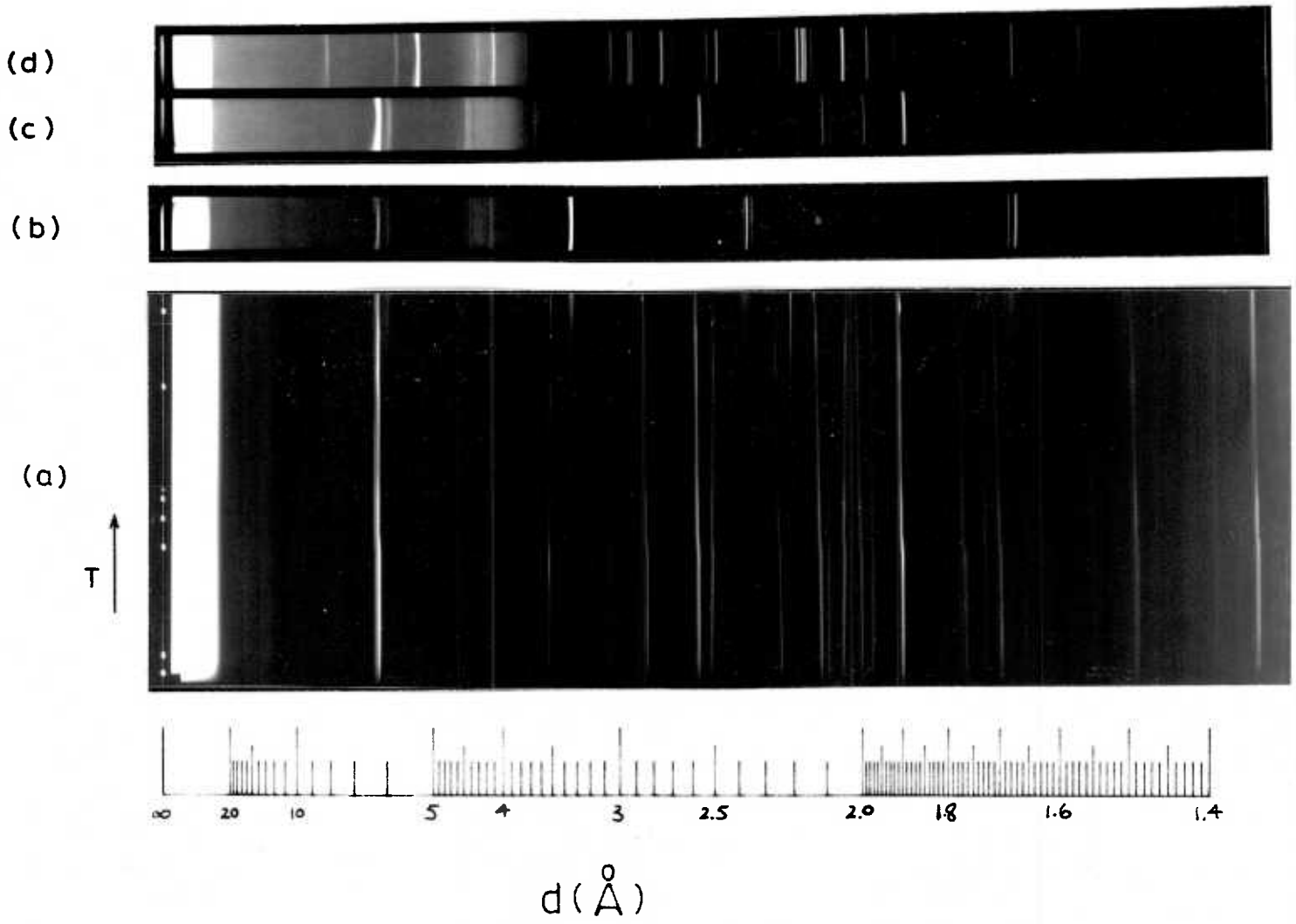


Figure 32: X-ray Diffraction Results of the Studies of Thermal Stability of $Mo_6S_{7.7}$
(a) High temperature study with a Guinier-Lenne camera; (b) The product of the (a) taken at r.t. (c) Sample heat-treated at 485°C; (d) Sample heat-treated at 1000°C.

clear. The only observation in this investigation which agrees with the previous work is the existence of Mo_2S_3 and Mo phases in the decomposition product at 1000°C, but they are by no means the only products. At this stage, to continue this investigation became very laborious and the study was called off.

(b) Lithium molybdenum sulphide:

The reaction between the binary compound $Mo_6S_{7.85}$ and n-BuLi is fairly violent if the glass container is swirled. The reaction is exothermic, and when the heat is released at a fast rate, the n-hexane solvent boils. This phase of the reaction ceases after roughly three hours. The x-ray diffraction pattern of the reaction product is very close to the starting binary compound. The values of a_R and α_R increase by 0.08% and 0.02% respectively. These minute changes in the lattice parameters do not provide firm evidence for the formation of the ternary phase, although reaction of some sort has undoubtedly happened. Further evidence supports the formation of the ternary phase. The thermal stability of the lithiated sample at 471°C indicates that the ternary phase is indeed formed (table 11). The AA analysis also confirms lithium in the phase and its content corresponds to a formula $Li_{2.0}Mo_6S_{7.85}$. The lithium content is slightly higher than the estimated 1.92 based on the result of the acid-base titration of n-BuLi.

The MoS_2 peak is again seen in the x-ray diffraction pattern of the lithiated compound. Though the amount, estimated by the intensity of the peak, is small, it would be better to avoid its presence and the consequent interference with properties. As outlined in the previous chapter, the reduced sulphur content will suppress the formation of this impurity phase. Thus, $Li_xMo_6S_{7.7}$ was prepared likewise. No MoS_2 is found in this phase. The lithium content of the ternary phase as determined by AA spectroscopy is (x =) 2.41 which is higher than the titration result (x =) 2.21. The value measured by AA spectroscopy appears too high as the amount of reagent used is not enough to produce such a high lithium content.

Table 11: X-ray Diffraction Results of Lithium Molybdenum Sulphides and the Binary Phase

	$Mo_6S_{7.85}$		$Li_{2.2}Mo_6S_{7.85}$		HT* $Li_{2.2}Mo_6S_{7.85}$	
hkl	d	I/Io	d	I/Io	d**	I/Io
101	6.38	100	6.385	100	6.421	100
			6.092	12.2	6.134	6.3
110	4.582	6.3	4.582	12.3	4.63	6.8
021	3.728	5.8			3.77	7.2
003	3.620	8.5	3.613	16.5	3.591	8.9
202	3.206	5.0	3.204	14.0	3.219	6.4
	3.109	4.0	3.113	14.2		
	3.028	4.1				
211	2.894	21.7	2.900	19.2	2.93	17.1
122	2.631	35.2	2.633	23.5	2.644	2.9
104	2.573	13.6	2.575	12.8	2.557	11.9
220	2.296	10.9	2.3	9.9	2.319	7.8
024	2.245	3.3				
131	2.162	2.3	2.165	15.6	2.181	16.7
033	2.142	7.6	2.143	8.8	2.146	6.9
015	2.1	10.8	2.101	6.2	2.084	9.1
312	2.046	15.9	2.046	12.8	2.060	11.3
214	2.017	9.9	2.02	9.4	2.018	11.1
	1.988	3.3				
223	1.941	32.6	1.942	20.0	1.947	27.0
	1.902	3.9				
006	1.814	4.3			1.815	5.2
321	1.8	6.2	1.802	7.4		
125	1.763	4.9	1.765	6.7		
232	1.730	11.5	1.732	9.8	1.744	8.2
134	1.715	3.2				
116	1.686	2.7				
a_R (Å)	6.426		6.431		-	
α_R (°)	91.26		91.28		-	

* Heat-treated at 454°C for 17H and 471°C for 22H

** Without internal standard

3. Hot-pressing Lithium Molybdenum Sulphide:

3-1. Experimental:

The hot-pressing technique was selected to prepare dense samples for conductivity measurement. The lithium molybdenum sulphide powder was cold-pressed in an 8 mm steel die with a 'G' clamp inside a dry box. The pellets were encapsulated with Pt inside the box. The capsule was then transferred to the hot-press apparatus into a $\frac{1}{2}$" alumina die if for pressing at low temperature or a graphite die if inductive heating was required for higher temperature. The pressure on the graphite die was 5×10^7 Nm^{-2}, and 9×10^7 Nm^{-2} for alumina die. BN powder was used to surround the capsule. Overnight pumping with suitable heating helped to get rid of the adsorbed species on the powder. The pressing time was two hours. The pressed sample was examined by x-ray diffraction. A rectangular bar specimen was cut with a high speed diamond saw. The density of the sample was inferred from the weight and dimensions of that specimen.

3-2. Results and Discussions:

A full investigation covering a wide range of temperature has not been attempted. Table 12 lists the results of the hot-pressing of lithium Chevrel phase.

Table 12: Results of Hot-pressing $Li_xMo_6S_{8-y}$

Materials	Temp. (°C)	Pressure (Nm^{-2})	Density (gm/cm^3)	Phases
$Li_{1.9}Mo_6S_{7.85}$	1325	5×10^7	-	TP + MoS_2
$Li_{1.9}Mo_6S_{7.85}$	950	9×10^7	-	TP + MoS_2
$Li_{2.2}Mo_6S_{7.7}$	950	9×10^7	4.63 (88%)	TP + MoS_2 (trace)

The temperature appears to have some effect on the phase. Thermal decomposition of the ternary phase to MoS_2 takes place at as low a temperature as 950°C. This severely restricts the use of high

temperatures which are essential to fabricate dense samples. Using the high lithium and low sulphur content material and a reasonably high temperature, the sample obtained is still contaminated by MoS_2 and with a density of merely 88% theoretical value. No further effort was put into this development to pursue the optimum hot-pressing conditions. The sample with lowest MoS_2 contamination was then used in the electrochemical studies.

III. Electrochemical Studies on Lithium Molybdenum Sulphide:

1. Lithium Solid Electrolytes:

The thermodynamic and transport properties of lithium molybdenum sulphide were studied in the solid state electrochemical assembly. To conduct this type of measurement, a lithium solid electrolyte is required. Two lithium solid electrolytes, $Li_{14}Zn(GeO_4)_4$ (LISICON) and $Li_{4-x}Si_{1-x}P_xO_4$ (LISPO) were chosen for their high lithium conductivity at about 300°C and the relatively simple preparation procedures.

(a) LISICON:

The starting materials were Li_2CO_3, GeO_2 and ZnO (all Specpure, Johnson Mattheys). The dried components at appropriate weights were ground together with an agate pestle and mortar. The mixture was fired in an alumina crucible in air at 1100°C overnight. The product was in a 'cake' form and it was ground to powder again. Pellets were made from the powder by cold-pressing in an 8 mm steel die. The pellets were encapsulated with Pt and hot-pressed in a $\frac{1}{2}$" alumina die with Al_2O_3 powder surrounding under oxygen atmosphere at 1000°C for 30 minutes at a pressure of 9×10^7 Nm^{-2}. The resultant density of the sample was 2.96 gm/cm^3 corresponding to 86.2% theoretical value. The x-ray diffractometer results (table 13) agreed well with the reported crystallographic data (7). The ionic conductivity of a bar specimen was measured by the four-point DC method (fig. 33). Various constant ionic currents were passed through the bar in both directions. The stable voltage response on the ionic probes was immediate. Ohm's

Table 13: X-ray Diffraction Results for LISICON

d	I/Io	hkl*	d	I/Io	hkl*
5.405	16.2	200	2.150	5.3	321
4.634	17	101	2.098	8.8	302
4.238	8.7	-	2.049	4.1	420
4.088	100.0	210	2.002	6.3	020, 022
3.969	56.1	011	1.946	6.5	230
3.726	37.2	201, 111	1.933	5.3	031
3.202	16.4	-	1.905	9.	131, 421
3.122	17.0	-	1.867	9.8	222, 402
3.028	5.8	-	1.821	5.6	231
2.710	51.4	220, 400	1.742	7.1	322
2.674	27.3	311	1.704	6.2	331
2.589	26.5	-	1.685	4.3	103
2.569	27.4	002	1.647	6.4	013, 430
2.535	5.8	-	1.637	4.7	113, 203
2.489	12.8	410	1.605	7.4	132, 422
2.398	7.2	401, 221	1.565	17.2	040
2.324	12.6	202	1.506	6.3	023, 313, 240
2.241	7.2	411	1.492	5.3	123
2.18	7.2	212	1.339	5.7	042

* Indexes based on the lattice parameters given in ref. (7)

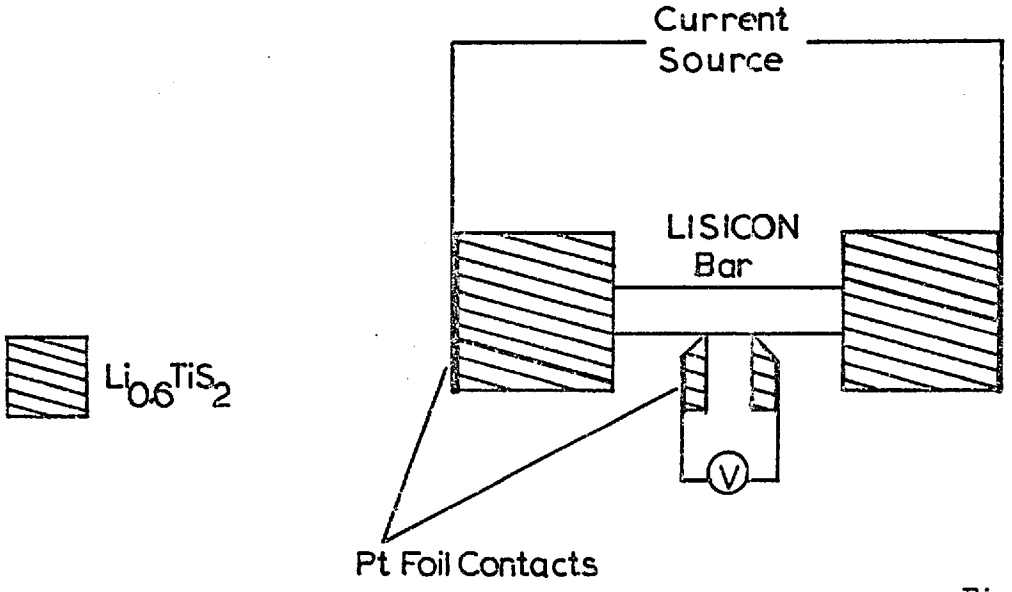


Figure 33: Experimental Set-up of 4-point DC Conductivity Measurement on LISICON

law was obeyed and from the measured resistance value, the ionic conductivity was calculated and plotted in figure 34 and the values are given in table 14.

(b) LISPO:

The composition of the sample was $Li_{3.6}Si_{0.6}P_{0.4}O_4$. An acetone slurry of Li_2CO_3, SiO_2 and $(NH_4)_2 HPO_4$ in appropriate ratio was ground until the acetone had evaporated. The powder was heated to 110°C under vacuum for about 16 hours to expel the ammonia, and then at 800°C for 24 hours. The resulting material was ground and re-fired until x-ray diffraction showed no further changes. The final pattern agreed with the reported crystallographic data (63). The powder thus prepared was cold-pressed in the dry box. A thick pellet about 1 cm long was loaded into an 8 mm graphite die. The die was transferred to the apparatus and the whole system was evacuated overnight. The hot-pressing was performed at 950°C under vacuum. The applied pressure on the pellet was maintained at 3×10^7 Nm^{-2} for the first hour and gradually decreased when the system was left on overnight. The hot-pressed pellet was translucent under light or when wetted with ethanol. The resultant density was 2.30 gm/cm^3 which was 96.5% of theoretical value. No ionic conductivity was measured on this particular batch of samples. Samples prepared by the same procedures with comparable density were measured by an AC conductivity method (63) and the values were in agreement with those of Shannon et al. (64).

In view of the better ionic conductivity at low temperature, LISPO is used as electrolyte, through which the ionic current passes. The LISICON is used as ionic probes, for which high ionic conductivity is not as critical as for the electrolyte. This set-up enables the whole system to be operated at lower temperatures which will be advisable when the sulphur vapour pressure of lithium molybdenum sulphide is unknown. Another reason for using LISPO as electrolyte is its stability in contact with pure lithium. This is vital in the calibration of lithium activity in Chevrel phase w.r.t. pure lithium.

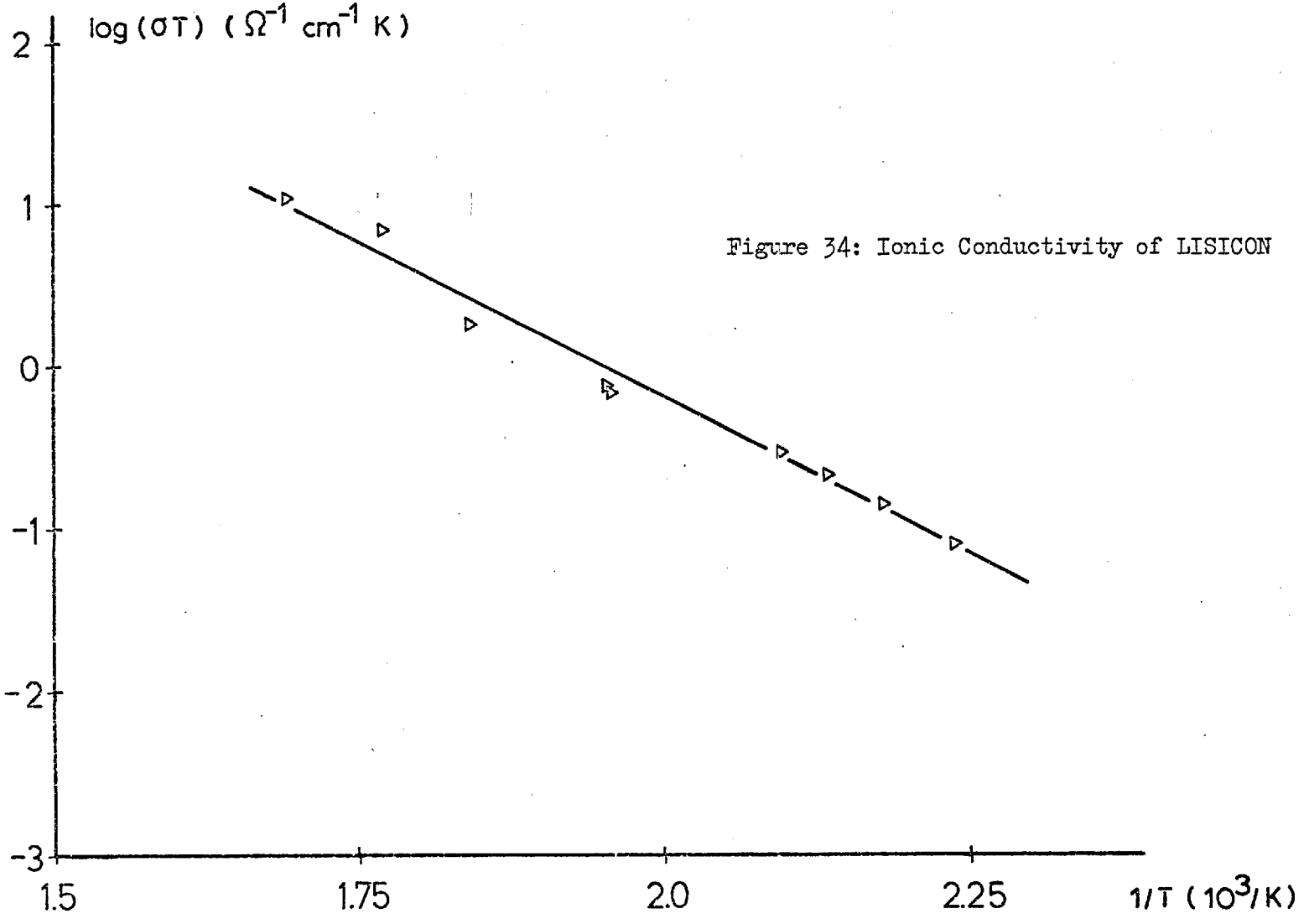


Figure 34: Ionic Conductivity of LISICON

Table 14: The Ionic Conductivities and the Activation Energy for Conduction of LISICON

$T^{o}K$	$\sigma (ohm^{-1} cm^{-1})$
477	6.2×10^{-4}
476.8	6.06×10^{-4}
468.5	4.58×10^{-4}
459	3.05×10^{-4}
447	1.8×10^{-4}
477	5.44×10^{-4}
512	1.48×10^{-3}
543.3	3.35×10^{-3}
511	1.34×10^{-3}
565	1.23×10^{-2}
591	1.85×10^{-2}

$E_a = 0.76$ eV

2. Calibration of Lithium Activity in the Lithium Molybdenum Sulphide:

Ideally, the lithium activity in the lithium SSE materials should be calibrated with pure lithium. Lithium metal has been used as reference electrode in aprotic solvent electrolyte cells. However, discrepancies in the voltage between the sample and reference electrode are often found in the literature. It is suggested that the difference is caused by the chemical reaction which occurs between the lithium metal and the electrolyte. On the other hand, the inclusion of pure lithium as reference electrode in the solid-state electrochemical cell is very difficult with the equipment used in the present investigation. Fresh deposits of lithium at an inert electrode should provide a means to calibrate the lithium activity w.r.t. pure lithium.

2-1. Experimental:

The rig used was a vacuum-tight system which, while used, was flushed with high purity argon gas further purified by passing over $Mg(ClO_4)_2$ and titanium at 750°C. The oxygen partial pressures of the argon gas directly at the outlet of the purification unit and after flow through the rig were measured with an oxygen meter to be 5.3×10^{-11} and 1.4×10^{-10} atm. respectively. A lump of lithium metal was placed inside the rig in a nickel crucible and used as a getter. The electrochemical cell assembly is given in figure 35. The inert electrode at which lithium was deposited was a piece of nickel mesh (N. Greening (Warrington) Ltd., 80 x 80 mesh) spot-welded onto a piece of nickel foil (Goodfellow Metals, 99.99+%). The lithium molybdenum sulphide was used as a lithium source and LISPO was used as electrolyte. These materials were prepared as previously described. The sample being calibrated was obtained by hot-pressing $Li_{2.2}Mo_6S_{7.7}$ at 950°C.

The whole system was evacuated at about 150°C for a few hours. The argon gas was let through the system while the

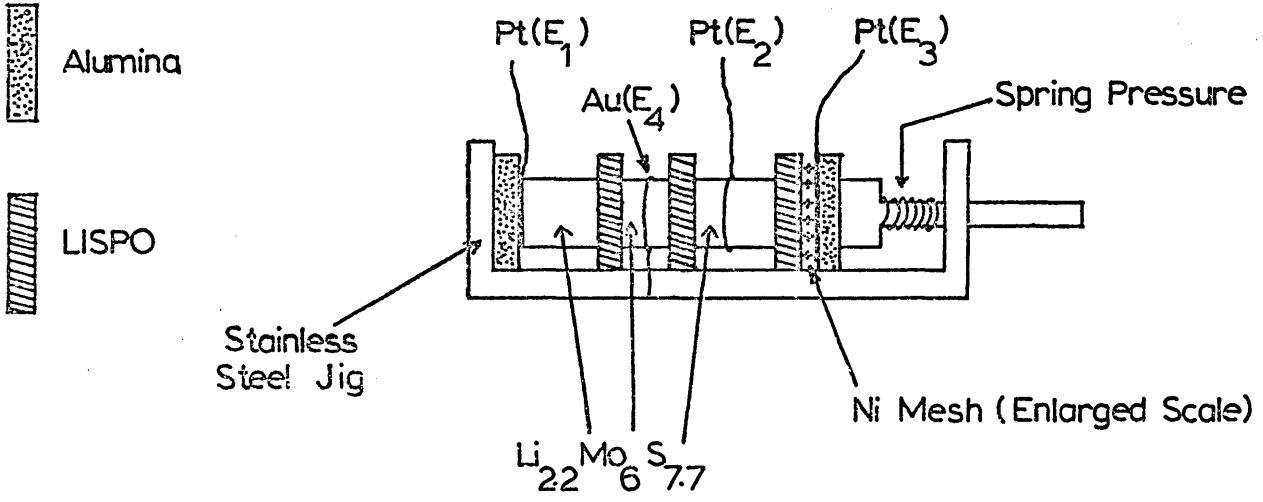


Figure 35: Assembly of the $Li_{2.2}Mo_6S_{7.7}$ Electrochemical Cell

temperature was brought to the desired value. Having reached thermal equilibrium, the gas was turned off. A constant current was passed from E_1 to E_3 to deposit lithium on the Ni mesh. The current should be high enough to register a polarisation of above 2.2 volts between E_3 and E_2. The current was kept passing for another day after this value of polarisation had been measured. The decay of the voltage across E_3 and E_2 was monitored when the current was turned off. The equilibrium value was obtained by extrapolating the exponential curve. These procedures were repeated at different temperatures.

2-2. Results and Discussions:

The results are given in figure 36 and summarised in table 15. The reproducibility of the

Table 15: Experimental Results on the Calibration of Lithium Molybdenum Sulphide

i (uA)	Q Passed (C)	Temp.(°C)	Equilibrium Voltage (volts)	Δt (hours)
20	2.23	310.3	2.06	8.73
20	1.44	310.3	2.06	9.72
10	0.22	255.0	2.07	10.62
5	0.90	220.3	2.11	21.33

Δt: time interval between the current switch-off and the sudden drop in the voltage (fig. 36)

equilibrium voltage is quite remarkable. Apparently, about one coulomb of charge should be passed before a reasonable voltage can be registered. It can be seen that the voltage decreases as the temperature increases. This indicates a small negative entropy term which is consistent with what will be expected from transferring molten lithium into a solid phase. Similar experiments were found very difficult to perform at temperatures

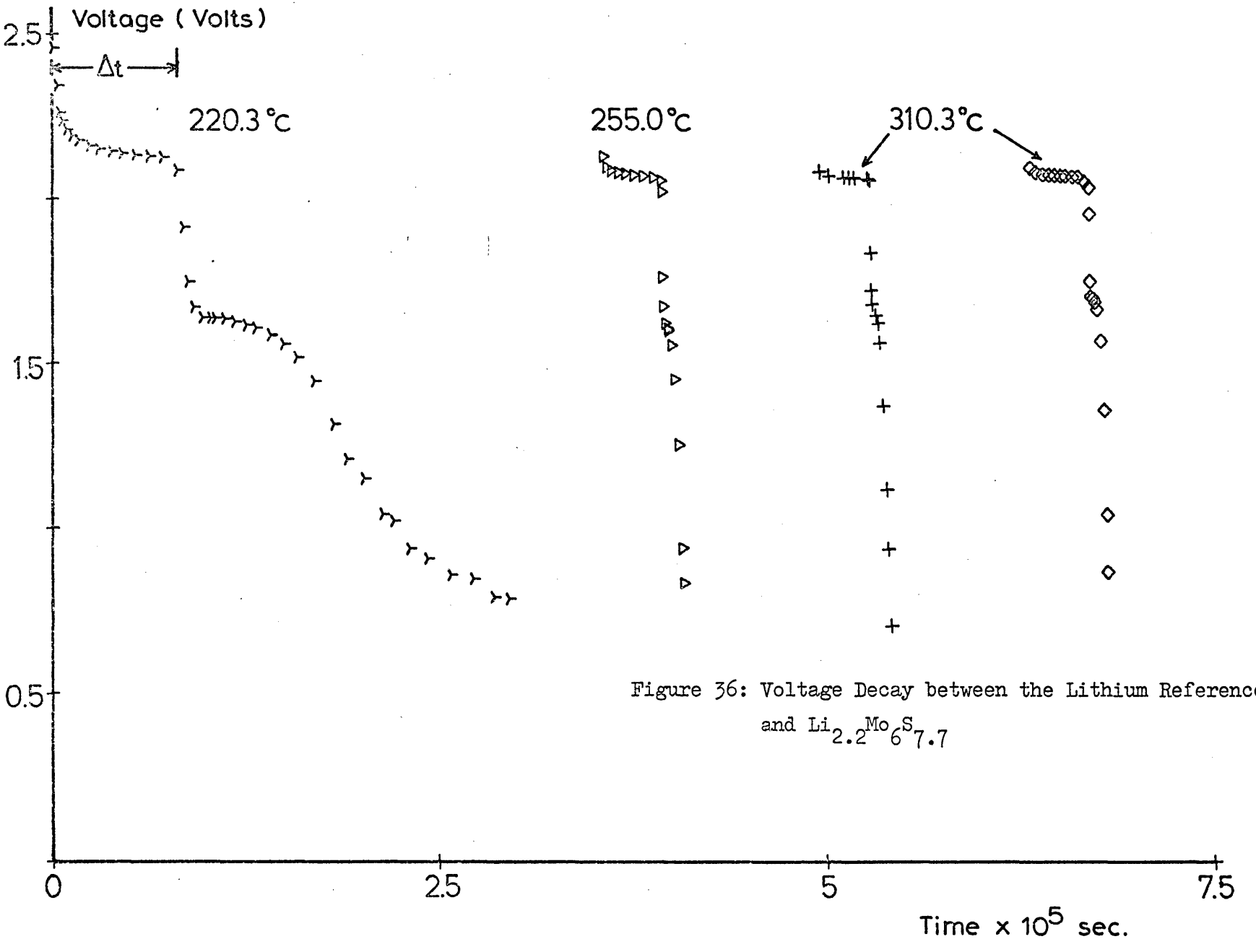


Figure 36: Voltage Decay between the Lithium Reference Electrode and $Li_{2.2}Mo_6S_{7.7}$

above 350°C. It was difficult to get the required polarisation across E_3 and E_4 even at a current as high as 50 mA. The actual reason for this observation is not clear. Nevertheless, one can speculate that the high temperature encourages reaction of the liquid lithium with the surrounding substances, e.g. the gaseous molecules or the impurities on the nickel substrate.

By least-square method, the voltage (in volts) as function of temperature (°K) can be expressed by the formula:

$$E = 2.35 - 5.2 \times 10^{-4} T \qquad (r = -0.89)$$

The voltage at 25°C as calculated from this formula is 2.2 volts. It should be pointed out that this value is not very accurate, as the equilibrium voltages at 310.3 and 255°C are too close together to allow a precise linear extrapolation of the voltage to lower temperatures. Another interesting feature of this series of experiments is the drastic drop in voltage after about 21 hours followed by a slow decay (a kink is seen at higher temperatures) (fig. 38). The time interval is apparently proportional to the temperature and the number of coulombs passed. This suggests that the stability of the lithium deposit depends on the temperature and the purity of the nickel substrate. This argument is based on the assumptions that the high temperatures enhance the possible side reactions and the early lithium deposit reacts with, for instance, nickel oxide and cleans up the electrode. There are very few reports about the reaction between liquid lithium and nickel. The only available information is the very low solubility of nickel (0.006 w/o) in liquid lithium at 200°C (50). What reaction is responsible for the second voltage plateau (around 1.6 V), is by no means clear at this stage.

3. Thermodynamic Properties of Lithium Molybdenum Sulphide

All attempts to measure the thermodynamic data of the lithium Chevrel phase have failed. It was extremely difficult to obtain any stable voltage between the sample and the reference,

with the same assembly as the calibration work (fig. 35). It was thought that the LISPO when in contact with the Pt/Rh electrical lead acted as an oxygen electrode. Wherever possible the Pt/Rh leads were rearranged to avoid this happening, and for the thin sample, gold wire was used for its weak catalytic properties even if the wire was in touch with LISPO. The unsteady voltage persisted after the change. The cause(s) of this phenomenon has/ have not been found out, and this part of the study had to be abandoned.

4. Transport Properties of Lithium Molybdenum Sulphide

Despite the failure of the thermodynamic study on lithium molybdenum sulphide, 6-point conductivity measurements have been carried out. The results are given below.

4-1. Experimental:

Hot-pressed lithium molybdenum sulphide of composition $Li_{2.2}Mo_6S_{7.7}$ was used as sample and reference electrodes on the ionic probes. The lithium source and sink were also lithium molybdenum sulphide, but with rather high MoS_2 contamination. LISPO slices about 0.7 mm thick were used as electrolyte. Ionic probes were LISICON. All materials were prepared as previously described. The cell was assembled inside the dry box to ensure a better interfacial contact between the specimens. The cell and the experimental procedures of the measurement were identical to those used for the copper analogue.

4-2. Results and Discussions:

The lithium conductivity in this sample appears to be quite poor. The only reasonable result obtained was at 415°C and with a current as low as 5μA (fig. 37 & 38). The lithium ionic

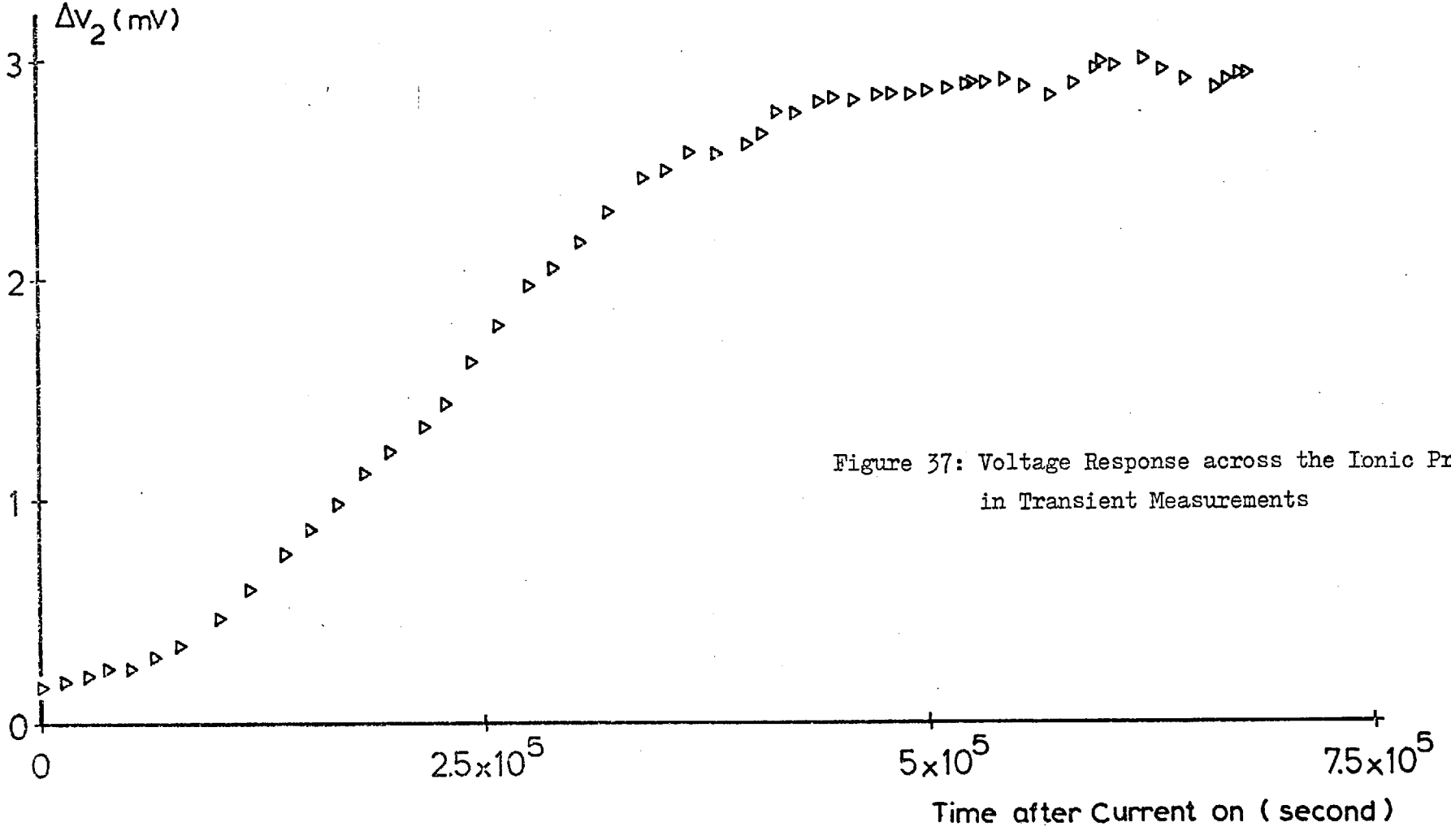


Figure 37: Voltage Response across the Ionic Probes in Transient Measurements

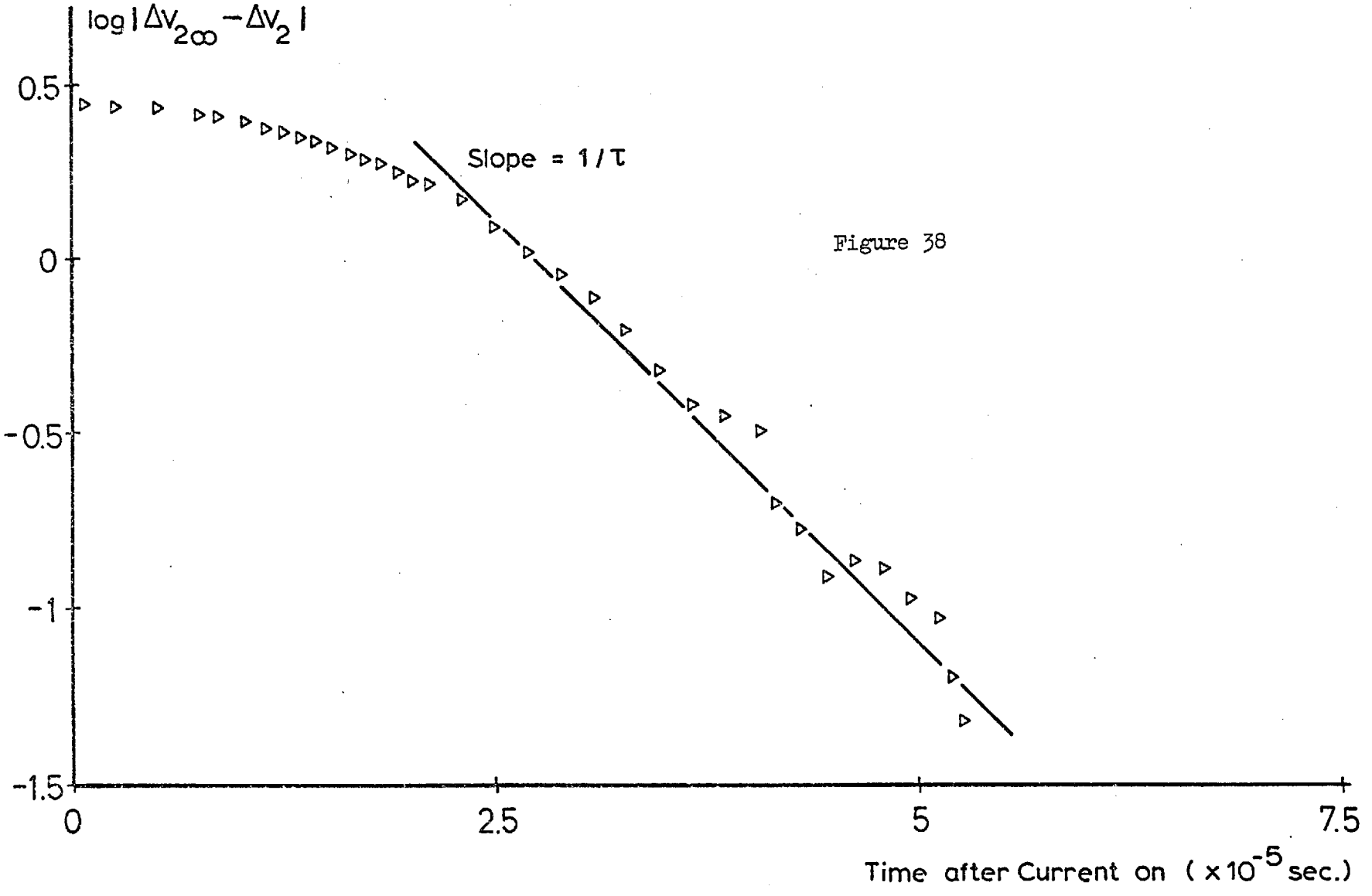

log | Δv2∞ − Δv2 |
0.5
0
-0.5
-1
-1.5
Slope = 1/τ
0
2.5
5
7.5
Time after Current on (x 10-5 sec.)

Figure 38

conductivity and the chemical diffusion coefficient of the sample at 415°C are estimated to be 3.4×10^{-4} ($ohm^{-1}cm^{-1}$) and 3.5×10^{-7} cm^2/s respectively. These values are much lower than those of copper in the similar lattice.

Despite the fact that the density of the sample is not extremely high, the lithium conductivity is very disappointing. If one recalls the lattice parameters of the lithium Chevrel compound (II 2-2.(b)), one will find the values are comparable with the binary phase. It is acceptable to argue that the similarity between two x-ray diffraction patterns is because of the comparatively low scattering factor of lithium. The low α_R value of the lithium phase indicates that the lithium ions are not delocalised to M_1 and M_2 sites. The localised lithium ions will not be very mobile and a low transport rate results.

In Chevrel compounds, the 3s and 3p orbitals of the sulphur atom are used to form the Mo_6S_8 unit. The valency of the sulphur atom is -2. When lithium dissolves into the phase, electrons are donated to the vacant energy level of the Mo_6S_8 host and lithium becomes a singly charged cation. Any possibility of forming a d-p π bond between sulphur and lithium can be ruled out because there is no electron available. Therefore, the lithium ion is held in the lattice by Coulombic force. For this ionicity requirement, the lithium ion takes up a higher coordination site, viz. the central cavity, instead of the more covalent tetrahedral M_1 and M_2 sites. A similar situation does not happen in copper Chevrel compound because the d^{10} orbital of copper is capable of forming the d-p π bond and the covalence results in the delocalisation of copper ions.

The slow diffusion rate of lithium ions in the Chevrel phase also explains the failure of the ionic exchange experiment. The establishment of ionic equilibrium between the solid and the melt is strongly hindered by the slow transport of lithium in the solid phase. The resultant situation is that the mobile copper ions are removed from the solid, and the solid matrix, without the stabilisation of the lithium ions, becomes crumbly.

IV. Summary and Conclusions:

Lithium molybdenum sulphide was prepared by lithiating the binary compound Mo_6S_{8-y}. The formation of a ternary phase was confirmed by AA spectroscopy and the thermal stability test. The x-ray diffraction pattern of the ternary phase was found to resemble closely the binary phase with only little change of the lattice parameters. Samples with density up to 88% theoretical value were prepared by hot-pressing $Li_{2.2}Mo_6S_{7.7}$ powder at 950°C and 9×10^7 Nm^{-2} under vacuum. The hot-pressed sample was contaminated by MoS_2 indicating that the lithiated sample was not very stable at high temperatures. Thermodynamic studies by solid state electrochemical methods failed to produce any sensible results. The lithium activity was calibrated w.r.t. freshly deposited lithium on a nickel substrate. The equilibrium voltage of the lithium molybdenum sulphide ($Li_{2.2}Mo_6S_{7.7}$) w.r.t. liquid lithium at r.t. was estimated to be about 2.2 volts. The $(\partial E/\partial T)$ term was a very small negative quantity. A low chemical diffusion coefficient of lithium in the Chevrel phase $\tilde{D} = 3.5 \times 10^{-7}$ cm^2/s at 415°C was determined by 6-point conductivity measurements.

An attempt was also made to prepare the lithium molybdenum sulphide by the ionic exchange technique. The approach was not fruitful, mainly due to the slow diffusion rate of lithium in the solid phase.

To prepare the binary compound, hydrochloric acid with air, and ferric solution were both able to produce satisfactory results. The acid was found more reliable as the other reagent might give undesired MoS_2. The sulphur vapour pressure of the binary compound was found to be quite high. Through a series of high temperature experiments on the binary compound, the thermal decomposition was proved to be very complicated. No clear picture about the formation of MoS_2 from Mo_6S_8 was developed, though the appearance of MoS_2 was seen at a lower temperature (394°C) than previously reported (468°C).

CONCLUDING REMARKS AND FURTHER WORKS

Copper molybdenum sulphide has been proved to be a 3-dimensional fast ionic conductor. It should be a suitable model to test the applicability of the solid state battery. In light of the fact that Chevrel compound can be sputtered (65), interfacial studies can be performed on this material with copper solid electrolytes, which are now under investigation in the Solid State Ionics Group at Imperial College.

The copper molybdenum sulphide system is by no means fully understood. The phase diagram proposed here is only a limited one, and is subject to error in the sulphur content. The effect of sulphur non-stoichiometry on the copper solubility in the phase and its mobility has hardly been investigated. The optimum composition for fast copper diffusion has yet to be found. The problem of MoS_2 separation from the Mo_6S_8 lattice, especially in the lithium compound, should be solved by more careful crystallographic work.

The results gained on the lithium analogue are not satisfactory. Indeed, there are some unknown factors operating in the system which give peculiar results, noticeable on the thermodynamic study. Recent investigations on $NiPS_3$ indicate that the behaviour of lithium in this phase depends on whether n-BuLi reagent or the electrochemical method is used to introduce lithium (66, 67). Had this effect also happened in the sample used in the present investigation, the other lithium behaviour should certainly be looked at. It is further suggested that the electrochemical substitution of copper with lithium by passing a current from a lithium source to a copper sink may produce a phase stabilised by copper ions with mobile lithium ions. This would be analogous to Li^+-Na^+ β-alumina which is basically a sodium β-alumina lattice with exclusive lithium mobility.

It can also be seen that a lattice suitable for copper transport may not necessarily be good for lithium diffusion. The different characteristics between the diffusing species account for the discrepancy. Perhaps the strategy adopted in this project

should be revised.

The lithium conductor is probably the most difficult one to find or synthesise. The present synthesis principles are not at all adequate. The ionic environment required for rapid lithium diffusion has produced a 2-dimensional lattice with a bottleneck which is not wide enough. No doubt the 3-dimensional framework will be a better choice but such a lattice is likely to impose high activation energy for diffusion. Further development and effort should be concentrated on finding suitable conditions for rapid lithium ionic transport.

APPENDIX

MATHEMATICAL BACKGROUND OF THE DIFFUSION MEASUREMENTS

The phenomenological equations for diffusion are given as

$$J_i = L_{ii} \nabla \bar{\mu}_i + L_{ij} \nabla \bar{\mu}_j + \ldots\ldots \quad [A1]$$

$$J_j = L_{ji} \nabla \bar{\mu}_i + L_{jj} \nabla \bar{\mu}_j + \ldots\ldots \quad [A2]$$

where J_i : the flux of i species, L_{ij} : general transport coefficient and $\bar{\mu}_i$: the electrochemical potential of species i. The last term can be expressed as :

$$\bar{\mu}_i = \mu_i + z_i F \varphi \quad [A3]$$

where μ_i & z_i are the chemical potential and charge of i species respectively, F is Faraday constant & φ is the average electrical potential. The equations [A1] & [A2] can be simplified by the Onsager relation

$$L_{ij} = L_{ji} \quad [A4]$$

The conductivity of species i (σ_i) is obtained as the quotient of the current density of that species (i_i) and the negative value of the gradient of the driving potential in a sample of uniform cross-section & uniform composition for stationary conditions. Therefore, in the absence of the chemical potential gradient, e.g. [A1] can be re-written

$$J_i = L_{ii} z_i F \nabla\varphi + L_{ij} z_j F \nabla\varphi + \ldots\ldots\ldots$$

$$= i_i / z_i F$$

By definition $\sigma_{ij} = i_i / -\nabla\varphi = - L_{ij} z_i z_j F^2$

or $L_{ij} = - \sigma_{ij} / z_i z_j F^2 \quad [A5]$

Now, equations [A1] & [A2] become

$$J_i = -\frac{\sigma_{ij}}{z_i^2 F^2}\nabla\bar{\mu}_i - \frac{\sigma_{ij}}{z_i z_j F^2}\nabla\bar{\mu}_j - \ldots\ldots\ldots\ldots\ldots \quad [A6]$$

$$J_j = -\frac{\sigma_{ij}}{z_i z_j F^2}\nabla\bar{\mu}_i - \frac{\sigma_{ij}}{z_j^2 F^2}\nabla\bar{\mu}_j - \ldots\ldots\ldots\ldots\ldots \quad [A7]$$

The transport can also be described in terms of diffusion. When the diffusion takes place in a non-equilibrium situation and more than one diffusing species is involved (which is the case in mixed conductors), the processes can be described by one chemical diffusion coefficient $\tilde{D}$ (or sometimes known as the ambipolar diffusion coefficient). It can be defined as the flux of particles per unit concentration gradient (Fick's law).

$$\tilde{D} = -J_i/\nabla C_i \quad [A8]$$

To correlate the conductivity and the chemical diffusion coefficient, one has to find the relationship between the chemical potential and the concentration. This can be obtained by the use of the thermodynamic equation

$$\mu_i = \mu_i^0 + RT \ln a_i$$

Thus,

$$\nabla\mu_i = \frac{\partial\mu_i}{\partial a_i}\frac{\partial a_i}{\partial C_i}\nabla C_i = \frac{RT}{C_i}\frac{\partial \ln a_i}{\partial \ln C_i}\nabla C_i$$

$$= \frac{RT}{C_i}\xi_i \nabla C_i \quad [A9]$$

where ξ_i is equal to $(\partial \ln a_i / \partial \ln C_i)$ and is designated the thermodynamic factor.

When a constant current (i) is passed through a sample and the current is carried by one mobile ion and electron, one has

$$i/F = z_1 J_1 + z_2 J_2$$

(The subscripts 1 and 2 are for electron and ion respectively). By substituting the appropriate terms and eliminating $\nabla\varphi$, one has

$$J_2 = - \frac{(\sigma_{11}\sigma_{22} - \sigma_{12}^2)}{\sigma_o} \frac{RT\nabla c_2}{F^2} \left(\frac{\xi_1}{z_1^2 c_1} + \frac{\xi_2}{z_2^2 c_2} \right) + \frac{i\,(\sigma_{22} + \sigma_{12})}{F z_2 \sigma_o} \qquad [A10]$$

where $\sigma_o = \sigma_{11} + \sigma_{22} + 2\sigma_{12}$ is known as the total conductivity. If the σ_{11}, σ_{22} and σ_{12} are independent of composition, the i-containing term will be independent of the space variables. Equation [A10] can then be split into 2 parts:

$$(a) \quad J_{2\,(ext)} = i\,(\sigma_{22} + \sigma_{12}) / z_2 F \sigma_o \qquad [A10a]$$

$$(b) \quad J_{2\,(diff)} = - \frac{(\sigma_{11}\sigma_{22} - \sigma_{12}^2)}{\sigma_o} \frac{RT\nabla c_2}{F^2} \left(\frac{\xi_1}{z_1^2 c_1} + \frac{\xi_2}{z_2^2 c_2} \right) \qquad [A10b]$$

and the corresponding chemical diffusion coefficient is

$$\tilde{D} = - \frac{J_{2(diff)}}{\nabla c_2} = \frac{(\sigma_{11}\sigma_{22} - \sigma_{12}^2)}{\sigma_o} \frac{RT}{F^2} \left(\frac{\xi_1}{z_1^2 c_1} + \frac{\xi_2}{z_2^2 c_2} \right)$$

$$\text{or} \quad \tilde{D} = - \frac{(\sigma_{11}\sigma_{22} - \sigma_{12}^2)}{\sigma_o} \frac{\vartheta}{F^2} \qquad [A11]$$

where $$\vartheta = RT \left(\frac{\xi_1}{z_1^2 C_1} + \frac{\xi_2}{z_2^2 C_2} \right)$$

In 4-point transient measurements, a constant ionic flux is passed through the sample. The time variation of the diffusion equation now has to be considered. For one dimensional transport (X direction), the equation is

$$\frac{\partial C_2}{\partial t} = - \frac{\partial J_2}{\partial X} \qquad [A12]$$

Assuming $\tilde{D}$ is constant, and solving equation [A12] with the boundary conditions:

$C_1 = C_{1,0}$, $C_2 = C_{2,0}$ at $t = 0$

$$\frac{\partial C_2}{\partial X} = - \frac{i_2 F}{z_2} \frac{(\sigma_{11} + \sigma_{12})}{(\sigma_{11}\sigma_{22} - \sigma_{12}^2)} / \vartheta \qquad \text{at } X = 0, L$$

$$\frac{\partial C_1}{\partial X} = \frac{i_2 F}{z_1} \frac{(\sigma_{11} + \sigma_{12})}{(\sigma_{11}\sigma_{22} - \sigma_{12}^2)} / \vartheta \qquad \text{at } X = 0, L$$

($C_{i,0}$: initial concentration of i species)

the solutions, analogous to Yokota's treatment (68), are

$$C_1 = C_{1,0} + \frac{i_2 F L}{z_1 (\sigma_{11}\sigma_{22} - \sigma_{12}^2)} (\vartheta)^{-1}$$

$$\left[\frac{X}{L} - \tfrac{1}{2} + \phi \left(\frac{X}{L} , \frac{t}{\tau} \right) \right] \qquad [A13]$$

By charge neutrality $(C_1 - C_{1,0}) z_1 + (C_2 - C_{2,0}) z_2 = 0$, one has

$$c_2 = c_{20} - \frac{i_2 F L}{z_2 (\sigma_{11}\sigma_{22} - \sigma_{12}^2)} (\vartheta)^{-1}$$

$$[\frac{X}{L} - \tfrac{1}{2} + \phi (\frac{X}{L} , \frac{t}{\tau})] \qquad [A14]$$

where L is the length of the sample and the function ϕ is defined as

$$\phi (\frac{X}{L} , \frac{t}{\tau}) = \frac{4}{\pi^2} \sum_{m=0}^{\infty} \frac{1}{(2m + 1)^2} \exp [- (2m + 1)^2 \frac{t}{\tau}]$$

$$\cos [(2m + 1) \frac{\pi X}{L}] \qquad [A15]$$

and $1/\tau$, the time rate at which the stationary polarisation is attained, is defined as

$$\frac{1}{\tau} = \tilde{D} \frac{\pi^2}{L^2} = \frac{\pi^2}{L^2} \frac{(\sigma_{11}\sigma_{22} - \sigma_{12}^2)}{c_o} \frac{\vartheta}{F^2} \qquad [A16]$$

The potential difference between the ionic probes is the measure of the free energy change in transferring one mole of the ion from one contact point (X_1) to the other (X_2).
Therefore,

$$-\Delta V_2 = \Delta \bar{\mu}_2 / z_2 F \qquad [A17]$$

The flux equations, when expressed in their diffusion terms, read

$$J_1 = - \frac{\sigma_{11}}{z_1^2 F^2} \frac{\partial \bar{\mu}_1}{\partial X} - \frac{\sigma_{12}}{z_1 z_2 F^2} \frac{\partial \bar{\mu}_2}{\partial X}$$

$$= - \tilde{D} \frac{\partial c_1}{\partial X} + \frac{i_2 (\sigma_{11} + \sigma_{12})}{F z_1 \sigma_o} \qquad [A18]$$

A similar equation can be obtained for J_2. Combining J_1 and J_2 and eliminating $\partial \bar{\mu}_1/\partial X$, one has

$$\frac{\partial \bar{\mu}_2}{\partial X} = \vartheta z_2^2 \frac{\partial C_2}{\partial X} \frac{(\sigma_{11} + \sigma_{12})}{\sigma_o} - \frac{i_2 z_2 F}{\sigma_o} \qquad [A19]$$

Therefore,

$$\Delta \bar{\mu}_2 = \int_{X_1}^{X_2} \frac{\partial \bar{\mu}_2}{\partial X} \, dX$$

$$= [\vartheta z_2^2 \frac{(\sigma_{11} + \sigma_{12})}{\sigma_o} \int_{X_1}^{X_2} \frac{\partial C_2}{\partial X} \, dX] - \frac{i_2 z_2 F}{\sigma_o} (X_2 - X_1)$$

Substituting eq. [A14] for $(C_2 - C_{20})$, and assuming the probes are symmetric with the centre of the bar, then $(X_2 - \frac{L}{2}) = (\frac{L}{2} - X_1)$ and $\phi(\frac{X_2}{L}, \frac{t}{\tau}) = -\phi(\frac{X_1}{L}, \frac{t}{\tau})$, one has

$$\Delta \bar{\mu}_2 = -\frac{z_2 F i_2 \Delta X \sigma_{11}}{(\sigma_{11}\sigma_{22} - \sigma_{12}^2)}$$

$$- \frac{2 z_2 F i_2 L (\sigma_{11} + \sigma_{12})^2}{\sigma_o (\sigma_{11}\sigma_{22} - \sigma_{12}^2)} \phi(\frac{X}{L}, \frac{t}{\tau})$$

and $\Delta V_2 = \frac{\Delta \bar{\mu}_2}{z_2 F}$

$$= - \frac{i_2 \Delta X \sigma_{11}}{(\sigma_{11}\sigma_{22} - \sigma_{12}^2)}$$

$$- \frac{2 i_2 L (\sigma_{11} + \sigma_{12})^2}{\sigma_o (\sigma_{11}\sigma_{22} - \sigma_{12}^2)} \phi(\frac{X}{L}, \frac{t}{\tau}) \qquad [A20]$$

where $\Delta X = X_2 - X_1$. A similar equation for ΔV_1 can be obtained. When the steady state is reached, $t = \infty$, $\phi(\frac{X}{L}, 0) = 0$, therefore

$$\Delta V_{2,\infty} = - \frac{i_2 \Delta X \sigma_{11}}{(\sigma_{11}\sigma_{22} - \sigma_{12}^2)} \qquad [A20a]$$

If σ_{12} is assumed to be small, equation [A20a] reduces to

$$\sigma_{22} = - \frac{i_2}{(\Delta V_{2,\infty}/\Delta X)} \qquad [A20b]$$

This expression was also used by Wagner (69) to designate the electron-suppressed ionic conductivity σ_1'.

At the steady state, when the current is switched off, the flux equations change to

$$J_1 = - \tilde{D} \frac{\partial c_1}{\partial X} = - \frac{\sigma_{11}}{z_1^2 F^2} \frac{\partial \bar{\mu}_1}{\partial X} - \frac{\sigma_{12}}{z_1 z_2 F^2} \frac{\partial \bar{\mu}_2}{\partial X}$$

$$J_2 = - \tilde{D} \frac{\partial c_2}{\partial X} = - \frac{\sigma_{12}}{z_1 z_2 F^2} \frac{\partial \bar{\mu}_1}{\partial X} - \frac{\sigma_{22}}{z_2 F^2} \frac{\partial \bar{\mu}_2}{\partial X}$$

Following the same procedures, one can have

$$\Delta V_2 = \frac{2 i_2 L (\sigma_{11} + \sigma_{12})^2}{\sigma_o (\sigma_{11}\sigma_{22} - \sigma_{12}^2)} \phi \left(\frac{X}{L}, \frac{t}{\tau} \right) \qquad [A21]$$

As can be seen, from equations [A20] and [A21], the ionic-probe response is time dependent. The governing chemical diffusion coefficient can be determined by measuring the value of $(1/\tau)$ according to

$$\Delta V_2 - \Delta V_{2,\infty} = A \exp (- t/\tau) \qquad [A22]$$

where $\Delta V_{2,\infty}$ is the steady state voltage between the ionic probes and A is a constant. By equation [A16], $\tilde{D}$ can be calculated.

If the responses of electronic probes (ΔV_1) are followed, the values of σ_{11}, σ_{12} and σ_{22} can also be determined. From these values, an independent $\tilde{D}$ value can be calculated from equation [A11] if ϑ is known from the thermodynamic data of the system. Without measuring these terms, a rough test can still be done by assuming $\sigma_{12} = 0$ and $\sigma_{11} \gg \sigma_{22}$. Therefore equation [A11] becomes

$$\tilde{D} = - \frac{\sigma_{22}\vartheta}{F^2} \qquad [A23]$$

The derivations of ΔV_1 equations in terms of σ_{ij} are not given here. These equations and more details about this type of measurement can be found in references (70, 71).

References

1. B.B. Owens & G.R. Argue, Science, 157, 308 (1967).
2. R.D. Armstrong, R.S. Bulmer & T. Dickinson, J. Solid State Chem., 8, 219 (1973).
3. D.O. Raleigh, J. Electrochem. Soc., 124, 1157 (1977).
4. T. Takahashi & O. Yamamoto, J. Electrochem. Soc., 122, 83 (1975).
5. J.B. Goodenough, H. Y-P. Hong & J.A. Kafalas, Mat. Res. Bull., 11, 203 (1976).
6. H. Y-P. Hong, in 'Solid State Chemistry of Energy Conversion & Storage', Eds., J.B. Goodenough & M.S. Whittingham, Advances in Chemistry series no. 163, p. 179, American Chemical Society, Washington, D.C. (1977).
7. H. Y-P. Hong, Mat. Res. Bull., 13, 117 (1978).
8. U. v. Alpen, M.F. Bell, W. Wichelhans, K.Y. Cheung & G.J. Dudley, Electrichem. Acta, in press.
9. M.S. Whittingham, J. Electrochem. Soc., 123, 315 (1976).
10. D.A. Winn, J.M. Shemilt & B.C.H. Steele, Mat. Res. Bull., 11, 559 (1976).
11. B.G. Silbernagel & M.S. Whittingham, J. Chem. Phys., 64, 3670 (1976).
12. J.A. Wilson & A.D. Yoffe, Advances in Physics, 18, 193 (1969).
13. B.C.H. Steele, in 'Fast Ion Transport in Solids', Eds., W. van Gool, North-Holland, Amsterdam (1973).
14. B.C.H. Steele, in 'Superionic Conductors', Eds., G.D. Mahan & W.L. Roth, Plenum, N.Y. (1976).
15. B.C.H. Steele, in 'Mass Transport Phenomena in Ceramics', Materials Science Research, Vol. 9, Eds., R.A. Cooper & A.H. Heuer, Plenum, N.Y. (1975).
16. M.B. Armand, in 'Fast Ion Transport in Solids', Ed., W. van Gool, North-Holland, Amsterdam (1973).
17. M.B. Dines, Mat. Res. Bull., 10, 287 (1975).
18. M.S. Whittingham & F.R. Gamble, Mat. Res. Bull., 10, 363 (1975).
19. M.S. Whittingham, Proceedings of the Symposium on 'Electrode Materials & Process for Energy Conversion & Storage', J.D.E. McIntyre, S. Srinivasan & F.G. Will (Ed.), The Electrochemical Soc., (1977).

20. R.R. Chianelli & M.B. Dines, Inorg. Chem., 14, 2417 (1975).
21. D.W. Murphy, F.J. Disalvo, G.W. Hull & J.V. Waszczak, Inorg. Chem., 15, 17 (1976).
22. R.R. Chianelli, J. Crystal Growth, 34, 239 (1976).
23. A. Leblanc-Soreau, M. Danot, L. Trichet & J. Touxel, Mat. Res. Bull., 9, 191 (1974).
24. M.S. Whittingham & M.B. Dines, J. Electrochem. Soc., 124, 1387 (1977).
25. H. Gilman & F.K. Cartledge, J. Organometal. Chem., 2, 447 (1964).
26. P.F. Collins, C.W. Kamienski, D.L. Esmay & R.B. Ellestad, Anal. Chem., 33, 468 (1961).
27. J.R. Urwin and P.J. Reed, J. Organometal. Chem., 15, 1 (1968).
28. M.S. Whittingham, J. Electrochem. Soc., 122, 713 (1975).
29. O.W. Johnson, Phys. Rev., A136, 284 (1964).
30. B.F. Decker & J.S. Kasper, Acta Cryst., 10, 332 (1957).
31. T. Horlin, T. Niklewski & M. Nygren, Mat. Res. Bull., 7, 1515 (1972).
32. NBS Mono. 25, Sec. 1 (1962).
33. R. Chevrel, M. Sergent & J. Prigent, J. Solid State Chem., 3, 515 (1971).
34. M. Sergent, O. Fischer, M. Decroux, C. Perrin & R. Chevrel, J. Solid State Chem., 22, 87 (1977).
35. M. Sergent, R. Chevrel, C. Rossel & O. Fischer, J. Less-Common Metals, 58, 179 (1978).
36. M. Marezio, R.D. Dernier, J.P. Remeika, E. Corenzwit & B.T. Matthias, Mat. Res. Bull., 8, 657 (1973).
37. F.A. Cotton, J. Less-Common Metals, 54, 3 (1977).
38. O. Bars, J. Guillevic & D. Grandjean, J. Solid State Chem., 6, 48 (1973).
39. R. Chevrel, M. Sergent & J. Prigent, Mat. Res. Bull., 9, 1487 (1974).
40. J. Guillevic, O. Bars & D. Grandjean, Acta Cryst., B32, 1338 (1976).
41. K. Yvon, A. Paoli, R. Flukiger & R. Chevrel, Acta Cryst., B33, 3066 (1977).
42. K. Yvon & A. Paoli, Solid State Commun., 24, 41 (1977).

43. O. Fischer, A. Treyvand, R. Chevrel & M. Sergent, Solid State Commun., 17, 721 (1975).
44. M. Sergent & R. Chevrel, J. Solid State Chem., 6, 433 (1973).
45. L.F. Mattheiss & C.Y. Fong, Phys. Rev., B15, 1760 (1977).
46. R.D. Shannon, Acta Cryst., A32, 751 (1976).
47. J. Guillevic, O. Bars & D. Grandjean, J. Solid State Chem., 7, 158 (1973).
48. K. Yvon, Solid State Commun., 25, 327 (1978).
49. F.A. Cotton & G.W. Wilkinson, 'Advanced Inorganic Chemistry', 3/e, Interscience, N.Y. (1972).
50. R.P Elliott, 'Constitution of Binary Alloys', 1st Supplement, McGraw-Hill, N.Y. (1965).
51. J. Hauck, Mat. Res. Bull., 12, 1015 (1977).
52. R. Flukiger, R. Baillif & E. Walker, Mat. Res. Bull., 13, 743 (1978).
53. F. Bonino, M. Lazzari, G. Razzini, B. Rivolta & B. Scrosati, 2nd International Meeting on Solid Electrolytes, St. Andrews (1978).
54. J.M. Shemilt, Ph.D. Thesis, Imperial College, London (1978).
55. G.J. Dudley & B.C.H. Steele, in press.
56. G.J. Dudley, private communication.
57. T. Matsui & J.B. Wagner, Jr., J. Electrochem. Soc., 124, 941 (1977).
58. T. Takahashi, O. Yamamoto, S. Yamada & S. Hayashi, 2nd International Meeting on Solid Electrolytes, St. Andrews (1978).
59. R. Schollhorn, M. Kumpers & J.O. Besenhard, Mat. Res. Bull., 12, 781 (1977).
60. R. Schollhorn, M. Kumpers & D. Plorin, J. Less-Common Metals, 58, 55 (1978).
61. Y-F. Yu Yao & J.T. Kummer, J. Inorg. Nucl. Chem., 29, 2453 (1967).
62. G.C. Farrington & W.L. Roth, Electrochim. Acta, 22, 767 (1977).
63. S.C. Lloyd-Williams, Transfer Report, Imperial College (1977).
64. R.D. Shannon, B.E. Taylor, A.D. English & T.Berzins, Electrochim. Acta, 22, 783 (1977).
65. C.K. Banks, L. Kammerdiner & H.L. Luo, J. Solid State Chem., 15, 271 (1975).

66. C. Berthier, Y. Chabre & M. Minier, Solid State Commun., in press.
67. A. Le Mehaute, C.R. Acad. Sc. Paris, in press.
68. I. Yokata, J. Phys. Soc. Japan, 16, 2213 (1961).
69. C. Wagner, Progress Solid State Chem., 10, 3 (1975).
70. G.J. Dudley & B.C.H. Steele, in press.
71. G.J. Dudley & B.C.H. Steele, J. Solid State Chem., 21, 1 (1977).
72. T. Takahashi, O. Yamamoto, F. Matsuyama & Y. Noda, J. Solid State Chem., 16, 35 (1976).